ABSTRACT

HELTON, THOMAS DALE. Cloning and Characterization of Alternatively SplicedVoltage-Gated Calcium Channel Subunits. (Under the direction of William Alan Horne.)

Neuronal voltage gated Ca^{2+} channels are multimeric transmembrane protein structures that consist of at least four subunits, α_1, α_2/δ, and β. Homology screening of a human spinal cord cDNA library revealed that the α_{1A} and β_4 subunit subtypes undergo alternative splicing. The pore-forming α_{1A} subunit splice variants differ in C-terminal exon composition. The α_{1A}-C2 variant possesses exon 37a and exon 44 while the α_{1A}-C16 variant has exon 37b but lacks exon 44. Expression studies in *Xenopus* oocytes in conjunction with β subunit subtypes β_{1a}, β_{1b}, β_3, and β_4 demonstrated that the inclusion of exon 44 increased the rates of activation, inactivation, and recovery from inactivation of α_{1A} subunits while not affecting the voltage dependence of activation and inactivation.

Two alternatively spliced N-terminal variants of the β_4 subunit (β_{4a} and β_{4b}) were isolated from human spinal cord. The novel β_{4a} subunit has a 15 amino acid N-terminus while the β_{4b} subunit, previously identified in brain, has a 49 amino acid N-terminus. Expression of α_{1A}/β_{4a} or α_{1A}/β_{4b} complexes in Xenopus oocytes revealed that compared to β_{4a}, β_{4b} left-shifts the voltage dependence of activation and inactivation, decreases the rate of fast inactivation, increases the rate of slow inactivation, and increases the sensitivity of α_{1A} subunits to the cone snail toxin ω-CTx-MVIIC. Site directed mutagenesis revealed that four amino acids (G10, D13, P15, and P18) of the N-terminus are responsible for conveying the effects of β_{4b} on the α_{1A} subunit.

Cloning and Characterization of Alternatively Spliced Voltage-Gated Calcium Channel Subunits

by

Thomas Dale Helton

A Dissertation

Presented to the Faculty of the Graduate Faculty of

North Carolina State University

in partial fulfillment of the requirements for the Degree of

Doctor of Philosophy

COMPARATIVE BIOMEDICAL SCIENCES

Raleigh

July 2002

Dedication

To my parents, Charles and Barbara Helton, and my sister, Laura for their loving support.

Biographical Sketch

Thomas Dale Helton was born in Minneapolis, Minnesota on December 22nd, 1970, the first of two children to Charles and Barbara Helton. He has one sister, Laura, who is three years younger. After spending his first eight years in Minneapolis he and his family moved to Raleigh, North Carolina where he graduated from Ravenscroft High School in 1989. He attended Emory University in Atlanta, Georgia and graduated in 1993 with a bachelor's of science degree in biology. After graduation, he worked as a cardiac surgical technician at Wake County Medical Center in Raleigh, North Carolina for two years. Wishing to further his knowledge of biological systems he enrolled in the Master's program in physiology at North Carolina State University in 1995. Upon receiving his Master's in Physiology in 1997, he decided to continue his academic pursuits and entered the doctoral program in cell biology at North Carolina State University. After completing his Ph.D. in 2002, he accepted a post-doctoral position in the Department of Neuroscience at Brown University in Providence, Rhode Island.

Table of Contents

List of Tables

List of Figures

Chapter 1

INTRODUCTION: FUNCTIONAL AND STRUCTURAL DIVERSITY OF VOLTAGE-GATED CA^{2+} CHANNELS.

The calcium ion plays a major role as a second messenger in a wide array of cellular mechanisms. The efficacy of Ca^{2+} as a second messenger relies on the strict regulation of intracellular Ca^{2+} levels. At rest, intracellular Ca^{2+} concentration is approximately 10^{-7} M. In electrically excitable cells, changes in plasma membrane potential cause voltage-gated Ca^{2+} channels (VGCCs) to open and local Ca^{2+} levels to rise. These localized, transient increases enable Ca^{2+} as a second messenger to initiate important cellular processes including excitation-contraction coupling, gene transcription, and synaptic transmission (Tanabe *et al*., 1990; Sutton *et al*., 1999; Wheeler *et al*., 1994). This high degree of Ca^{2+}-dependent cellular process specialization has led to the evolution of a large diversity of Ca^{2+} channel subtypes.

Prior to the cloning era, electrophysiological and pharmocological experiments hinted at the possible wide diversity of Ca^{2+} channel phenotypes. Three voltage-gated Ca^{2+} channel subtypes, L-type (long-lasting current), T-type (transient current), and N-type (neither L- or T-type) were first distinguished in chick dorsal root ganglion cells (Nowycky et al., 1985). Subsequently, additional phenotypes were discovered in rat Purkinje cells (P/Q-type) and rat cerebellar granule cells (R-type) (Llinás et al., 1989; Randall and Tsien, 1995). L-, N-, P/Q-, and R-type channels are categorized as members of the high-voltage activated (HVA) family because they are activated by strong

depolarizations (+40 mV) from holding potentials ranging from –80 to –100 mV. In contrast, T-type channels are termed low-voltage activated (LVA) because they open in response to weaker membrane depolarizations (+10 to +20 mV) from resting membrane potentials of approximately –80mV. The phenotypic variability observed between Ca^{2+} channel subtypes is due to extensive structural and genetic diversity between Ca^{2+} channel subtypes and associated subunits. Voltage-gated Ca^{2+} channel complexes are multimeric membrane-spanning protein structures that provide a selective pathway for the entrance of Ca^{2+} into cells. Neuronal VGCCs consist of a minimum four distinct subunits (Figure 1.1), α_1, α_2/δ, and β (Liu *et al*., 1996). A fifth subunit, γ, a constituent of skeletal muscle VGCCs, has also been proposed to be a part of the neuronal VGCC complex (Leung et al., 1988; Letts *et al*., 1998). My thesis will focus on the effects of alternative subunit splicing on Ca^{2+} channel gating and pharmacology.

A. Overview of Structure and Function of Neuronal Ca^{2+} Channel Subunits:

1. α_1 Subunits:

The α_1 subunit forms the pore and contains the domains necessary for channel gating, voltage sensing, and toxin and auxiliary subunit binding (Catterall, 1996, Jones, 1998). It is greater than 2000 amino acids long (170 kDa) and is arranged into four homologous transmembrane spanning domains (DI-IV) (Figure 1.2). Kyte and Doolittle hydropathy plots of α_1 subunit sequence demonstrate that the hydrophobic regions of the protein correspond to the homologous transmembrane spanning domains (Tanabe et al., 1987). Each domain is linked by intracellular loops of varying lengths that contain binding sites for auxiliary β subunits (I-II linker) (De Waard et al., 1996), G-proteins, and Ca^{2+} binding proteins such as calmodulin, as well as protein kinase A (PKA) (DeJongh et

al., 1996), protein kinase C (PKC) (Bourinet et al., 1992; McHugh et al., 2000) and MAP kinase phosphorylation sites (Fitzgerald, 2000; Jones, 1998). Each domain consists of six transmembrane spanning segments (S1-S6), similar to segment structures of voltage gated Na^+ and K^+ channels (Figure 1.2). The S1-S3 segments are thought to form the lipid-facing wall of the channel, while the interior of the channel is lined by the S6 segments (Bezanilla, 2000). The S4 segment of each domain serves as the voltage-sensing component and contains highly conserved positively charged arginine or lysine amino acid residues at every third position. In response to changes in membrane voltage, the S4 segment moves outward and rotates under the influence of the electric field and initiates a conformational change that opens the pore (Bezanilla, 2000; Durell *et al*., 1998). The four domains are arranged in a circle-like pattern surrounding an aqueous pore (Figure 1.1) (Lipkind and Fozzard, 2001; Mitterdorfer J *et al*., 1998). The outer vestibule of each repeat is formed by the membrane associated, hydrophilic, extracellular S5-S6 linker (termed P-loop or H5). The P-loops project into the middle of the channel and form a selectivity filter near the outer mouth of the channel. The pore loops are well conserved within each VGCC class as well as between each of the four repeats. Each VGCC pore loop has a glutamate residue located at the same position. This structural arrangement is given a shorthand notation of EEEE (Yang et al., 1993). Site-directed mutagenesis of these glutamates has shown that they are the key for establishing the Ca^{2+} binding site that is crucial for Ca^{2+} selectivity (Yang *et al*., 1993 Nature; Tang *et al*., JBC 1993; Parent and Gopalakrishnan 1995; Heinemann *et al*., 1992). The corresponding pore loop residues in Na^+ channels, DEKA, when mutated to DEEE result in Na^+ channels that are Ca^{2+} permeable (Heinemann *et al*., 1992).

Ten known Ca^{2+} channel α_1 subunit gene classes (α_{1A} through α_{1I} and α_{1S}) have been defined by homology screening. These subunit genes are divided into 3 structurally and functionally related groups (Figure 1.3) (Ertel *et al*., 2000). The dihydropyridine sensitive L-type channels are termed $Ca_v1.1$-$Ca_v1.4$ (S, C, D, and F, respectively) while the dihydropyridine insensitive A, B, and E class channels are termed $Ca_v2.1$, $Ca_v2.2$, and $Ca_v2.3$, respectively. Recent evidence has shown, however, that the $Ca_v1.3$ channel, originally thought to be an HVA Ca^{2+} channel, actually has characteristics of low voltage-activated (LVA) Ca^{2+} channels (Xu and Lipscombe, 2001). The T-type LVA channels, not including $Ca_v1.3$, include the α_{1G}, α_{1H}, and α_{1I} class genes, $Ca_v3.1$-$Ca_v3.3$, respectively (Figure 1.3).

a. Ca_v1 Channels:

Ca_v1 channels were initially cloned from rat skeletal muscle t-tubules, and characterized electrophysiologically in Xenopus oocytes (Perez-Reyes et al., 1989). Ca_v1 channels have relatively large single channel conductances (approximately 25pS), and tend to inactivate slowly or not at all. Ca_v1 channels are highly sensitive to dihydropyridines and benzothiazepines, and these agents have been used extensively in treatment of various cardiovascular disorders including hypertension and cardiac arrhythmias. Ca_v1 channels are found on the post-synaptic surface of the neuromuscular junction as well as in association with ryanodine receptors in skeletal muscle t-tubules ($Ca_v1.1$), in cardiac muscle ($Ca_v1.2$), and in dendrites and somal regions of neurons ($Ca_v1.3$). Recently, a fourth L-type channel, $Ca_v1.4$, has been localized to rod active zones in the retina (Morgans, 2001). $Ca_v1.1$ and $Ca_v1.2$ channels are primarily involved

in initiating muscle contraction and modulating gene regulation. $Ca_v1.3$ channels modulate action potential propagation and gene transcription, while $Ca_v1.4$ channels appear to be involved in tonic glutamate release in retinal bi-polar cells (Catterall, 2000).

b. Ca_v2 Channels:

The non-L-type $Ca_v2.1$ channels are primarily located in pre-synaptic nerve termini and are intricately involved in the neurosecretory process (Wheeler et al. 1994; Turner and Dunlap, 1995). Two distinct phenotypes, P and Q, are attributed to alternatively spliced versions the $Ca_v2.1$ channel (Bourinet *et al* 1999; Moreno *et al*., 1997; Stea *et al*., 1994). Both P- and Q-type channels have unitary conductances in the range of 15pS but display varying rates of inactivation and varying sensitivities to channel blockers. The P-type channels have relatively slow inactivation kinetics (several seconds) (Mintz et al.,1992; Mintz and Bean 1993) and are highly sensitive to the funnel web spider (*Agelenopsis aperta*) venom ω-Aga-IVA (1nM) and to a lesser extent the cone snail toxin ω-CTx-MVIIC (Sather *et al*., 1993). The Q-type channels have rapid inactivation kinetics, less than 0.1 sec and are less sensitive to ω-Aga-IVA (200nM). The genotypic distinction between P- and Q-type channels has been difficult to establish in many neurons so most studies refer to P- and Q- type channels as one entity. In most circumstances, the designation P/Q-type serves to indicate ω-Aga-IVA sensitive $Ca_v2.1$ channels.

The $Ca_v2.2$ channel subtype, found primarily in pre-synaptic nerve terminals, and to a lesser extent in neuronal dendrites and cell bodies (Westenbroek *et al*., 1992), is also involved in neurotransmitter release from the pre-synaptic membrane. Like Ca_v1

channels, $Ca_v2.2$ is a member of the HVA channel family and has a unitary conductance of approximately 13-20pS. These channels are highly sensitive to the cone snail toxins ω-Conotoxin GVIA (ω-CTx-GVIA) and ω-conotoxin MVIIA (ω-CTx-MVIIA). Ziconotide (SNX-111) is the synthetic form of cone snail peptide ω-CTx-MVIIA and has been approved by the FDA for treatment of severe chronic pain. ω-CTx-MVIIA is a neuron-specific N-type calcium channel blocker with an analgesic and neuroprotective effects (Bowersox and Luther, 1998). Intrathecally administered, ziconotide produces analgesia by blocking neurotransmitter release from primary nociceptive afferents and prevents the propagation of pain signals to the brain. Unlike opioids, there have been no reports of development of tolerance after prolonged use, however, significant side effects have been reported (Penn and Paice, 2000; Jain , 2000).

Cerebellar granule cells also demonstrate a VGCC HVA component that is resistant (R-type) to dihydropyridines, ω-CTx-GVIA, and ω-Aga-IVA (Ellinor et al., 1993; Zhang et al., 1993; Randall and Tsien, 1995). R-type, or $Ca_v2.3$ channels, inactivate more rapidly than other HVA channels, have a unitary conductance of approximately 15pS, and are selectively blocked by the *Hysterocrates gigas* tarantula toxin SNX-482 and low concentrations of the divalent cation Ni^{2+} (30-50 μM) (Gasparini *et al*., 2001). $Ca_v2.3$ channels are coded for by the α_{1E} subunit gene and were thought to be primarily restricted to dendrites and cell bodies of most central neurons (Yokoyama *et al*., 1995) (Figure 1.3). However, selective pre-synaptic block of $Ca_v2.1$ and $Ca_v2.2$ channels does not completely suppress pre-synaptic calcium entry into fast glutamatergic synapses (Luebke *et al*., 1993; Takahashi and Momiyama, 1993; Wu and Saggau, 1995). This indicates that $Ca_v2.3$ channels are also located at pre-synaptic nerve terminals.

Further, $Ca_v2.3$ channels can contribute to fast excitatory synaptic transmission, demonstrating that $Ca_v2.3$ channels can cooperate with $Ca_v2.1$ and $Ca_v2.2$ channels in regulating synaptic transmission (Gasparini *et al*., 2001).

c. Ca_v3 Channels:

The low voltage-activated Ca_v3, or T-type, channel family represents a unique class of VGCCs. This family carries smaller unitary conductances (6-8pS), activates at lower membrane potentials (-60 mV to –70 mV) as compared to HVA channels (-40mV), and is mildly sensitive to dihydropyridines, highly sensitive to mibfradil, and is insensitive ω-CTx-GVIA, and ω-Aga-IVA. These channels were initially characterized in chick and rat sensory neurons and eventually cloned from rat brain (Carbone and Lux, 1984; Nilius *et al*., 1985; Perez-Reyes *et al*., 1998). Ca_v3 channels are primarily found in dendrites and the soma of central neurons but are also found in other tissues including heart, kidney, pancreas, smooth and skeletal muscle, lung, and placenta (Perez-Reyes, 1999). T-type channels, including the α_{1G-I} classes are designated $Ca_v3.1$-$Ca_v3.3$ respectively (Perez-Reyes, 1999). Initially, Ca_v3 channels were thought to be primarily involved in establishing and maintaining pacemaker current in cardiac pacemaker cells, however, they have also been found to play a pace making role in neurons as well. Since their activation potential is so close to the resting membrane potential of most cells, Ca_v3 channels can play a role in sustaining Ca^{2+} levels above resting cellular concentrations. In this respect they may be important in maintaining smooth muscle tone, as well as be an important determinant of cell proliferation and gene transcription (Perez-Reyes, 1999).

2. α_2/δ and γ subunits:

Voltage gated Ca^{2+} channel complexes also contain membrane associated α_2/δ and γ subunits (Figure 1.1). The approximately 1100 amino acid, 170 kDa, α_2/δ subunit was first co-purified with the α_1 subunit from rabbit skeletal muscle t-tubules (Curtis and Catterall *et al*., 1984). The human α_2 and δ subunits are encoded by the same gene (CACNA2) on chromosome 7q11.23 (Felix, 1999). The mature form of this subunit is produced by post-translational glycosylation of the α_2/δ protein and subsequent α_2-δ subunit disulfide linkage. The cloned α_2 subunit has several hydrophobic sequences but studies indicate that it is an extracellular protein attached to the membrane via its disulfide linkages to the δ subunit. The δ subunit possesses a transmembrane segment that anchors the complex to the plasma membrane (Felix, 1999). Co-expression of the α_2/δ subunit with various α_1 subunits results in an increase in the current densities as well as left-shifts the current-voltage (I-V) relationship and accelerates activation and inactivation kinetics of VGCC's (Singer *et al*., 1991; Welling *et al*., 1993; DeWaard and Campbell, 1995; Bangalore *et al*., 1996; Felix *et al*., 1997; Jones *et al*., 1998; Klugbauer *et al*., 1999). Three distinct CACNA2 α_2/δ genes have been identified (α_2/δ-1, -2, and -3) that vary in their tissue distribution; the α_2/δ-2 subunit is expressed in heart, pancreas, skeletal muscle, kidney, liver, and brain while the α_2/δ-1 and α_2/δ-3 subunits are expressed primarily in brain (Hobom *et al*., 2000; Klugbauer *et al*., 1999). The various α_2/δ subtypes have been shown to undergo alternative splicing.

The γ subunit is a VGCC complex associated subunit approximately 300 amino acids in length (36 kDa) and consists of four hydrophobic transmembrane spanning

domains and an intracellular amino and carboxy terminus (Figure 1.1). The γ subunit was first purified from rat skeletal muscle in conjunction with the α_{1S} subunit (Curtis and Catterall, 1984). Initially, γ subunits were believed to be associated solely with skeletal muscle VGCCs. However, recent evidence has demonstrated that the γ subunit may also be part of the neuronal VGCC complex (Kang *et al*., 2001). Subsequent experiments have determined that at least 8 γ genes (CACNG1-8) exist in rats and humans and can be found throughout the brain as well as in skeletal muscle and in heart (Chu *et al*., 2001; Letts *et al*., 1998). The role of γ subunits in VGCC function is unclear. Studies have shown that the γ subunit, when expressed with various α_1 and β subunits, has negligible effects on voltage-dependent gating. However the γ subunit may have other biological functions. Recently the γ2 subunit was shown to co-immunoprecipitate *in vitro* with both AMPA receptors and synaptic PDZ-domain containing proteins PSD-95, DLG, and ZO-1 suggesting that it may be required for synaptic targeting of AMPA receptors in cerebellar granule cells (Chu *et al*., 2001).

3. β Subunits

a. β Subunit Structure:

Similar to other VGCC subunits, Ca^{2+} channel β_1 subunits were initially purified and cloned from rat skeletal muscle t-tubule membranes as part of the dihydropyridine receptor complex (Curtis and Catterall, 1984; Ruth *et al*., 1989). Further experiments

resulted in the discovery of three additional β subunit subtypes (β_2-β_4) (Perez-Reyes 1992; Castellano *et al*., 1993a; Castellano *et al*., 1993b; Powers *et al*., 1992).

The four voltage-gated Ca^{2+} calcium channel β subunits arise from four separate genes (CACNB1-4) and each gene is composed of at least 13 exons. The human β_1 gene is located on chromosome 17q21-q22, β_2 on chromosome 10q12, β_3 on chromosome 12q13, and β_4 on chromosome 2q22-23 (Gregg *et al*., 1993; Park *et al*., 1997; Taviaux *et al*., 1997). Calcium channel β subunits range from 480-600 amino acids in length and have six predicted alpha helical regions. The amino acid sequences can be divided into five domains (A-E) based on amino acid sequence identity between representatives of each gene class (Figure 1.4) (Birnbaumer et al., 1998; Hanlon et al., 2002). Kyte-Doolittle analysis indicates that all five domains are cytosolic (Ruth *et al*., 1989; Hanlon *et al*., 1999). The poorly conserved A, C, and E domains are coded for by exons 1, 6, and 13, respectively, and the highly conserved B and D domains are coded by exons 2-5 and 7-12, respectively. Interestingly there appear to be two evolutionarily distinct A domains, a long and short version. The short forms are structurally unrelated while the longer forms show approximately 44% evolutionary relatedness (Figure 1.5). Homology screening using the β_1 subunit as a probe led to the discovery of several β_1 splice variants, β_{1a}-β_{1c}. The three differ in central (C) domain and C-terminal composition. Like β_1, several versions of the β_2 subunit have also been isolated, β_{2a}-β_{2c}, that differ in A and C domain structure. Recently, the β_4 subunit has also been shown to undergo alternative splicing (Helton and Horne, 2002). Currently, no β_3 subunit splice variants have been reported. Channel β subunits are expressed in numerous tissue types including brain,

skeletal muscle, heart, and spinal cord (Ludwig et al., 1997; Wittemann et al., 2000). While the various β subunit isoforms are present in most tissues, certain splice variants predominate. Skeletal muscle mainly expresses the β_{1a} isoform whereas β_{1b} and β_{1c} are found mostly in neuronal tissue (Powers et al., 1992). Heart predominantly expresses the β_{2a} subtype. Brain and spinal cord express β_{1b}, β_{2a}, β_3, and β_4 isoforms, however, β_3 and β_4 are more prevalent (Ludwig *et al*., 1997).

Recent protein modeling studies of the rat β_{1b} subunit suggest that the five β subunit domains (A-E) resemble structures found in members of the membrane-associated guanylate kinase (MAGUK) protein family (Hanlon et al., 1999) (Figure 1.4). MAGUK proteins act as molecular scaffolds for signaling pathway components at the plasma membranes of synaptic and neuromuscular junctions. They function by binding to cytoplasmic C-termini of transmembrane and intracellular signal transduction proteins (Dimitratos et al., 1999). They act to hold together elements of individual signaling pathways, increasing the efficiency and specificity of signaling interactions. Typically, MAGUK proteins possess guanylate kinase like binding regions preceded by protein-protein interaction SH3 and N-terminal PDZ domains (Hanlon and Wallace, 2002). Sequence homology modeling of the 597 amino acid long rat β_{1b} subunit produced PDZ-like, SH3-like, and guanylate kinase-like domains, however sequence homology was low (~17% for PDZ, ~27% for SH3, and ~18% for gyanylate kinase). Secondary structure prediction using Prodom and Pfam databases provide additional confirmation for presence of these structures. The N-terminal portion of the PDZ-like domain, or A-domain, comprised of approximately the first 100 amino acids, shares approximately 2% amino acid identity between β subunit subtypes. The SH3, or B-domain, amino acids

101-161, shares 65% identity between β subunit subtypes. The C-domain, amino acids 162-220, shows little similarity to other structure predictions and has only 11% identity between subtypes. The GK-like D-domain, amino acids 221-430, shares 78% identity between β subunit subtypes while the C-terminal E-domain demonstrates only 3% homology. These percentages are based on amino acid comparisons between human β_{1-4} subunits.

b. β subunit function:

Channel β subunits associate directly with the α_1 subunit by binding to a highly conserved region in the cytoplasmic loop that links transmembrane spanning domains I and II (I-II linker). This α interaction domain, or AID, consists of a minimal binding domain of 18 amino acids of which 9 are highly conserved between Ca_v1 and Ca_v2 channel classes (Pragnell *et al*., 1994). Interestingly, $Ca_v3.1$-3.3 channels do not possess a conserved AID region and do not appear to be modulated by Ca^{2+} channel β subunits (Perez-Reyes, 1999). Site directed mutagenesis experiments revealed three of the 9 conserved AID amino acids were critical for binding (DeWaard et al., 1996). The AID interacts with a highly conserved region of the β subunit called the β interaction domain or BID (Figure 1.5). The BID is mapped to first thirty amino acids of the N terminal region of the second high homology domain (D) of the β subunit (Walker and De Waard, 1998). The BID was identified by truncating the β_{1b} subunit to the shortest sequence capable of modulating α_1 subunit activity (Pragnell *et al*., 1994; De Waard *et al*., 1995; De Waard *et al*., 1996). Recently, $Ca_v2.1/\beta_{4b}$ subunit specific interactions have been

identified involving the N- and C-terminus of the α_{1A} subunit and the C-terminus of the β_{4b} subunit (Walker *et al*., 1998; Walker *et al*., 1999). This interaction may impart a β_4 subunit isoform specific regulation of the α_{1A} subunit. Recent evidence has shown that β_4 subunits co-localize with $Ca_v2.1$ and $Ca_v2.2$ channels in hippocampal neurons (Wittemann *et al*., 2000) pointing to specific $Ca_v2.1/\beta_4$ and $Ca_v2.2/\beta_4$ interactions at synaptic terminals. The AID-BID interaction is the minimal interaction responsible for augmenting current sizes and modulating channel kinetics (Pragnell *et al*., 1994). This interaction is believed to be responsible for augmenting VGCC current sizes by both increasing the number of functional channels in the membrane as well as increasing the probability that a channel will open at a specific voltage (DeWaard *et al*., 1995; Yamaguchi *et al*., 1998). While not all α_1 subunits possess a putative AID, all β subunits have the highly conserved BID and are capable of interacting with α_1 subunits.

Calcium channel β subunits appear to be required for normal channel expression and kinetic activity. In addition to augmenting Ca^{2+} currents, β subunits also modify activation and inactivation kinetics of α_1 subunits without altering deactivation. Regions of the β subunit have been attributed to the various affects on channel kinetics and membrane localization. The A and C domains have been shown to be important for modulating channel activation and inactivation kinetics while the E-domain has been implicated in membrane targeting of the α_1 subunit (Figure 1.4) (Helton and Horne, 2002; DeWaard and Campbell 1995; Lacerda et al., 1991; Tomlinson et al., 1993; DeWaard et al 1996).

Beta subunits modify the activation phase by affecting both the rate of activation (τ_{act}) as well as the membrane voltage at which the channels open (voltage-dependency of activation). Generally, β subunits subtypes 1-4, expressed with α_1 subunits, increase overall current densities while increasing the rate and lowering the voltage at which the α_1 subunits activate in comparison to the α_1 subunit expressed alone (Birnbaumer *et al*., 1998). In this respect, β subunits make the α_1 subunit more sensitive to smaller depolarizations in membrane voltage, facilitating a more rapid influx of Ca^{2+} at lower potentials. While not all α_1 subunit isoforms inactivate ($Ca_v1.1$-1.4 channels show little or no inherent inactivation), β subunits profoundly affect inactivation of neuronal $Ca_v2.1$-2.3 channels. Similar to activation, β subunits alter the rate (τ_{inact}) and voltage-dependency of inactivation. However, unlike activation, various β subunit isoforms affect inactivation differently. In the case of the $Ca_v2.3$ channel, β_1, β_3, and β_4, expressed in conjunction with α_{1E}, to differing degrees, increase the rate and lower the voltage-dependency of inactivation compared to α_{1E} alone (Ellinor *et al*., 1993; Jones *et al*., 1998). On the other hand, the β_2 subunit splice variant β_{2a} has the opposite effect on α_{1E}. The β_{2a} variant slows the rate of inactivation and raises the potential at which inactivation occurs. In some cases, β_{2a} can abolish inactivation altogether. This rightward shift in the voltage-dependency of inactivation and slowing of the τ_{inact} of the channel has been attributed to the N-terminus of the β_{2a} subunit (Olcese *et al*., 1994; Qin *et al*., 1996). The N-terminus of the β_{2a} subunit is 16 amino acids long with cystines at the 3rd and 4th amino acid positions. Studies have demonstrated that C3 and C4 are palmitoylated and may anchor the N-terminal portion of the β_{2a} subunit to the membrane, facilitating its unique

effects on the α_1 subunit. By mutating these cystines to serines (C3S, C4S), these unique β_{2a} effects were abolished (Qin *et al*., 1996). Therefore, β subunits not only modulate how fast Ca^{2+} enters the cell but also the amount and duration of Ca^{2+} influx at a given membrane potential.

4. VGCC modulation pathways:

VGCCs are modulated by several intracellular affector proteins including protein kinases A and C (PKA and PKC, respectively), guanine nucleotide-binding proteins (G-proteins) and Ca^{2+} binding proteins such as calmodulin. Skeletal $Ca_v1.1$ and cardiac $Ca_v1.2$ subtypes have been shown to be substrates for cyclic AMP (cAMP) dependent phosphorylation. PKA phosphorylation of sites on the I-II linker (serine 687) and C-terminus (serine 1854) of skeletal muscle α_{1S} subunits and corresponding sites of α_{1C} subunits increase the number of functional channels in the membrane and increase channel activity leading to a greater influx of Ca^{2+} during each membrane depolarization (Rotman *et al*., 1992. Rotman *et al*., 1995; DeJongh *et al*., 1996). In contrast to PKA, PKC phosphorylation of N-terminal PKC consensus sequences at positions 27 and 31 inhibits cardiac Ca^{2+} channel activity (McHugh *et al*., 2000).

$Ca_v2.1$ and $Ca_v2.2$ channels are regulated through several G-protein coupled pathways (Hille, 1994; Ikeda and Dunlap, 1999; Jones and Elmslie, 1997). G-proteins are molecules that act as transducers between ligand receptors in the plasma membrane and intracellular effector molecules. Heterotrimeric G-protein complexes consist of α, β, and γ subunits. G-proteins exist in two interconvertable states: the GDP-bound form which is inactive, in which all 3 subunits are bound, and the GTP-bound form which is active,

where the G_{α} and $G_{\beta\gamma}$ subunits are disassociated. When the G-protein complex is activated, the G-protein undergoes a conformational change allowing for G_{α} bound GDP to be exchanged for GTP. This exchange promotes the disassociation of the G_{α} and $G_{\beta\gamma}$ subunits. The disassociated G_{α} and $G_{\beta\gamma}$ subunits then interact with other proteins initiating or inhibiting various intracellular processes. For example $Ca_v2.2$ channels in rat sympathetic ganglion neurons are regulated by at least five different G-protein coupled pathways (Hille, 1994). These pathways represent a significant mechanism in controlling synaptic transmission and hormone secretion. In general, the $Ca_v2.2$, and to a lesser extent $Ca_v2.1$, type channels are inhibited by G-protein activation while $Ca_v2.3$ (R-type) are not. This inhibition is typically manifested by a positive shift and decrease in slope of the voltage dependence of activation, as well as a decrease in the rate of activation. A positive shift in the voltage dependence of activation means that a stronger membrane depolarization is required to activate the channel while a decrease in slope in the voltage dependence of activation denotes that the channels become less voltage dependent, thus activating over a wider range of potentials. The effect of G-proteins has been modeled as a shift between two channel states with different gating properties, reluctant and willing (Bean, 1989). The reluctant state is characterized by slower activation at more positive potentials while the willing state demonstrates more rapid activation during voltages within a physiological range. Activation of G-proteins shifts the channel to the reluctant state. This shift can be reversed by a series of strong positive depolarizations, also called pre-pulse facilitation.

It has been determined that the $G_{\beta\gamma}$ subunits of the G-protein complex are responsible for the regulatory effects of G-proteins on $Ca_v2.1$ and $Ca_v2.2$ type channels

(Herlitze *et al*., 1996; Zamponi *et al*., 1997; De Waard *et al*., 1997). Construction and analysis of channel chimeras in conjunction with G-protein binding experiments, site-directed mutagenesis, and expression studies suggest that the $G_{\beta\gamma}$ subunit binds to an overlapping region in the α_1 subunit AID (De Waard *et al*., 1997; Herlitze *et al*., 1997; Page *et al*., 1997; Zamponi *et al*., 1997). The highly conserved QQIER motif in the N-terminal region of the I-II linker of the Ca_v2 channel family is important for binding of $G\beta\gamma$ subunits although the specific residues responsible have not been directly mapped. Co-expression of peptides containing the QQIER motif and a C-terminal fragment with α_{1B} subunits in Xenopus oocytes blocked the inhibitory effects of $G_{\beta\gamma}$ suggesting that these peptides act by competing for $G_{\beta\gamma}$ binding, essentially acting as a $G_{\beta\gamma}$ sink (Zamponi et al., 1997). Furthermore, studies where the QQIER sequence in α_{1A} to was mutated to the α_{1C} QQLEE sequence, produced a reduction of $G_{\beta\gamma}$ modulation of $Ca_v2.1$ channels, (Herlitze *et al*., 1997). When QQIER sequence is mutated to QQIEE, $G_{\beta\gamma}$ inhibition is increased rather than decreased indicating that I381 is an important amino acid for facilitating $G_{\beta\gamma}$ inhibition (Herlitze *et al*., 1997). These results indicate that the I-II linker of the Ca_v2 family is an important region of interaction between $G_{\beta\gamma}$ subunits and Ca^{2+} channels. Recent evidence has also indicated that N- and C-terminal regions of VGCC's are also required for G-protein regulation. Chimeric studies where N- and the C-terminus of $Ca_v2.2$ were transferred to the $Ca_v2.1$ channel conferred full $G_{\beta\gamma}$ regulation on $Ca_v2.1$ and substitution of the I-II linker and or N-terminus of the $Ca_v2.2$ for corresponding regions of the $G_{\beta\gamma}$ resistant $Ca_v2.3$ subtype enhanced G-protein regulation of $Ca_v2.3$ (Page *et al*., 1997; Zhang *et al*., 1996).

Voltage-gated Ca^{2+} channels are also regulated by Ca^{2+} itself. L-type, $Ca_v1.2$ channels in the heart are potently regulated by intracellular Ca^{2+}. During long depolarizing stimuli, increased intracellular Ca^{2+} levels lead to an increase in the rate of channel inactivation. Calcium dependent inactivation is more rapid than voltage-dependent inactivation of these channels indicating that Ca^{2+} is a primary determinant of the duration of Ca^{2+} current (Haack and Rosenberg, 1994). This Ca^{2+}-dependent inactivation results from the binding of Ca^{2+} and calmodulin to the C-terminus of $Ca_v2.1$ channels (Soldatov *et al*., 1997; Soldatov et al., 1998; Zühlke *et al*., 1998). Calmodulin is a ubiquitous Ca^{2+} binding protein of the EF hand type that interacts with specific IQ binding motifs of various proteins. By mutating this C-terminal IQ motif in $Ca_v1.2$ channels, Ca^{2+}-dependent inactivation is abolished (Peterson *et al*., 1999; Qin *et al*., 1999; Zühlke *et al*., 1999). It is believed that calmodulin is constitutively bound to the IQ site and ready to bind Ca^{2+} to initiate Ca^{2+}-dependent inactivation. Pre-synaptic $Ca_v2.1$ channels are also susceptible to Ca^{2+}-dependent facilitation and inactivation. Similar to cardiac channels, $Ca_v2.1$ channels directly bind calmodulin in a Ca^{2+} dependent manner (Lee *et al*., 1999). Calcium-dependent binding of Ca^{2+}/calmodulin to a unique IQ motif in the C-terminus of $Ca_v2.1$ channels increases the rate and extent of voltage-dependent inactivation, and causes a Ca^{2+}-dependent facilitation of Ca^{2+} current, as well as enhancing recovery from inactivation (Lee *et al*., 2000).

5. Voltage-gated Ca^{2+} channels and synaptic transmission:

The neurosecretory process is highly reliant on calcium influx. $Ca_v2.1$, $Ca_v2.2$, and $Ca_v2.3$ channels are primarily located at pre-synaptic nerve terminals and are integral

components in the rapid release of neurotransmitter in response to a pre-synaptic membrane depolarization (Timmerman et al., 2002). Studies have shown that pre-synaptic neurotransmitter vesicles are clustered around Ca^{2+} channels in 0.3 μm^2 microdomains (Seagar and Takahashi, 1998). Transient, highly localized Ca^{2+} currents, occurring less than 200 μs after action potential arrival at the synaptic terminal, initiate neurotransmitter release in less than 1 ms (Sheng *et al*., 1998). At rest, the pre-synaptic intracellular Ca^{2+} is approximately 10^{-7} M; however, upon VGCC activation, the local Ca^{2+} concentrations rise as high as 200-300 μM, triggering neurotransmitter vesicle fusion with the pre-synaptic membrane (Sheng *et al*., 1998). Since intracellular Ca^{2+} concentration falls off steeply as a function of distance away from the Ca^{2+} channel, it was initially thought that low-affinity Ca^{2+} sensors were located in close proximity to voltage-gated Ca^{2+} channels at neurotransmitter release sites (Südhof and Rizo, 1996; Neher, 1998). Activation of these sensors by local Ca^{2+} concentrations of greater than 100 μM then triggered a phasic neurotransmitter release. However, recent Ca^{2+} uncaging experiments in the calyx of Held have demonstrated that rapid neurotransmitter release can occur at Ca^{2+} concentrations as low as 10 μM (Schneggenburger and Neher, 2000; Bollman et al., 2000). The end result is that neurotransmitter release is an n^4 function of Ca^{2+} concentration.

Many proteins have been implicated in pre-synaptic vesicle docking, fusion, and release of neurotransmitter into the synaptic cleft. Voltage-gated Ca^{2+} channel Ca_v2 subtypes are integral parts of this mechanism (Figure 1.6). Rat brain *in situ* hybridization and co-immunoprecipitation studies demonstrate that $Ca_v2.1$, 2.2, and 2.3 channels are highly localized to pre-synaptic nerve terminals of peripheral and central

neurons (Ludwig *et al*., 1997). The α_1 subunit II- III linker region of both $Ca_v2.1$ and 2.2 channels is believed to be the region responsible for interactions with vesicle docking and fusion proteins (Sheng *et al*., 1998). While $Ca_v2.1$ and 2.2 channels are essential for neurotransmitter release, several other vesicle docking and fusion proteins are also involved. Of these, synaptotagmin, synaptosome associated protein 25kDa (SNAP-25), vesicle associated membrane protein (VAMP, or synaptobrevin), and syntaxin 1A are closely associated with pre-synaptic $Ca_v.2.1$ and 2.2 channels (Figure 1.6).

Synaptotagmin is an 65 kDa protein composed of an intravesicular N-terminal domain, a single transmembrane domain, and a large C-terminal domain which contains two Ca^{2+} binding C2 domains (C2A and C2B) that are homologous to C2 domains found in Ca^{2+} activated isoforms of protein kinase C (Brose et al., 1992). Current evidence suggests that synaptotagmin may be the Ca^{2+} dependent mediator of the neurotransmitter release mechanism (Charvin *et al*., 1997; Fossier *et al*., 1999). Calcium binding to the C2A and C2B domains of synaptotagmin initiates insertion of synaptotagmin into acidic phospholipids that comprise the pre-synaptic membrane. This Ca^{2+} dependent insertion is very rapid and is postulated to initiate the fusion of pre-synaptic and vesicular membranes. Synaptotagmin interacts with various components of the pre-synaptic neurotransmitter release complex. Synaptotagmin binds to syntaxin 1A through the C2A domain (Chapman *et al*., 1995; Kee and Scheller, 1996), and to the II-III linker of $Ca_v2.1$ and $Ca_v2.2$ channels (synprint site, amino acids 780-969 of $Ca_v2.1$ and 710-1090 $Ca_v2.2$) in a Ca^{2+} dependent manner (Charvin *et al*., 1998; Sheng *et al*., 1997; Wiser *et al*., 1997; Tobi *et al*., 1998; Kim and Catterall, 1997).

Syntaxin 1A is a 35kDa protein primarily expressed in the pre-synaptic plasma membrane where it is anchored by a C-terminal transmembrane spanning segment (Figure 1.6). Syntaxin 1A plays a major role in membrane fusion and neurotransmitter release, as determined in loss-of-function studies in the *Drosophila melanogaster* syntaxin 1A gene (Broadie *et al*., 1995; Schulze *et al*., 1995; Wu *et al*., 1998; Wu et al., 1999) and in biochemical studies where syntaxin 1A is cleaved by botulinum C1 toxin inhibiting exocytosis (Schiavo *et al*., 1995; Blasi *et al*., 1993; Hayashi *et al*., 1994). The cytoplasmically oriented N-terminus contains three heptad repeats which are characteristic of coiled-coil protein structures. The C-terminal third of syntaxin 1A (aa 181-288) interacts with the II-III linker of $Ca_v2.1$ and 2.2 channels (Sheng *et al*., 1994; Rettig *et al*., 1996) and synaptotagmin (Seagar *et al*., 1998; Sheng *et al*., 1998). When the pre-synaptic neurotransmitter release complex is incomplete, individual SNARE proteins such as syntaxin can have an inhibitory effect on voltage-gated Ca^{2+} channel function. Two-electrode voltage clamp experiments in *Xenopus* oocytes, involving the BI-2 and rbA isoforms of the α_{1A} subunit and β_3 subunits, demonstrate that the co-expression of syntaxin 1A, which interacts directly with the II-III linker of the α_{1A} subunit, significantly reduces α_{1A} current sizes and dramatically left-shifts the voltage-dependency of inactivation (Bezprozvanny *et al*., 1995; Zhong *et al*., 1999). This results in a marked reduction in the number of voltage-gated Ca^{2+} channels available to facilitate neurotransmitter release, creating a negative feedback mechanism against premature neurotransmitter release. This inhibition would allow for proper vesicle docking and fusion assembly and coordinated neurotransmitter release in response to changes in pre-synaptic membrane voltage.

Other neurotransmitter release complex components include VAMP (or synaptobrevin) and SNAP25 (Figure 1.6). VAMP is an 18 kDa integral vesicle protein that binds to syntaxin and SNAP-25 (Zheng and Bobich, 1998). VAMP may play a role in disruption of the pre-synaptic membrane during vesicle fusion (Fisher and Bourque, 2001). SNAP-25 is a 25 kDa plasma membrane associated protein that also interacts with the DII-III linker of $Ca_v2.1$ and 2.2 channels (Seagar *et al*., 1998; Sheng *et al*., 1998). SNAP-25 may act to stabilize the neurotransmitter release complex as studies have shown that when cleaved by botulinum toxin A, neurotransmitter release is reduced (Blasi *et al*., 1993 Nature). Synaptotagmin, syntaxin 1A, SNAP-25, and VAMP are collectively referred to as synaptosome receptor (SNARE) proteins.

At low resting Ca^{2+} concentrations (less than 10 μM) neurotransmitter vesicles are pre-docked at or near the voltage-gated calcium channel microdomains in the pre-synaptic terminal via a low affinity interaction between VAMP, syntaxin, and SNAP-25 (Figure 1.6) (Fossier *et al*., 1999). As the pre-synaptic membrane is depolarized, the initial rise in intracellular Ca^{2+} concentration (10-20 μM) increases VAMP/syntaxin/SNAP-25 coupling, perhaps increasing the energetic driving force for the early priming steps of the vesicle fusion/ neurotransmitter release mechanism. As Ca^{2+} concentrations increase above 30 μM, the complex dissociates, leading to the Ca^{2+}-dependent binding of synaptotagmin and vesicle fusion. While other proteins may also be involved, this process is thought to form the core of the vesicle fusion/ release mechanism.

There is evidence suggesting that alternative splicing of VGCCs affects the fusion-release mechanism. The α_{1A} subunits of $Ca_v2.1$ channels undergo alternative II-III

linker splicing that produces channels with varying syntaxin 1A and SNAP-25 affinity (Sheng *et al*., 1994). The $Ca_v2.1$ α_{1A} isoforms rbA (rat brain) and BI (rabbit brain) have alternatively spliced II-III linkers leading to altered binding affinity for syntaxin 1A and SNAP 25. The BI isoform binds both syntaxin and SNAP 25 while the rbA isoform only binds syntaxin 1A. The BI and rbA isoforms are shown to be differentially distributed in rat brain (Sakurai *et al*., 1995). The II-III linker of the N-type α_{1B} subunit also undergoes alternative splicing, resulting in β subunit specific changes in voltage-dependence of inactivation (Pan and Lipscombe, 2000). These results imply that a neuron could modulate the efficiency of synaptic transmission by regulating the expression of different isoforms of $Ca_v2.1$ and 2.2 channels.

6. Calcium Channel Mutations and Disease:

Several mouse and human neurological disorders have been linked to mutations in genes encoding voltage-gated Ca^{2+} channel α_1 and β subunits. These mutations include single amino acid substitutions and nonsense/truncated proteins as well as deletion and aberrant transcript mutations. These neurological disorders are now referred to as Ca^{2+} channelopathies.

a. Human Mutations:

The several human neurological disorders have been definitively linked to mutations in α_1 and β subunits. The human retinal recessive disorder, X-linked congenital stationary night blindness (xlCSNB), manifests as various levels of night blindness with reduced day vision and visual acuity accompanied by myopia, nystagmus,

and strabismus. A Ca^{2+} channel mutation has been mapped to a region of the X chromosome, Xp11.23, where the $Ca_v1.4$ gene has been located (Bech-Hansen et al., 1998; Strom et al., 1998). These channels have only recently been discovered and are expressed only in the retina. These channels are thought to be responsible for neurotransmitter release in photoreceptor pre-synaptic nerve terminals. Over 20 mutations have been linked to xlCSNB, 14 are nonsense mutations leading to truncated or deleted proteins, 5 are missense mutations leading to substitutions of conserve amino acids, and 1 is a splice/donor site mutation (Nakamura et al., 2001). Several mutations involve 3 amino acid substitutions located in the pore forming loops of the DIII and DIV S6 domains, regions thought to form portions of the channel pore perhaps altering channel selectivity for Ca^{2+} or affecting channel gating. Other mutations include premature truncations that lead to non-functioning channels. These loss-of-function mutants would decrease pre-synaptic Ca^{2+} influx and tonic glutamate release in darkness leading to depolarization of bipolar cells in darkness.

Other Ca^{2+} channel α_1 mutations have been linked to several human neurological disorders. Familial hemiplegic migraine (FHM), episodic ataxia type-2 (EA-2), and spinocerebellar ataxia type-6 (SCA-6), are a family of neurological disorders linked to mutations in $Ca_v2.1$ channels. These channels are located pre-synaptically throughout the central nervous system with high expression in the cerebellum, especially in Purkinje and cerebellar granule cells (Westenbroek et al., 1995). Familial hemiplegic migraine is a rare autosomal dominant disorder characterized by an early childhood onset of intermittent unilateral weakness and paralysis lasting for hours to days with certain cases showing nystagmus, slow progressive ataxia and cerebellar atrophy. This disorder has

been mapped to chromosome 19p13, the gene identified to code for the $Ca_v2.1$ channel (Ophoff et al., 1996; Terwindt et al., 2001). Of the 12 different missense mutations associated with FHM, several are located in important functional regions of the $Ca_v2.1$ channel. Three mutations substitute neutral amino acids for positive arginines in the S4 voltage sensors, 2 mutations are in the pore-lining segments (p-loops) near important glutamates in the Ca^{2+} selectivity filter, and 3 are found in S6 segments. These mutations alter $Ca_v2.1$ channel density in neuronal membranes (Hans et al., 1999), as well as alter single channel conductances, voltage-dependencies of activation, and rates of both inactivation and recovery from inactivation (Ophoff et al., 1996). It is unclear whether these mutations lead to a gain- or loss-of-function in terms of Ca^{2+} influx, however these mutations may affect $Ca_v2.1$ in different neuron subtypes or may affect Ca^{2+} influx in different compartments of the same neuron, for example synaptic terminals versus dendrites.

EA-2 is an autosomal dominant disorder characterized by episodic ataxia (including truncal instability, unsteady gate and loss of limb coordination), vertigo, and progressive cerebellar ataxia and atrophy (Ophoff et al., 1998). The disorder has been mapped to the same locus on chromosome 19 as FHM. More than 15 mutations have currently been identified, most lead to prematurely truncated proteins (Denier et al., 1999; Yue et al., 1997). However, 3 mutations have been identified as missense mutations in critical areas such as p-loops, voltage-sensors and S6 segments. Investigation of these mutations indicates a loss of function of $Ca_v2.1$ channels without affecting channel expression (Friend et al., 1999).

Spinocerebellar ataxia type-6 is an inherited neurodegenerative disorder characterized by progressive ataxia and cerebellar degeneration. This condition is a member of a group of neurodegenerative disorders called poly-glutamine expansion disorders, which include Huntington's disease and Kennedy's disease. SCA-6 is caused by CAG nucleotide expansion repeats that code for poly-glutamine expansions ranging from 35-135 repeats (Zhuchenko et al., 1997) in the 3' end of exon 47 of $Ca_v2.1$ channels. Exon 47 is an alternatively spliced exon that is expressed when 5 nucleotides are inserted into an in-frame stop codon, leading to the expression of exon 47. Poly-glutamine expansions have been demonstrated to lead to aggregation of $Ca_v2.1$ channels in the cytoplasm of Purkinje cells (Ishikawa et al., 1999, Matsuyama et al., 1999) as well as shifts in steady-state inactivation of human $Ca_v2.1$ channels in HEK 293 cells (Toru et al., 2000).

A mutation in the human voltage-gated Ca^{2+} β_4 subunit has also been linked to neurodegenerative disorders characterized by generalized epilepsy, seizures, and episodic ataxia. A mutation in the CACNB4 gene in chromosome 2q22-23 leads to a premature truncation of the voltage-gated Ca^{2+} channel β_4 subunit. Expression of this mutant with $Ca_v2.1$ channels in *Xenopus* oocytes showed slight slowing of fast inactivation (Escayg *et al*., 2000).

b. Mutations in Mice:

Several spontaneous recessive mutations in the $Ca_v2.1$ channel gene have been characterized in mice. These mutations identified in four recessive neurological mouse mutants, and named according to their phenotype, include *tottering (cacna1a^{tg})*, *leaner*

(cacna1a$^{tg\text{-}1a}$), *rolling Nagoya (cacna1a$^{tg\text{-}rol}$)*, and *rocker (cacna1a^{rkr})* (Fletcher et al., 1996; Burgess and Noebels, 1999; Mori et al., 2000; Zwingman et al., 2001). The *tottering*, *rolling*, and *rocker* phenotypes arise from 3 different missense mutations: *tottering* is caused by a mutation in the DII S5-S6 linker (P601L), *rocker* is caused by a mutation in the DIII S5-S6 linker (T1310K), and *rolling* is caused by a substitution of a neutral glycine for a conserved positively charged arginine (R1262G) in the DIII S4 voltage-sensor. The *leaner* phenotype is caused by a splice-site mutation producing a frameshift leading to $Ca_v2.1$ splice products with abnormal C-terminal sequences. Homozygous *tottering*, *leaner*, and *rocker* mice exhibit intermittent seizures (similar to human absence epilepsy) and various levels of ataxia. Mice exhibiting the *leaner* phenotype have more pronounced ataxic symptoms as well as immune system deficiencies (Burgess et al., 1999).

Another mouse neurological disorder has been attributed to the voltage-gated Ca^{2+} channel β_4 subunit. The *lethargic (cacnb4^{lh})* phenotype is similar to that of *tottering* but with more pronounced ataxia and immune system deficiencies (Burgess et al., 1999a). Mutations in the mouse cacnb4 gene lead to premature truncations of the β_4 subunit. The β_4 subunit is thought to primarily be expressed with $Ca_v2.1$ and $Ca_v2.2$ channels in pres-ynaptic terminals. Studies have demonstrated an increase in expression of the β_{1b} subunit in forebrain and cerebellum in lethargic mutants and an increase of β_{1b} and β_3 association with $Ca_v2.1$ and $Ca_v2.2$ channels in mouse pre-synaptic nerve terminals indicating that increased expression of other β subunit subtypes may compensate for the loss of a functional β_4 subunit. (Burgess et al., 1999b; McEnery et al., 1998). Studies comparing the wild type (wt) and *lethargic* $Ca_v2.1$ mouse channels in Purkinje cells demonstrate

similar voltage-dependent properties as well as synaptic transmission and pharmacological profiles in pre-synaptic Ca^{2+} influx in CA3-CA1 synapses in wt and lethargic hippocampal slices (Burgess et al., 1999b; Qian and Noebels, 2000).

References

Bangalore R, Mehrke G, Gingrich K, Hofmann F, Kass RS (1996) Influence of L-type Ca channel alpha 2/delta-subunit on ionic and gating current in transiently transfected HEK 293 cells. Am J Physiol. 270:H1521-528.

Bean BP (1989) Neurotransmitter inhibition of neuronal calcium currents by changes in channel voltage dependence. Nature. 340:153-156.

Bech-Hansen NT, Naylor MJ, Maybaum TA, Pearce WG, Koop B, Fishman GA, Mets M, Musarella MA, Boycott KM (1998) Loss-of-function mutations in a calcium-channel alpha1-subunit gene in Xp11.23 cause incomplete X-linked congenital stationary night blindness. Nat Genet. 19:264-267.

Bezanilla F (2000) The voltage sensor in voltage-dependent ion channels. Physiol Rev. 80:555-592.

Bezprozvanny I, Scheller RH, Tsien RW (1995) Functional impact of syntaxin on gating of N-type and Q-type calcium channels. Nature. 378:623-626.

Birnbaumer L, Qin N, Olcese R, Tareilus E, Platano D, Costantin J, Stefani E (1998) Structures and functions of calcium channel beta subunits. J Bioenerg Biomembr. 30:357-375.

Bollmann JH, Sakmann B, Borst JG (2000) Calcium sensitivity of glutamate release in a calyx-type terminal. Science. 289:953-957.

Blasi J, Chapman ER, Yamasaki S, Binz T, Niemann H, Jahn R (1993) Botulinum neurotoxin C1 blocks neurotransmitter release by means of cleaving HPC-1/syntaxin. EMBO J. 12:4821-4828.

Bourinet E, Soong TW, Sutton K, Slaymaker S, Mathews E, Monteil A, Zamponi GW, Nargeot J, Snutch TP (1999) Splicing of alpha 1A subunit gene generates phenotypic variants of P- and Q-type calcium channels. Nat Neurosci. 2:407-415.

Bowersox SS, Luther R (1998) Pharmacotherapeutic potential of omega-conotoxin MVIIA (SNX-111), an N-type neuronal calcium channel blocker found in the venom of Conus magus. Toxicon. 36:1651-1658.

Broadie K, Prokop A, Bellen HJ, O'Kane CJ, Schulze KL, Sweeney ST (1995) Syntaxin and synaptobrevin function downstream of vesicle docking in Drosophila. Neuron. 15:663-673.

Brose N, Petrenko AG, Südhof TC, Jahn R (1992) Synaptotagmin: a calcium sensor on the synaptic vesicle surface. Science. 256:1021-1025.

Burgess DL, Biddlecome GH, McDonough SI, Diaz ME, Zilinski CA, Bean BP, Campbell KP, Noebels JL (1999b) Beta subunit reshuffling modifies N- and P/Q-type Ca2+ channel subunit compositions in lethargic mouse brain. Mol Cell Neurosci. 13:293-311.

Burgess DL, Noebels JL (1999) Single gene defects in mice: the role of voltage-dependent calcium channels in absence models. Epilepsy Res. 36:111-122.

Carbone E, Lux HD (1984) A low voltage-activated, fully inactivating Ca channel in vertebrate sensory neurones. Nature.;310:501-502.

Castellano A, Wei X, Birnbaumer L, Perez-Reyes E (1993a) Cloning and expression of a neuronal calcium channel beta subunit. J Biol Chem. 268:12359-12366.

Castellano A, Wei X, Birnbaumer L, Perez-Reyes E (1993b) Cloning and expression of a third calcium channel beta subunit. J Biol Chem. 268:3450-3455.

Catterall WA, Seagar MJ, Takahashi M (1988) Molecular properties of dihydropyridine-sensitive calcium channels in skeletal muscle. J Biol Chem. 263:3535-3538.

Catterall WA (1996) Molecular properties of sodium and calcium channels. J Bioenerg Biomembr. 28:219-230.

Catterall WA (2000) Structure and regulation of voltage-gated Ca2+ channels. Annu Rev Cell Dev Biol.
16:521-555.

Chapman ER, Hanson PI, An S, Jahn R (1995) Ca2+ regulates the interaction between synaptotagmin and syntaxin 1. J Biol Chem. 270:23667-23671.

Charvin N, L'eveque C, Walker D, Berton F, Raymond C, Kataoka M, Shoji-Kasai Y, Takahashi M, De Waard M, Seagar MJ (1997) Direct interaction of the calcium sensor protein synaptotagmin I with a cytoplasmic domain of the alpha1A subunit of the P/Q-type calcium channel. EMBO J. 16:4591-4596.

Chu PJ, Robertson HM, Best PM (2001) Calcium channel gamma subunits provide insights into the evolution of this gene family. Gene. 280:37-48.

Curtis BM, Catterall WA (1984) Purification of the calcium antagonist receptor of the voltage-sensitive calcium channel from skeletal muscle transverse tubules. Biochemistry. 23:2113-2118.

De Jongh KS, Murphy BJ, Colvin AA, Hell JW, Takahashi M, Catterall WA (1996) Specific phosphorylation of a site in the full-length form of the alpha 1 subunit of the cardiac L-type calcium channel by adenosine 3',5'-cyclic monophosphate-dependent protein kinase. Biochemistry. 35:10392-10402.

De Waard M, Campbell KP (1995) Subunit regulation of the neuronal alpha 1A Ca2+ channel expressed in Xenopus oocytes. J Physiol. 485:619-634.

De Waard M, Liu H, Walker D, Scott VE, Gurnett CA, Campbell KP (1997) Direct binding of G-protein betagamma complex to voltage-dependent calcium channels. Nature. 385:446-450.

De Waard M, Scott VE, Pragnell M, Campbell KP (1996) Identification of critical amino acids involved in alpha1-beta interaction in voltage-dependent Ca2+ channels. FEBS Lett. 380:272-276.

Denier C, Ducros A, Vahedi K, Joutel A, Thierry P, Ritz A, Castelnovo G, Deonna T, Gerard P, Devoize JL, Gayou A, Perrouty B, Soisson T, Autret A, Warter JM, Vighetto A, Van Bogaert P, Alamowitch S, Roullet E, Tournier-Lasserve E (1999) High prevalence of CACNA1A truncations and broader clinical spectrum in episodic ataxia type 2. Neurology. 52:1816-1821.

Dimitratos SD, Woods DF, Stathakis DG, Bryant PJ (1999) Signaling pathways are focused at specialized regions of the plasma membrane by scaffolding proteins of the MAGUK family. Bioessays. 21:912-921.

Dunlap K, Luebke JI, Turner TJ (1995) Exocytotic Ca2+ channels in mammalian central neurons. Trends Neurosci. 18:89-98.

Durell SR, Hao Y, Guy HR (1998) Structural models of the transmembrane region of voltage-gated and other K+ channels in open, closed, and inactivated conformations. J Struct Biol. 121:263-284.

Ellinor PT, Zhang JF, Randall AD, Zhou M, Schwarz TL, Tsien RW, Horne WA (1993) Functional expression of a rapidly inactivating neuronal calcium channel. Nature. 363:455-458.

Ertel EA, Campbell KP, Harpold MM, Hofmann F, Mori Y, Perez-Reyes E, Schwartz A, Snutch TP, Tanabe T, Birnbaumer L, Tsien RW, Catterall WA (2000) Nomenclature of voltage-gated calcium channels. Neuron. 25:533-535.

Escayg A, De Waard M, Lee DD, Bichet D, Wolf P, Mayer T, Johnston J, Baloh R, Sander T, Meisler MH (2000) Coding and noncoding variation of the human calcium-channel beta4-subunit gene CACNB4 in patients with idiopathic generalized epilepsy and episodic ataxia. Am J Hum Genet. 66:1531-1539.

Felix R, Gurnett CA, De Waard M, Campbell KP (1997) Dissection of functional domains of the voltage-dependent Ca2+ channel alpha2delta subunit. J Neurosci. 17:6884-6891.

Felix R (1999) Voltage-dependent Ca2+ channel alpha2delta auxiliary subunit: structure, function and regulation. Receptors Channels. 6:351-362.

Fitzgerald EM (2000) Regulation of voltage-dependent calcium channels in rat sensory neurones involves a Ras-mitogen-activated protein kinase pathway. J Physiol. 527:433-444.

Fisher TE, Bourque CW (2001) The function of Ca(2+) channel subtypes in exocytotic secretion: new
perspectives from synaptic and non-synaptic release. Prog Biophys Mol Biol. 77:269-303.

Flockerzi V, Oeken HJ, Hofmann F, Pelzer D, Cavalie A, Trautwein W (1986) Purified dihydropyridine-binding site from skeletal muscle t-tubules is a functional calcium channel. Nature. 323:66-68.

Fossier P, Tauc L, Baux G (1999) Calcium transients and neurotransmitter release at an identified synapse. Trends Neurosci. 22:161-166.

Freise D, Held B, Wissenbach U, Pfeifer A, Trost C, Himmerkus N, Schweig U, Freichel M, Biel M, Hofmann F, Hoth M, Flockerzi V (2000) Absence of the gamma subunit of the skeletal muscle dihydropyridine receptor increases L-typeCa2+ currents and alters channel inactivation properties. J Biol Chem. 275:14476-14481.

Friend KL, Crimmins D, Phan TG, Sue CM, Colley A, Fung VS, Morris JG, Sutherland GR, Richards RI (1999) Detection of a novel missense mutation and second recurrent mutation in the CACNA1A gene in individuals with EA-2 and FHM. Hum Genet. 105:261-265.

Gasparini S, Kasyanov AM, Pietrobon D, Voronin LL, Cherubini E (2001) Presynaptic R-type calcium channels contribute to fast excitatory synaptic transmission in the rat hippocampus. J Neurosci. 21:8715-8721.

Gregg RG, Powers PA, Hogan K (1993) Assignment of the human gene for the beta subunit of the voltage-dependent calcium channel (CACNLB1) to chromosome 17 using somatic cell hybrids and linkage mapping. Genomics. 15:185-187.

Haack JA, Rosenberg RL (1994) Calcium-dependent inactivation of L-type calcium channels in planar lipid bilayers. Biophys J. 66:1051-1060.

Hanlon MR, Berrow NS, Dolphin AC, Wallace BA (1999) Modelling of a voltage-dependent Ca2+ channel beta subunit as a basis for understanding its functional properties. FEBS Lett. 445:366-370.

Hanlon MR, Wallace BA (2002) Structure and function of voltage-dependent ion channel regulatory beta subunits. Biochemistry. 2002 41:2886-2894.

Hans M, Luvisetto S, Williams ME, Spagnolo M, Urrutia A, Tottene A, Brust PF, Johnson EC, Harpold MM, Stauderman KA, Pietrobon D (1999) Functional consequences of mutations in the human alpha1A calcium channel subunit linked to familial hemiplegic migraine. J Neurosci. 19:1610-1619.

Hayashi T, McMahon H, Yamasaki S, Binz T, Hata Y, Sudhof TC, Niemann H (1994) Synaptic vesicle membrane fusion complex: action of clostridial neurotoxins on assembly. EMBO J. 13:5051-5061.

Heinemann SH, Terlau H, Stuhmer W, Imoto K, Numa S (1992) Calcium channel characteristics conferred on the sodium channel by single mutations. Nature. 356:441-443.

Helton TD, Horne WA (2002) Alternative splicing of the beta 4 subunit has alpha1 subunit subtype-specific effects on Ca2+ channel gating. J Neurosci. 22:1573-1582.

Herlitze S, Garcia DE, Mackie K, Hille B, Scheuer T, Catterall WA (1996) Modulation of Ca2+ channels by G-protein beta gamma subunits. Nature. 380:258-262.

Herlitze S, Hockerman GH, Scheuer T, Catterall WA (1997) Molecular determinants of inactivation and G protein modulation in the intracellular loop connecting domains I and II of the calcium channel alpha1A subunit. Proc Natl Acad Sci U S A. 94:1512-1516.

Hille B (1994) Modulation of ion-channel function by G-protein-coupled receptors. Trends Neurosci. 17:531-536.

Hobom M, Dai S, Marais E, Lacinova L, Hofmann F, Klugbauer N (2000) Neuronal distribution and functional characterization of the calcium channel alpha2delta-2 subunit. Eur J Neurosci. 12:1217-1226.

Ikeda SR, Dunlap K (1999) Voltage-dependent modulation of N-type calcium channels: role of G protein subunits. Adv Second Messenger Phosphoprotein Res. 33:131-151.

Ishikawa K, Fujigasaki H, Saegusa H, Ohwada K, Fujita T, Iwamoto H, Komatsuzaki Y, Toru S, Toriyama H, Watanabe M, Ohkoshi N, Shoji S, Kanazawa I, Tanabe T, Mizusawa H. (1999)Abundant expression and cytoplasmic aggregations of [alpha]1A voltage-dependent calcium channel protein associated with neurodegeneration in spinocerebellar ataxia type 6. Hum Mol Genet. 8:1185-1193.

Jain KK. (2000) An evaluation of intrathecal ziconotide for the treatment of chronic pain. Expert Opin Investig Drugs. 9:2403-2410.

Jones SW, Elmslie KS (1997) Transmitter modulation of neuronal calcium channels. J Membr Biol. 155:1-10.

Jones SW (1998) Overview of voltage-dependent calcium channels. J Bioenerg Biomembr. 30(4):299-312.

Kang MG, Chen CC, Felix R, Letts VA, Frankel WN, Mori Y, Campbell KP (2001) Biochemical and biophysical evidence for gamma 2 subunit association with neuronal voltage-activated Ca2+ channels. J Biol Chem. 276:32917-32924.

Kee Y, Scheller RH (1996) Localization of synaptotagmin-binding domains on syntaxin. J Neurosci. 16:1975-1981.

Kim DK, Catterall WA (1997) Ca2+-dependent and -independent interactions of the isoforms of the alpha1A subunit of brain Ca2+ channels with presynaptic SNARE proteins. Proc Natl Acad Sci U S A. 94(26):14782-14786.

Klugbauer N, Lacinova L, Marais E, Hobom M, Hofmann F (1999) Molecular diversity of the calcium channel alpha2delta subunit. J Neurosci. 19:684-691.

Lacerda AE, Kim HS, Ruth P, Perez-Reyes E, Flockerzi V, Hofmann F, Birnbaumer L, Brown AM (1991) Normalization of current kinetics by interaction between the alpha 1 and beta subunits of the skeletal muscle dihydropyridine-sensitive Ca2+ channel. Nature. 352:527-530.

Lee A, Scheuer T, Catterall WA (2000) Ca2+/calmodulin-dependent facilitation and inactivation of P/Q-type Ca2+ channels. J Neurosci. 20:6830-6838.

Lee A, Wong ST, Gallagher D, Li B, Storm DR, Scheuer T, Catterall WA. Ca2+/calmodulin binds to and modulates P/Q-type calcium channels. Nature. 399:155-159.

Letts VA, Felix R, Biddlecome GH, Arikkath J, Mahaffey CL, Valenzuela A, Bartlett FS 2nd, Mori Y, Campbell KP, Frankel WN (1998) The mouse stargazer gene encodes a neuronal Ca2+-channel gamma subunit. Nat Genet. 19:340-347.

Leung AT, Imagawa T, Block B, Franzini-Armstrong C, Campbell KP (1988) Biochemical and ultrastructural characterization of the 1,4-dihydropyridine receptor from rabbit skeletal muscle. Evidence for a 52,000 Da subunit. J Biol Chem. 263:994-1001.

Lipkind GM, Fozzard HA (2001) Modeling of the outer vestibule and selectivity filter of the L-type Ca2+ channel. Biochemistry. 40:6786-6794.

Liu H, De Waard M, Scott VE, Gurnett CA, Lennon VA, Campbell KP (1996) Identification of three subunits of the high affinity omega-conotoxin MVIIC-sensitive Ca2+ channel. J Biol Chem. 271:13804-13810.

Llinas RR, Sugimori M, Cherksey B (1989) Voltage-dependent calcium conductances in mammalian neurons. The P channel. Ann N Y Acad Sci. 560:103-111.

Ludwig A, Flockerzi V, Hofmann F (1997) Regional expression and cellular localization of the alpha1 and beta subunit of high voltage-activated calcium channels in rat brain. J Neurosci. 17:1339-1349.

Luebke JI, Dunlap K, Turner TJ (1993) Multiple calcium channel types control glutamatergic synaptic transmission in the hippocampus. Neuron. 11:895-902.

Matsuyama Z, Wakamori M, Mori Y, Kawakami H, Nakamura S, Imoto K (1999) Direct alteration of the P/Q-type Ca2+ channel property by polyglutamine expansion in spinocerebellar ataxia 6. J Neurosci. 19:RC14.

McEnery MW, Copeland TD, Vance CL (1998) Altered expression and assembly of N-type calcium channel alpha1B and beta subunits in epileptic lethargic (lh/lh) mouse. J Biol Chem. 273:21435-21438.

McHugh D, Sharp EM, Scheuer T, Catterall WA (2000) Inhibition of cardiac L-type calcium channels by protein kinase C phosphorylation of two sites in the N-terminal domain. Proc Natl Acad Sci U S A. 97:12334-12338.

Mintz IM, Bean BP (1993) GABAB receptor inhibition of P-type Ca2+ channels in central neurons. Neuron. 10:889-898.

Mintz IM, Venema VJ, Swiderek KM, Lee TD, Bean BP, Adams ME (1992) P-type calcium channels blocked by the spider toxin omega-Aga-IVA. Nature. 355:827-829.

Mitterdorfer J, Grabner M, Kraus RL, Hering S, Prinz H, Glossmann H, Striessnig J (1998) Molecular basis of drug interaction with L-type Ca2+ channels. J Bioenerg Biomembr. 30:319-334.

Moreno H, Rudy B, Llinas R (1997) Beta subunits influence the biophysical and pharmacological differences between P- and Q-type calcium currents expressed in a mammalian cell line. Proc Natl Acad Sci U S A. 94:14042-14047.

Morgans CW (2001) Localization of the alpha(1F) calcium channel subunit in the rat retina. Invest Ophthalmol Vis.Sci. 42:2414-2418.

Mori Y, Wakamori M, Oda S, Fletcher CF, Sekiguchi N, Mori E, Copeland NG, Jenkins NA, Matsushita K, Matsuyama Z, Imoto K (2000) Reduced voltage sensitivity of activation of P/Q-type Ca2+ channels is associated with the ataxic mouse mutation rolling Nagoya (tg(rol)). J Neurosci. 20:5654-5662.

Nakamura M, Ito S, Terasaki H, Miyake Y (2001) Novel CACNA1F mutations in Japanese patients with incomplete congenital stationary night blindness. Invest Ophthalmol Vis Sci. 42:1610-166.

Neher E (1998) Vesicle pools and Ca2+ microdomains: new tools for understanding their roles in neurotransmitter release. Neuron. 20:389-399.

Nilius B, Hess P, Lansman JB, Tsien RW (1985) A novel type of cardiac calcium channel in ventricular cells. Nature. 316:443-446.

Nowycky MC, Fox AP, Tsien RW (1985) Three types of neuronal calcium channel with different calcium agonist sensitivity. Nature. 316:440-443.

Olcese R, Qin N, Schneider T, Neely A, Wei X, Stefani E, Birnbaumer L (1994) The amino terminus of a calcium channel beta subunit sets rates of channel inactivation independently of the subunit's effect on activation. Neuron. 13:1433-1438.

Ophoff RA, Terwindt GM, Frants RR, Ferrari MD (1998) P/Q-type Ca2+ channel defects in migraine, ataxia and epilepsy. Trends Pharmacol Sci. 19:121-127.

Ophoff RA, Terwindt GM, Vergouwe MN, van Eijk R, Oefner PJ, Hoffman SM, Lamerdin JE, Mohrenweiser HW, Bulman DE, Ferrari M, Haan J, Lindhout D, van Ommen GJ, Hofker MH, Ferrari MD, Frants RR (1996) Familial hemiplegic migraine and episodic ataxia type-2 are caused by mutations in the Ca2+ channel gene CACNL1A4. Cell. 87:543-552.

Pan JQ, Lipscombe D (2000) Alternative splicing in the cytoplasmic II-III loop of the N-type Ca channel alpha 1B subunit: functional differences are beta subunit-specific. J Neurosci. 20:4769-4775.

Parent L, Gopalakrishnan M (1995) Glutamate substitution in repeat IV alters divalent and monovalent cation permeation in the heart Ca2+ channel. Biophys J. 69:1801-1813.

Park SH, Suh YS, Kim H, Rhyu IJ, Kim HL (1997) Chromosomal localization and neural distribution of voltage dependent calcium channel beta 3 subunit gene. Mol Cells. 7:200-203.

Penn RD, Paice JA (2000) Adverse effects associated with the intrathecal administration of ziconotide. Pain. 85:291-296.

Perez-Reyes E, Castellano A, Kim HS, Bertrand P, Baggstrom E, Lacerda AE, Wei XY, Birnbaumer L (1992) Cloning and expression of a cardiac/brain beta subunit of the L-type calcium channel. J Biol Chem. 267:1792-1797.

Perez-Reyes E, Cribbs LL, Daud A, Lacerda AE, Barclay J, Williamson MP, Fox M, Rees M, Lee JH (1998) Molecular characterization of a neuronal low-voltage-activated T-type calcium channel. Nature. 391:896-900.

Perez-Reyes E, Kim HS, Lacerda AE, Horne W, Wei XY, Rampe D, Campbell KP, Brown AM, Birnbaumer L (1989) Induction of calcium currents by the expression of the alpha 1-subunit of the dihydropyridine receptor from skeletal muscle. Nature. 340:233-236.

Perez-Reyes E (1999) Three for T: molecular analysis of the low voltage-activated calcium channel family. Cell Mol Life Sci. 56:660-669.

Peterson BZ, DeMaria CD, Adelman JP, Yue DT (1999) Calmodulin is the Ca2+ sensor for Ca2+ -dependent inactivation of L-type calcium channels. Neuron. 22:549-558.

Powers PA, Liu S, Hogan K, Gregg RG (1992) Skeletal muscle and brain isoforms of a beta-subunit of human voltage-dependent calcium channels are encoded by a single gene. J Biol Chem. 267:22967-22972.

Pragnell M, De Waard M, Mori Y, Tanabe T, Snutch TP, Campbell KP (1994) Calcium channel beta-subunit binds to a conserved motif in the I-II cytoplasmic linker of the alpha 1-subunit. Nature. 368:67-70.

Qian J, Noebels JL (2000) Presynaptic Ca(2+) influx at a mouse central synapse with Ca(2+) channel subunit mutations. J Neurosci. 20:163-170.

Qin N, Olcese R, Bransby M, Lin T, Birnbaumer L (1999) Ca2+-induced inhibition of the cardiac Ca2+ channel depends on calmodulin. Proc Natl Acad Sci U S A. 96:2435-2438.

Qin N, Olcese R, Zhou J, Cabello OA, Birnbaumer L, Stefani E (1996) Identification of a second region of the beta-subunit involved in regulation of calcium channel inactivation. Am J Physiol. 271:C1539-1545.

Randall A, Tsien RW (1995) Pharmacological dissection of multiple types of Ca2+ channel currents in rat cerebellar granule neurons. J Neurosci. 15:2995-3012.

Rettig J, Sheng ZH, Kim DK, Hodson CD, Snutch TP, Catterall WA (1996) Isoform-specific interaction of the alpha1A subunits of brain Ca2+ channels with the presynaptic proteins syntaxin and SNAP-25. Proc Natl Acad Sci U S A. 93:7363-7368.

Rotman EI, De Jongh KS, Florio V, Lai Y, Catterall WA (1992) Specific phosphorylation of a COOH-terminal site on the full-length form of the alpha 1 subunit of the skeletal muscle calcium channel by cAMP-dependent protein kinase. J Biol Chem. 267:16100-16105.

Rotman EI, Murphy BJ, Catterall WA (1995) Sites of selective cAMP-dependent phosphorylation of the L-type calcium channel alpha 1 subunit from intact rabbit skeletal muscle myotubes. J Biol Chem. 270:16371-16377.

Ruth P, Rohrkasten A, Biel M, Bosse E, Regulla S, Meyer HE, Flockerzi V, Hofmann F (1989) Primary structure of the beta subunit of the DHP-sensitive calcium channel from skeletal muscle. Science. 245:1115-1118.

Sakurai T, Hell JW, Woppmann A, Miljanich GP, Catterall WA (1995) Immunochemical identification and differential phosphorylation of alternatively spliced forms of the alpha 1A subunit of brain calcium channels. J Biol Chem. 270:21234-21242.

Sather WA, Tanabe T, Zhang JF, Mori Y, Adams ME, Tsien RW (1993) Distinctive biophysical and pharmacological properties of class A (BI) calcium channel alpha 1 subunits. Neuron. 11:291-303.

Schiavo G, Shone CC, Bennett MK, Scheller RH, Montecucco C (1995) Botulinum neurotoxin type C cleaves a single Lys-Ala bond within the carboxyl-terminal region of syntaxins. J Biol Chem. 270:10566-10570.

Schneggenburger R, Neher E (2000) Intracellular calcium dependence of transmitter release rates at a fast central synapse. Nature. 406:889-893.

Schulze KL, Broadie K, Perin MS, Bellen HJ (1995) Genetic and electrophysiological studies of Drosophila syntaxin-1A demonstrate its role in nonneuronal secretion and neurotransmission. Cell. 80:311-320.

Seagar M, Takahashi M (1998) Interactions between presynaptic calcium channels and proteins implicated in synaptic vesicle trafficking and exocytosis. J Bioenerg Biomembr. 30:347-356.

Sheng ZH, Rettig J, Takahashi M, Catterall WA (1994) Identification of a syntaxin-binding site on N-type calcium channels. Neuron. 13:1303-1313.

Sheng ZH, Westenbroek RE, Catterall WA (1998) Physical link and functional coupling of presynaptic calcium channels and the synaptic vesicle docking/fusion machinery. J Bioenerg Biomembr. 30:335-345.

Singer D, Biel M, Lotan I, Flockerzi V, Hofmann F, Dascal N (1991) The roles of the subunits in the function of the calcium channel. Science. 253:1553-1557.

Soldatov NM, Oz M, O'Brien KA, Abernethy DR, Morad M (1998) Molecular determinants of L-type Ca2+ channel inactivation. Segment exchange analysis of the carboxyl-terminal cytoplasmic motif encoded by exons 40-42 of the human alpha1C subunit gene. J Biol Chem. 273:957-963.

Soldatov NM, Zuhlke RD, Bouron A, Reuter H (1997) Molecular structures involved in L-type calcium channel inactivation. Role of the carboxyl-terminal region encoded by exons 40-42 in alpha1C subunit in the kinetics and Ca2+ dependence of inactivation. J Biol Chem. 272:3560-3566.

Stea A, Tomlinson WJ, Soong TW, Bourinet E, Dubel SJ, Vincent SR, Snutch TP (1994) Localization and functional properties of a rat brain alpha 1A calcium channel reflect similarities to neuronal Q- and P-type channels. Proc Natl Acad Sci U S A. 91:10576-10580.

Strom TM, Nyakatura G, Apfelstedt-Sylla E, Hellebrand H, Lorenz B, Weber BH, Wutz K, Gutwillinger N, Ruther K, Drescher B, Sauer C, Zrenner E, Meitinger T, Rosenthal A, Meindl A (1998) An L-type calcium-channel gene mutated in incomplete X-linked congenital stationary night blindness. Nat Genet. 19:260-263.

Südhof TC, Rizo J (1996) Synaptotagmins: C2-domain proteins that regulate membrane traffic. Neuron. 17:379-388.

Sutton KG, McRory JE, Guthrie H, Murphy TH, Snutch TP (1999) P/Q-type calcium channels mediate the activity-dependent feedback of syntaxin-1A. Nature. 401:800-804.

Takahashi T, Momiyama A (1993) Different types of calcium channels mediate central synaptic transmission. Nature. 366:156-158.

Tanabe T, Beam KG, Adams BA, Niidome T, Numa S (1990) Regions of the skeletal muscle dihydropyridine receptor critical for excitation-contraction coupling. Nature. 346:567-569.

Tanabe T, Takeshima H, Mikami A, Flockerzi V, Takahashi H, Kangawa K, Kojima M, Matsuo H, Hirose T, Numa S (1987) Primary structure of the receptor for calcium channel blockers from skeletal muscle. Nature. 328:313-318.

Tang S, Mikala G, Bahinski A, Yatani A, Varadi G, Schwartz A (1993) Molecular localization of ion selectivity sites within the pore of a human L-type cardiac calcium channel. J Biol Chem. 268:13026-13029.

Taviaux S, Williams ME, Harpold MM, Nargeot J, Lory P (1997) Assignment of human genes for beta 2 and beta 4 subunits of voltage-dependent Ca2+ channels to chromosomes 10p12 and 2q22-q23. Hum Genet. 100:151-154.

Terwindt GM, Ophoff RA, van Eijk R, Vergouwe MN, Haan J, Frants RR, Sandkuijl LA, Ferrari MD; Dutch Migraine Genetics Research Group. (2001) Involvement of the CACNA1A gene containing region on 19p13 in migraine with and without aura. Neurology. 56:1028-1032.

Timmermann DB, Westenbroek RE, Schousboe A, Catterall WA (2002) Distribution of high-voltage-activated calcium channels in cultured gamma-aminobutyric acidergic neurons from mouse cerebral cortex. J Neurosci Res. 67:48-61.

Tobi D, Wiser O, Trus M, Atlas D (1998) N-type voltage-sensitive calcium channel interacts with syntaxin, synaptotagmin and SNAP-25 in a multiprotein complex. Receptors Channels. 6:89-98.

Tomlinson WJ, Stea A, Bourinet E, Charnet P, Nargeot J, Snutch TP (1993) Functional properties of a neuronal class C L-type calcium channel. Neuropharmacology. 32:1117-1126.

Toru S, Murakoshi T, Ishikawa K, Saegusa H, Fujigasaki H, Uchihara T, Nagayama S, Osanai M, Mizusawa H, Tanabe T (2000) Spinocerebellar ataxia type 6 mutation alters P-type calcium channel function. J Biol Chem. 275:10893-10898.

Turner TJ, Dunlap K (1995) Pharmacological characterization of presynaptic calcium channels using subsecond biochemical measurements of synaptosomal neurosecretion. Neuropharmacology. 34:1469-1478.

Walker D, Bichet D, Campbell KP, De Waard M (1998) A beta 4 isoform-specific interaction site in the carboxyl-terminal region of the voltage-dependent Ca2+ channel alpha 1A subunit. J Biol Chem. 273:2361-2367.

Walker D, Bichet D, Geib S, Mori E, Cornet V, Snutch TP, Mori Y, De Waard M (1999) A new beta subtype-specific interaction in alpha1A subunit controls P/Q-type Ca2+ channel activation. J Biol Chem. 274:12383-12390.

Walker D, De Waard M (1998) Subunit interaction sites in voltage-dependent Ca2+ channels: role in channel function. Trends Neurosci. 21:148-154.

Welling A, Bosse E, Cavalie A, Bottlender R, Ludwig A, Nastainczyk W, Flockerzi V, Hofmann F (1993) Stable co-expression of calcium channel alpha 1, beta and alpha 2/delta subunits in a somatic cell line. J Physiol. 471:749-765.

Westenbroek RE, Hell JW, Warner C, Dubel SJ, Snutch TP, Catterall WA (1992) Biochemical properties and subcellular distribution of an N-type calcium channel alpha 1 subunit. Neuron. 9:1099-1115.

Wheeler DB, Randall A, Tsien RW (1994) Roles of N-type and Q-type Ca2+ channels in supporting hippocampal synaptic transmission. Science. 264:107-111.

Wiser O, Tobi D, Trus M, Atlas D (1997) Synaptotagmin restores kinetic properties of a syntaxin-associated N-type voltage sensitive calcium channel. FEBS Lett. 404:203-207.

Wittemann S, Mark MD, Rettig J, Herlitze S (2000) Synaptic localization and presynaptic function of calcium channel beta 4-subunits in cultured hippocampal neurons. J Biol Chem. 275:37807-37814.

Wong W, Newell EW, Jugloff DG, Jones OT, Schlichter LC (2002) Cell surface targeting and clustering interactions between heterologously expressed PSD-95 and the Shal voltage-gated potassium channel, Kv4.2. J Biol Chem. 277:20423-20430.

Wu LG, Saggau P. Block of multiple presynaptic calcium channel types by omega-conotoxin-MVIIC at hippocampal CA3 to CA1 synapses. J Neurophysiol. 1995 May;73(5):1965-72.

Wu MN, Fergestad T, Lloyd TE, He Y, Broadie K, Bellen HJ (1999) Syntaxin 1A interacts with multiple exocytic proteins to regulate neurotransmitter release in vivo. Neuron. 23:593-605.

Wu MN, Littleton JT, Bhat MA, Prokop A, Bellen HJ (1998) ROP, the Drosophila Sec1 homolog, interacts with syntaxin and regulates neurotransmitter release in a dosage-dependent manner. EMBO J. 17:127-139.

Xu W, Lipscombe D (2001) Neuronal Ca(V)1.3alpha(1) L-type channels activate at relatively hyperpolarized membrane potentials and are incompletely inhibited by dihydropyridines. J Neurosci. 21:5944-5951.

Yamaguchi H, Hara M, Strobeck M, Fukasawa K, Schwartz A, Varadi G (1998) Multiple modulation pathways of calcium channel activity by a beta subunit. Direct evidence of beta subunit participation in membrane trafficking of the alpha1C subunit. J Biol Chem. 273:19348-19356.

Yang J, Ellinor PT, Sather WA, Zhang JF, Tsien RW (1993) Molecular determinants of Ca2+ selectivity and ion permeation in L-type Ca2+ channels. Nature. 366:158-161.

Yokoyama CT, Westenbroek RE, Hell JW, Soong TW, Snutch TP, Catterall WA (1995) Biochemical properties and subcellular distribution of the neuronal class E calcium channel alpha 1 subunit. J Neurosci. 15:6419-6432.

Yue Q, Jen JC, Nelson SF, Baloh RW (1997) Progressive ataxia due to a missense mutation in a calcium-channel gene. Am J Hum Genet. 61:1078-1087.

Zamponi GW, Bourinet E, Nelson D, Nargeot J, Snutch TP (1997) Crosstalk between G proteins and protein kinase C mediated by the calcium channel alpha1 subunit. Nature. 385:442-446.

Zhang JF, Randall AD, Ellinor PT, Horne WA, Sather WA, Tanabe T, Schwarz TL, Tsien RW (1993) Distinctive pharmacology and kinetics of cloned neuronal Ca2+ channels and their possible counterparts in mammalian CNS neurons. Neuropharmacology. 32:1075-1088.

Zheng X, Bobich JA (1998) A sequential view of neurotransmitter release. Brain Res Bull. 47:117-128.

Zhong H, Yokoyama CT, Scheuer T, Catterall WA (1999) Reciprocal regulation of P/Q-type Ca2+ channels by SNAP-25, syntaxin and synaptotagmin. Nat Neurosci. 2:939-941.

Zhuchenko O, Bailey J, Bonnen P, Ashizawa T, Stockton DW, Amos C, Dobyns WB, Subramony SH, Zoghbi HY, Lee CC (1997) Autosomal dominant cerebellar ataxia (SCA6) associated with small polyglutamine expansions in the alpha 1A-voltage-dependent calcium channel. Nat Genet. 15:62-69.

Zuhlke RD, Pitt GS, Deisseroth K, Tsien RW, Reuter H (1999) Calmodulin supports both inactivation and facilitation of L-type calcium channels. Nature. 399:159-162.

Zuhlke RD, Reuter H (1998) Ca2+-sensitive inactivation of L-type Ca2+ channels depends on multiple cytoplasmic amino acid sequences of the alpha1C subunit. Proc Natl Acad Sci U S A. 95:3287-3294.

Zwingman TA, Neumann PE, Noebels JL, Herrup K (2001) Rocker is a new variant of the voltage-dependent calcium channel gene Cacna1a. J Neurosci. 21:1169-1178.

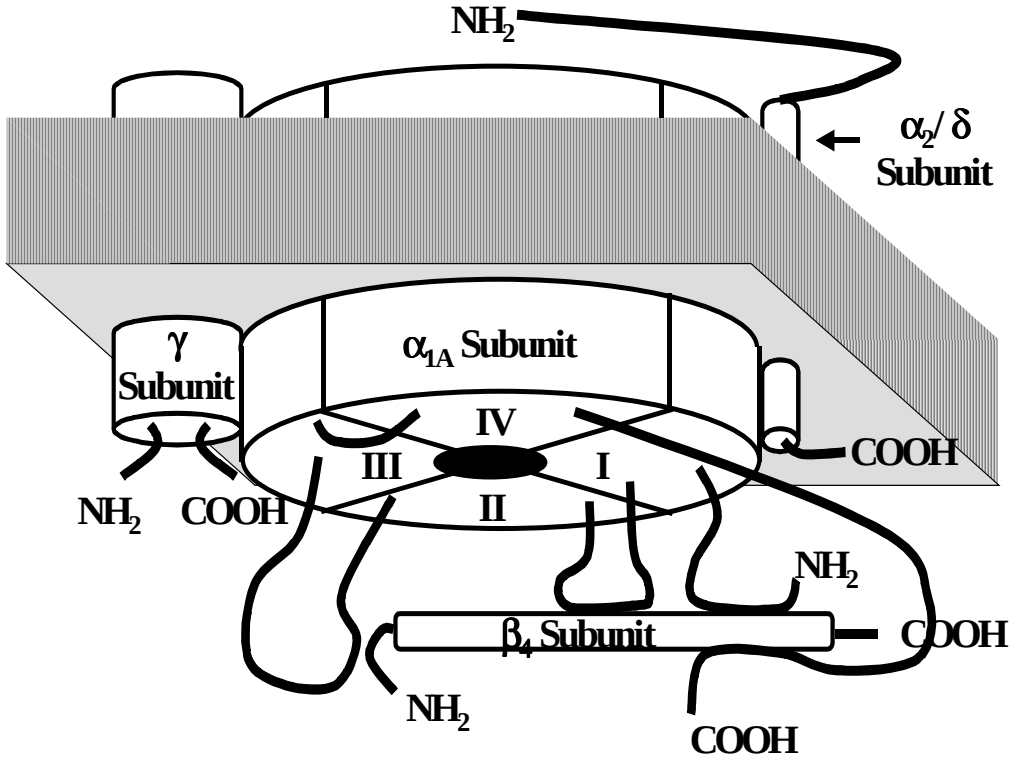

Figure 1.1. Voltage-gated Ca^{2+} channel α_{1A}, α_2/δ, β_4, and γ, subunits.

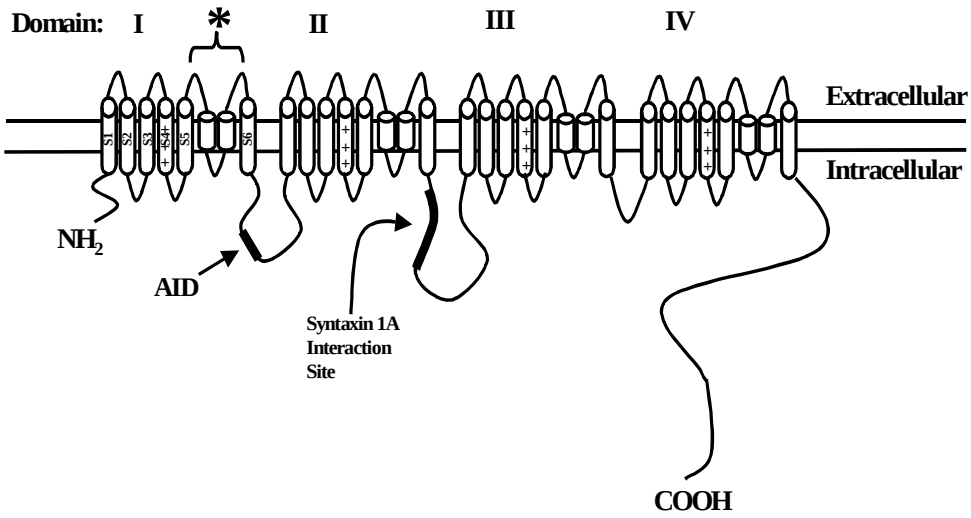

Figure 1.2. Membrane topology of the α_{1A} subunit of voltage-gated calcium channel. The alpha interaction domain (AID) located at amino acids 383-400 on the I-II linker and the syntaxin 1A interaction site at amino acids 722-1036 on the II-III linker are also depicted. The * represents 1 of 4 pore-forming regions of the channel. Transmembrane segment S4 is the putative voltage sensor for voltage-gated calcium channels.

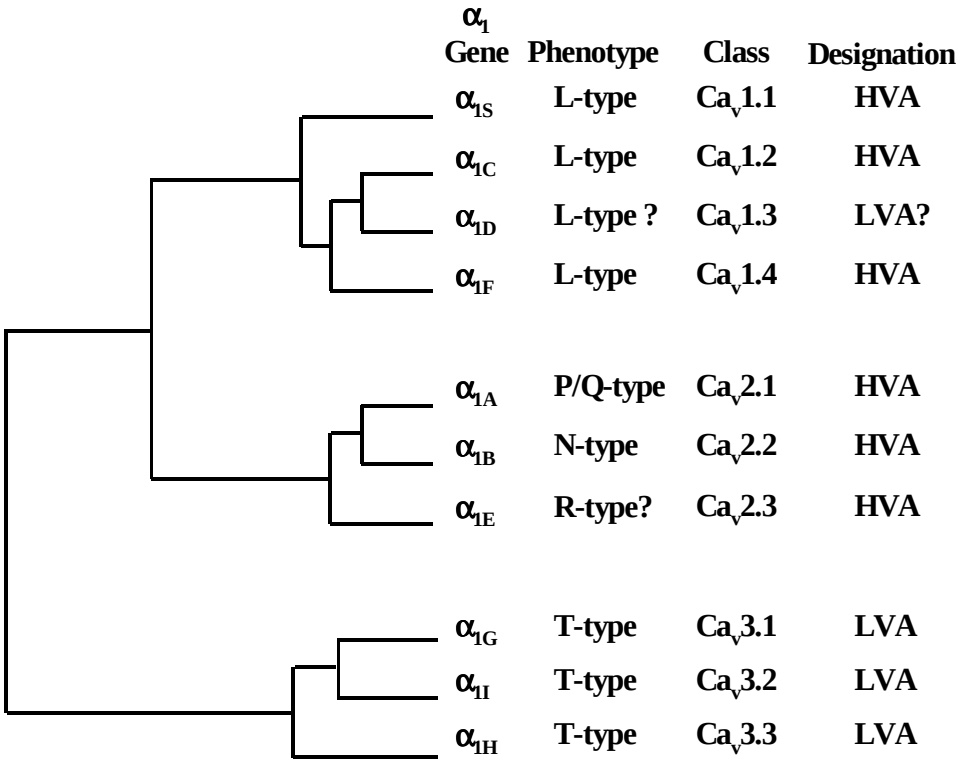

Figure 1.3. Phylogenetic tree representing the Ca^{2+} channel α_1 subunit genes and corresponding phenotypes, classes and designations. Phylogenetic tree is based on amino acid alignments of transmembrane spanning S1-S6 segments of each class. HVA= high voltage-activated, LVA= low voltage-activated. (Perez-Reyes, 1999).

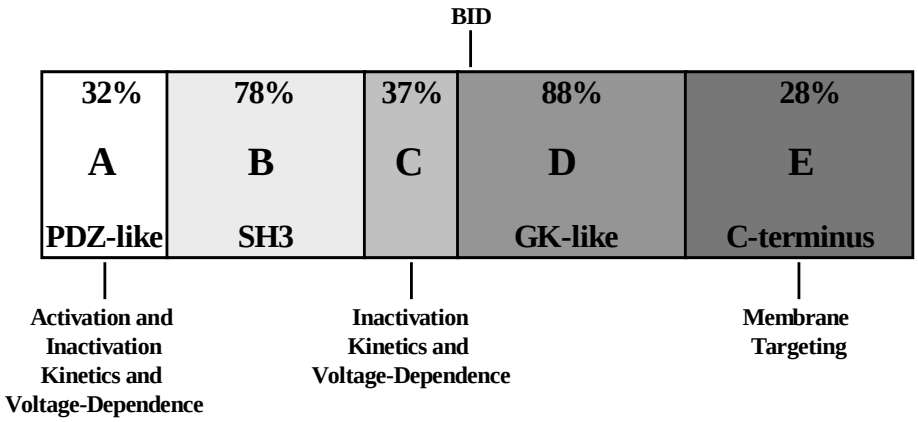

Figure 1.4. Schematic map showing key domain structural and functional features of the Ca^{2+} channel β subunit. Percentages represent amino acid identities between human β subunit isoforms. Putative structural domains are indicated with phenotypic effects on channel activity. A-E represent homology domains. BID= β interaction domain. (Hanlon *et al.*, 2002).

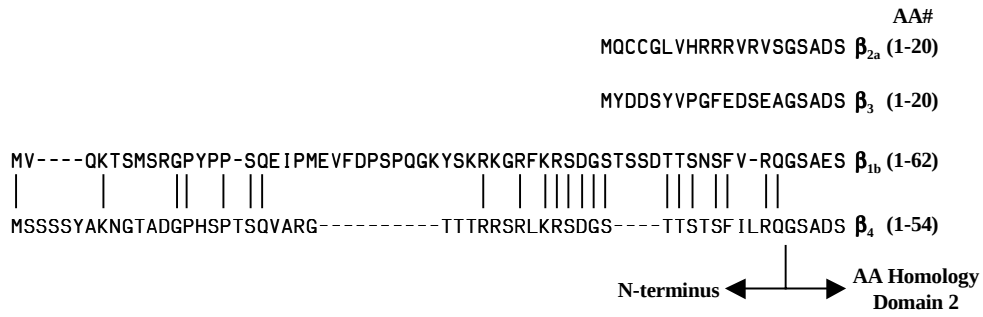

Figure 1.5. Amino (N-) terminal alignment of human β subunits. Two short N-termini (β_{2a} and β_3 are evolutionarily unrelated althought they are identical in length (15 amino acids). β_{1b} and β_4 have longer N-termini (62 and 54 amino acids, respectively) and demonstrate a 44% identity between subunits. AA=amino acid.

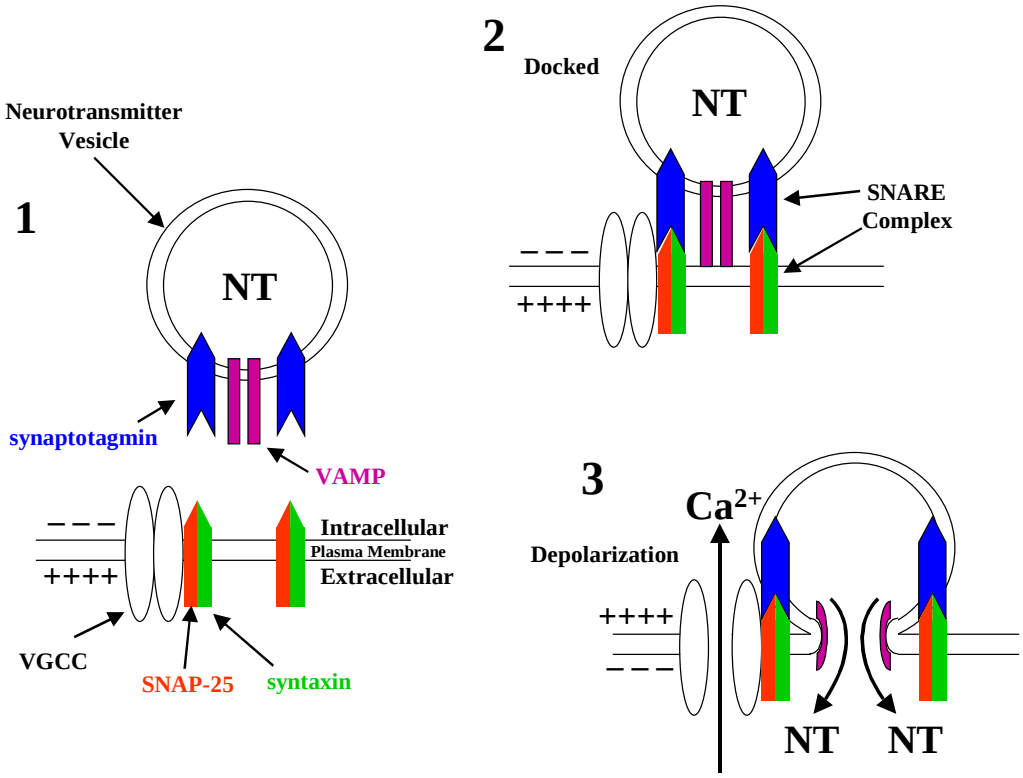

Figure 1.6. SNARE hypothesis for neurotransmitter release. 1. Components of SNARE complex. 2. Docking of neurotransmitter vesicle at pre-synaptic membrane via SNARE complex interactions. 3. Ca^{2+} dependent vesicle fusion with pre-synaptic membrane in response to membrane depolarization.

Chapter 2

C-TERMINAL ALTERNATIVE SPLICING CHANGES THE GATING PROPERTIES OF A HUMAN SPINAL CORD CALCIUM CHANNEL ALPHA1A SUBUNIT

Abstract

The calcium channel α_{1A} subunit gene codes for proteins with diverse structure and function. This diversity may be important for fine tuning neurotransmitter release at central and peripheral synapses. The α_{1A} C-terminus, which serves a critical role in processing information from intracellular signaling molecules, is capable of undergoing extensive alternative splicing. The purpose of this study was to determine the extent to which C-terminal alternative splicing affects some of the fundamental biophysical properties of α_{1A} subunits. Specifically, the biophysical properties of two alternatively spliced α_{1A} subunits were compared. One variant was identical to an isoform identified previously in human brain, and the other was a novel isoform isolated from human spinal cord. The variants differed by two amino acids (NP) in the extracellular linker between transmembrane segments IVS3 and IVS4, and in two C-terminal regions encoded by exons 37 and 44. Expression in *Xenopus* oocytes demonstrated that the two variants were similar with respect to current-voltage relationships and the voltage-dependence of steady-state activation and inactivation. However, the rates of activation, inactivation, deactivation, and recovery from inactivation were all significantly slower for the spinal cord variant. A chimeric strategy demonstrated that the inclusion of the sequence encoded by exon 44 specifically affects the rate of inactivation. These findings

demonstrate that C-terminal structural changes alone can influence the way in which α_{1A} subunits respond to a depolarizing stimulus, and add to the developing picture of the C-terminus as a critical domain in the regulation of Ca^{2+} channel function.

Introduction

Multiple types of high voltage-activated Ca^{2+} channels (L, N, P, Q, and R) coordinate a variety of Ca^{2+}-dependent processes, including gene expression, signal propagation, and neurotransmitter release (Tsien et al., 1991; Zhang et al., 1993; Dunlap et al., 1995). These channels can be distinguished by their biophysical and pharmacological properties. L- and R-type channels, found on cell bodies and proximal dendrites, regulate gene transcription and signal propagation (Westenbroek et al., 1990; Murphy et al., 1991; Yokoyama et al., 1995), while synaptic N-, P- and Q-type channels regulate neurotransmitter release (Turner et al., 1992; Takahashi and Momiyama, 1993; Wheeler et al., 1994). The Ca^{2+} channel complex consists of four subunits, α_1, α_2/δ, β and γ. With the exception of P- and Q- type channels, the different neuronal Ca^{2+} channel phenotypes arise primarily from the expression of five unique α_1 subunit genes (Tsien et al., 1991; Jun et al., 1999). These genes (A-E) are differentially distributed throughout brain and spinal cord (Murphy et al., 1991; Takahashi and Momiyama, 1993; Westenbroek et al., 1998) and encode large proteins consisting of four homologous domains (I–IV) containing six transmembrane segments each (S1-S6) (Tsien et al., 1991, Zhang et al., 1993).

Alternative splicing of the α_{1A} gene results in the expression of multiple Ca^{2+} channel phenotypes (Sutton et al., 1998; Bourinet et al., 1999; Hans et al., 1999; Jun et al., 1999). Splicing of two amino acids (NP) in the α_{1A} IVS3-IVS4 linker affects rates of

activation, inactivation, voltage-dependence of inactivation, and the affinity of α_{1A} for ω-Aga IVA (Sutton et al., 1998; Bourinet et al., 1999; Hans et al., 1999, Lin et al., 1999). The biophysical and pharmacological properties of α_{1A} Ca^{2+} channels are also influenced by intracellular signaling molecules. Co-expression of α_{1A} with different β subunit subtypes alters inactivation rates and ω-Aga IVA affinity (Moreno et al., 1997). Generally, α_{1A} subunit function is inhibited by interactions with G proteins or syntaxin-1A (Zhang et al., 1996; Qin et al., 1997; Sutton et al., 1999), and enhanced by protein kinase C (Zamponi et al., 1997; Bourinet et al., 1999). Calcium-activated calmodulin has dual effects on α_{1A} subunit function (Lee et al., 1999).

Determination of genomic exon-intron boundaries (Ophoff et al., 1996) and isolation of several α_{1A} C-terminal splice variants (Zhuchenko et al., 1997) suggest that there are four exons between IVS3-IVS4 and the C-terminal stop codon that undergo alternative splicing. This implies that sixteen combinations of these four exons are possible. Eight combinations have already been isolated from human brain (Ophoff et al., 1996; Zhuchenko et al., 1997, Hans et al., 1999). In this study, a ninth is isolated from human spinal cord. Biophysical characterization of this α_{1A} variant reveals that its rates of activation, inactivation, deactivation and recovery from inactivation are all significantly slower than an α_{1A} variant from cerebellum. The rate of inactivation was especially affected by sequence encoded by a single exon. These findings suggest that variation in α_{1A} C-terminal structure provides an added mechanism for functional diversity among neuronal Ca^{2+} channel subtypes.

Materials and Methods

Human spinal cord library screening

Calcium channel subunit cDNAs were isolated from an oligo(dT) and random primed human spinal cord λgt11 5' stretch cDNA library (Clontech, Palo Alto, CA) using a non-radioactive digoxigenin labeling and colorimetric detection system (Roche Molecular Biochemicals, Indianapolis, IN). The library was constructed from mRNA isolated from whole spinal cords pooled from 26 male/female Caucasians, ages 16 – 75, who died of sudden death syndrome. The insert size range of the library was 0.8 – 7.0 kb (average size 1.7 kb). Plaque-purified phage DNAs were isolated using a Lambda Prep Kit (Qiagen, Santa Clara, CA), and digested with the restriction endonuclease *EcoR*I (Roche Molecular Biochemicals, supplier of all endonucleases used). Southern blot analysis was used to assess insert size. cDNA isolates were ligated into pBluescriptII (Stratagene, La Jolla, CA) for sequencing. The inserts were subjected to exonuclease III/SI nuclease digestion (Erase-A-Base®, Promega, Madison, WI) prior to sequencing. PCR-based cycle sequencing (FS chemistry from PE Biosystems, Foster City, CA) with universal primers and custom internal primers (Genosys, The Woodlands, TX) was used for each clone. Sequence was obtained using an ABI Prism 310 Genetic DNA analyzer, and data were analyzed using ABI Prism DNA Sequencing Software version 2.12 (PE Biosystems). Sequence comparisons, alignments and restriction maps were performed using Lasergene Software (DNAStar, Madison, WI). 5' RACE (Roche Molecular Biochemicals) was used with human spinal cord polyA$^+$ RNA (Clontech) to create a 5' probe for the α_{1A} screening. This RNA came from a pool of 92 male/female Caucasians, ages 16-75, who died from sudden death syndrome.

The library screening process was initiated with a cDNA probe (α_1-EST) obtained from the NCBI dbEST database (1.8 kb human fetal brain α_{1A} fragment; Genbank H14053). Clone α_1-9, extending from nucleotides 3416 to the 3' untranslated region, was the longest of twenty-four 3' cDNAs isolated in the first rounds of screening. Five α_1 cDNAs were isolated in a second round, in which a 1 kb 5' *EcoR*I fragment of clone α_1-9 was used as probe. The longest clone isolated in this round, extending from nucleotide 2399 to 4551, was subsequently labeled and used as a probe to identify α_1-38 (which contained an *EcoR*I/*EcoR*I fragment from 1800 to 4551). In order to isolate the 5' portion of the α_{1A} sequence, a probe containing nucleotides 946 to 1800 was created by RT-PCR with human spinal cord RNA. Library screening with this probe yielded 14 cDNAs, one of which, clone α_1-80, extended from the 5' untranslated region to a region beyond the *EcoR*I site at nucleotide 1800.

Clone construction and sequencing

Full-length spinal cord α_{1A} cDNAs were assembled in several steps. Initially, PCR was performed using PFU Polymerase (Stratagene) and custom primers (Genosys) to truncate the 5' untranslated region of α_1-80 and to insert an idealized Kozak (Kozak, 1991) sequence into the shortened 5' end of the construct. The resulting 1.1 kb fragment was then ligated into the pT-Adv vector (Clontech) and sequenced to ensure that there were no polymerase errors. This PCR product was cut using the restriction endonuclease *Not*I and the resulting fragment was ligated into *EcoR*V/*Not*I prepared pBluescriptII. The untruncated α_1-80 was cut with *Not*I and the resulting 900 bp fragment was then ligated

into the shortened 5' clone using *Not*I. The resulting clone (referred to as 5'short) spans from the shortened 5' untranslated sequence to the *EcoR*I site at nucleotide1800.

In the next step, a 3' cDNA extending from nucleotide 3826 to the 3' untranslated region of the clone, α_1-10, was cut with *Not*I to eliminate the *EcoR*I site located in the polylinker of pBluescriptII. The construct was then cut with *Sac*I, blunted using Klenow fragment (Roche Molecular Biochemicals), and cut with *EcoR*I to yield a 3.5 kb fragment spanning from the *EcoR*I site at 4551 to the 3' untranslated region. This fragment was ligated into *EcoR*I/*Sma*I prepared pBluescriptII, removed with *EcoR*I/*BamH*I, and ligated into the *EcoR*I/*BamH*I cut vector containing 5' short. Thus, the resulting construct (5'short + 3') extended from the shortened 5' untranslated region to the *EcoR*I site at 1800, and continued from the *EcoR*I site at 4551 to the 3' untranslated region. In the final step, an *EcoR*I fragment of α_1-38 extending from 1801 to 4550 was cloned into *EcoR*I cut 5'short + 3'. The fully constructed clone, $\alpha_{1A\text{-}C1}$, was then sequenced to ensure the fidelity of the construction process. Exchanging the C-terminal domain of $\alpha_{1A\text{-}C1}$ with that of α_1-EST and α_1-9 created $\alpha_{1A\text{-}C2}$ and $\alpha_{1A\text{-}C16}$, respectively. Thus, both $\alpha_{1A\text{-}C2}$ and $\alpha_{1A\text{-}C16}$ are constructed of the same cDNAs up to nucleotide 4550 but then contain segments of different cDNAs beyond this point.

The rabbit Chβ_{1a} and α_{2a}/δ clones used in this study were provided by T. Tanabe (Tokyo Medical And Dental Univ., Tokyo, Japan). The Chβ_{1b}, β_3 and β_4 subunits were cloned from the same human spinal cord library described above and are nearly identical to previously reported sequences (Chβ_{1b}: Genbank M923303, Chβ_3: Genbank U07139 and Chβ_4: Genbank U95020).

Electrophysiology and data analysis

Standard *Xenopus laevis* oocyte expression methods were used to characterize the α_{1A} splice variants. Briefly, full-length α_{1A} subunit cDNA was *in vitro* transcribed (Ambion, Austin, TX). The resulting cRNA was injected into defolliculated *Xenopus laevis* oocytes (stage V-VI) along with equimolar ratios of rabbit α_2a/δ and Chβ cRNAs (0.40 μg/ml α_{1A}; 0.16 μg/ml α_2a/δ; 0.08 μg/ml Chβ in a total of 46 nl). Ca^{2+} channel currents were recorded by standard two-microelectrode voltage clamp techniques using a Warner amplifier (OC-725B) at room temperature (20 – 22°C) and data collected using pCLAMP6 software (Axon Instruments, Foster City, CA). The bath solution contained the following: 40 mM $Ba(OH)_2$, 40 mM TEA-OH, 2 mM KOH, 5 mM HEPES, pH adjusted to 7.4 with methanesulphonic acid. Microelectrodes were filled with 3M KCl and the resistances of the current and voltage electrodes were 0.3-1.5 MΩ. Data were filtered at 2 kHz and sampled at 10 kHz. Currents were recorded 6-18 days post-injection. The holding potential of all experiments was -100 mV unless otherwise noted. Control oocytes (α_{1A} alone or uninjected oocytes) did not yield currents larger than 50 nA. Due to lower expression levels when Chβ subunits other than the rabbit Chβ_{1a} were utilized, currents as low as 150 nA were included in the initial portion of the study. Only currents greater than 0.5 μA were analyzed for the remainder of this work. In order to diminish the contamination due to the Ca^{2+}-activated Cl^- channels, currents that exhibited slow deactivation (τ > 10 msec) were excluded from analysis. The leak current and capacitive current transients were subtracted on-line by a standard P/4 protocol. Data were analyzed

using pCLAMP6 and Excel 7.0 (Microsoft, Redmond, WA). For statistical analysis, a one-way ANOVA test was employed followed by a Fisher's PLSD test using Statview software (SAS Institute Inc., Cary, NC).

Results

Two α_{1A} C-terminal splice variants, $\alpha_{1A\text{-}C2}$ and $\alpha_{1A\text{-}C16}$, are the focus of this study (Figure 2.1A). These variants were assembled from a parent spinal cord construct, $\alpha_{1A\text{-}C1,}$ and thus are identical up to homology domain IV. Sequencing of the $\alpha_{1A\text{-}C1}$ cDNA through domain IV revealed only three differences when compared to an α_{1A} cDNA isolated from human cerebellum (Genbank AF004883). A deletion (ΔG419) previously identified in rat brain was found in the region encoding the intracellular linker between homology domains I and II (Bourinet et al., 1999). A mutation resulting in a charge change (M537R) was found in the region encoding transmembrane segment IIS2. A nine nucleotide deletion resulting in the loss of amino acids 726-728 (VEA) was found in the region encoding the intracellular linker between homology domains II and III. This deletion has been identified in another α_{1A} variant from human brain (Genbank U79666). The spinal cord $\alpha_{1A\text{-}C1}$ cDNA did not contain a six nucleotide insertion which codes for the amino acid sequence NP in the extracellular linker between IVS3 and IVS4. The α_1-EST and α_1-9 C-terminal cDNAs used to construct $\alpha_{1A\text{-}C2}$ and $\alpha_{1A\text{-}C16}$, respectively, differed from the C-terminus of $\alpha_{1A\text{-}C1}$ and other α_{1A} clones in sequences that could be traced to specific exon-intron boundaries (Ophoff et al., 1996). The α_1-EST cDNA did not extend to domain IV and therefore $\alpha_{1A\text{-}C2}$, like $\alpha_{1A\text{-}C1}$, lacks NP (Figure 2.1A). The

α_1-9 cDNA contained the NP exon and this region is therefore present in $\alpha_{1A\text{-}C16}$. The α_1-EST cDNA contained one version of exon 37 (37a), whereas α_1-9 contained a second (37b). There are nine amino acid changes in this region including one charge change (L1851K, Figure 2.1B). The α_1-EST cDNA contained 12 amino acids encoded by exon 44, whereas α_1-9 did not. Interestingly, five of these amino acids are positively charged (Figure 2.1B). A 3' GGCAG insert in exon 46 that would extend the open reading frame to exon 47, though present in $\alpha_{1A\text{-}C1}$ (data not shown), was not found in either α_1-EST or α_1-9 (Figure 2.1A). Thus, neither $\alpha_{1A\text{-}C2}$ nor $\alpha_{1A\text{-}C16}$ contains the approximately 240 amino acid domain encoded by exon 47. The end result is that $\alpha_{1A\text{-}C2}$ is identical to the human cerebellar clone described above, and $\alpha_{1A\text{-}C16}$ represents a novel spinal cord clone containing a unique arrangement of NP and C-terminal exons.

To determine the functional consequences of C-terminal splicing, both $\alpha_{1A\text{-}C2}$ and $\alpha_{1A\text{-}C16}$ were co-expressed with rabbit α_2a/δ and a rabbit $Ch\beta_{1a}$, or a human $Ch\beta_{1b}$, $Ch\beta_3$, or $Ch\beta_4$ subunit in *Xenopus* oocytes. Representative current traces demonstrate that $\alpha_{1A\text{-}C2}$ inactivates more rapidly than $\alpha_{1A\text{-}C16}$ when associated with $Ch\beta_{1a}$ $Ch\beta_{1b}$ or $Ch\beta_3$ subunits (Figure 2.2A-C; see below). When co-expressed with the $Ch\beta_4$ subunit, the $\alpha_{1A\text{-}C2}$ complex appears to inactivate at approximately the same rate as $\alpha_{1A\text{-}C16}$ (Figure 2.2D) although the low expression levels of this complex make interpretation difficult. As seen in Figure 2.2A, the deactivation rate of the $\alpha_{1A\text{-}C2}$ variant was slightly faster than for $\alpha_{1A\text{-}C16}$ ($\tau_{deactivation}$ [$\alpha_{1A\text{-}C2}$]= 5.6 ± 0.3 msec at –80 mV mV (n=7); $\tau_{deactivation}$ [$\alpha_{1A\text{-}C16}$]= 6.6 ± 0.3 msec at –80 mV (n=6)). When expressed with each of the Chβ subunits, the current-voltage relationships of $\alpha_{1A\text{-}C2}$ and $\alpha_{1A\text{-}C16}$ were essentially indistinguishable (Figure 2.2).

With all Chβ subunits, both α_{1A} variants had peak inward currents at +15 to +20 mV. Additionally, the voltages at which 1% of the maximal current was obtained were nearly identical ($Ch\beta_{1a}/\alpha_{1A\text{-}C2}$ = -19.2 +/- 4.4 mV while $Ch\beta_{1a}/\alpha_{1A\text{-}C16}$ = -19.5 +/- 5.0 mV; this measurement was not obtained with the other Chβ subunits due to poor expression levels). Co-expression of the rabbit $Ch\beta_{1a}$ subunit yielded currents 2-5 times higher than with any of the human Chβ subunits (Fig.2A-D). The goal of this study was to determine the effect of C-terminal α_{1A} splicing upon the function of the channel, independent of Chβ binding to the region. Therefore, the remainder of the study was carried out with the $Ch\beta_{1a}$ subunit since it does not appear to bind to this region of the α_{1A} subunit and has the most robust expression levels (Walker et al., 1998).

The voltage-dependency of activation, as determined from tail current measurements, was similar between $\alpha_{1A\text{-}C2}$ and $\alpha_{1A\text{-}C16}$ (Figure 2.3A: $V_{1/2}$ [$\alpha_{1A\text{-}C2}$] = 9.5 mV ± 1.4 mV and $V_{1/2}$ [$\alpha_{1A\text{-}C16}$] = 7.3 mV ± 1.1 mV), as was the voltage dependency of steady-state inactivation (Figure 2.3B:$V_{1/2}$ [$\alpha_{1A\text{-}C2}$] = -37.9 mV ± 1.4 mV and $V_{1/2}$ [$\alpha_{1A\text{-}C16}$] = -34.3 mV ± 1.5 mV). The time constants of activation and inactivation were described with a single exponential (Figs. 3C and 3D). The time constants of activation of the $\alpha_{1A\text{-}C16}$ variant, however, were much slower than that of $\alpha_{1A\text{-}C2}$ and varied with membrane potential (Figure 2.3E). The taus of activation of $\alpha_{1A\text{-}C16}$ ranged from 6.15 ± 0.40 msec at 0 mV to 1.24 ± 0.06 msec at +30 mV, whereas those of $\alpha_{1A\text{-}C2}$ ranged from 2.07 ± 0.51 msec at 0 mV to 0.75 ± 0.12 msec at +30 mV. The time constants of inactivation of the $\alpha_{1A\text{-}C16}$ variant were also slower than that of $\alpha_{1A\text{-}C2}$ (Figure 2.3F). The taus of inactivation of $\alpha_{1A\text{-}C2}$ ranged from 347 ± 69 msec at -10 mV to 175 ± 11 msec at

+50 mV, whereas those of $\alpha_{1A\text{-}C16}$ ranged from 984 ± 325 msec at -10 mV to 338 ± 46 msec at +50 mV. Analysis of the correlation between peak current and tau of inactivation demonstrates that slow activation of the Cl_{Ca} current did not contaminate the apparent rates of inactivation (r=0.304).

Since α_{1A} subunits are expressed primarily at synapses, and high frequency trains of action potentials govern neurotransmitter release, recovery from inactivation was characterized as a means of predicting how $\alpha_{1A\text{-}C2}$ versus $\alpha_{1A\text{-}C16}$ might respond to repetitive stimulation. Interestingly, at -40 and -60 mV, the rates of recovery from inactivation of $\alpha_{1A\text{-}C2}$ and $\alpha_{1A\text{-}C16}$ are not significantly different (Figure 2.4- A and D). However, at more negative potentials, the $\alpha_{1A\text{-}C2}$ subunit recovers from inactivation more rapidly than the $\alpha_{1A\text{-}C16}$ subunit (Figure 2.4- B, C, and D). A comparison of the fits of these recovery rates with a single exponential function reveals that the differences in recovery rates become more apparent at increasingly negative potentials (Figure 2.4D), showing that the rate of recovery from inactivation of the $\alpha_{1A\text{-}C2}$ subunit is more voltage dependent than that of $\alpha_{1A\text{-}C16}$. Although this difference is greater at potentials not likely to be seen physiologically (-100 to -120 mV), the recovery rate is still significantly different between -70 and -90 mV: at -70mV ($\alpha_{1A\text{-}C2}$ = 398 ± 19 msec; $\alpha_{1A\text{-}C16}$ = 469 ± 23 msec); at -80mV ($\alpha_{1A\text{-}C2}$ = 234 ± 11 msec; $\alpha_{1A\text{-}C16}$ = 321 ± 19 msec); at -90 mV ($\alpha_{1A\text{-}C2}$ = 178 ± 6 msec; $\alpha_{1A\text{-}C16}$ = 251 ± 15 msec). The voltage-dependence of the recovery from inactivation is shifted by approximately 10 mV in the physiological range (Figure 2.4D).

Given that the most obvious structural difference between $\alpha_{1A\text{-}C2}$ and $\alpha_{1A\text{-}C16}$ is the presence of the highly charged 12 amino acid segment encoded by exon 44 (Figure

2.1A), a chimera was constructed in order to characterize the influence of this segment on channel gating. The chimera, $\alpha_{1A\text{-}C14}$, is identical to $\alpha_{1A\text{-}C16}$ except that it contains the 12 amino acids encoded by exon 44. As expected, the voltage-dependencies of activation and steady-state inactivation of $\alpha_{1A\text{-}C14}$ were similar to $\alpha_{1A\text{-}C16}$ ($V_{1/2Activation}$ [$\alpha_{1A\text{-}C14}$] = 6.7 ± 1.3 mV; $V_{1/2Inactivation}$ [$\alpha_{1A\text{-}C14}$]= -33.0 ± 1.1 mV). The differences between the rates of activation (Figure 2.5C) and deactivation (at -80 mV: $\tau_{deactivation}$ [$\alpha_{1A\text{-}C14}$]= 6.3 ± 0.4 msec) and the rates of recovery from inactivation (at -100 mV: $\tau_{recovery}$ = 216 ± 19 msec; at -80 mV: $\tau_{recovery}$ = 316 ± 31 msec; at -60 mV: $\tau_{recovery}$ = 520 ± 63 msec) were not statistically significant. The most striking difference between the two variants was the enhancement of the rate of inactivation of $\alpha_{1A\text{-}14}$ relative to $\alpha_{1A\text{-}C16}$ (Figure 2.5- A, B, and D). Moreover, these rates were similar to those of $\alpha_{1A\text{-}C2}$, ranging from 198 ± 14 msec at 0 mV to 133 ± 16 msec at +50 mV.

In order to determine whether the effects of the amino acid segment encoded by exon 44 upon the rate of inactivation were background dependent, this exon was removed from $\alpha_{1A\text{-}C2}$ to create $\alpha_{1A\text{-}C4}$. Thus, $\alpha_{1A\text{-}C4}$, is identical to $\alpha_{1A\text{-}C2}$ except that it lacks the 12 amino acids encoded by exon 44. The effect of the removal of exon 44 was indeed to slow the rate of inactivation (Figure 2.6A, 6B and 6D) without significantly affecting the voltage-dependency of activation ($V_{1/2}$ [$\alpha_{1A\text{-}C4}$] = 7.7 mV ± 1.0 mV) or inactivation ($V_{1/2}$ [$\alpha_{1A\text{-}C4}$] = -31.4 mV ± 1.2 mV). Interestingly, this construct had a slower rate of activation (Figure 2.6A, 6B and 6C).

Discussion

The gating properties of neuronal Ca^{2+} channels are determined by multiple structural domains within the α_1 subunit (Tsien et al., 1991; Catterall, 1995). Our results indicate that C-terminal alternative splicing can influence some of these properties. The C-terminus of the α_{1A} subunit is encoded by twelve exons, numbered 36 through 47 (Ophoff et al., 1996), of which four exons, 37, 44, 46, and 47, undergo alternative splicing (Zhuchenko et al., 1997). Depending on the pattern of splicing, the C-terminus may vary from 436 to 517 amino acids. Binding sites for several intracellular signaling molecules, which affect channel gating, have been identified within this sequence. An EF-hand Ca^{2+}-binding motif can be aligned to sequence encoded by exons 36 and 37 (de Leon et al., 1995). Calmodulin has been shown to bind to a region of the C-terminus encoded by exon 40 (Peterson et al., 1999) and to a calmodulin-binding domain (CBD) identified in the region encoded by exon 42 (Lee et al., 1999). Calcium-dependent binding of calmodulin to the CBD-motif speeds inactivation and recovery from inactivation and produces a long-lasting facilitation of Ca^{2+} current (Lee et al., 1999). Calcium channel β_4 subunit binding to a region encoded by exons 43-47 has been shown to enhance the rate of inactivation (Walker et al., 1998). In addition, the C-terminus appears to be essential for modulation by $G_{\beta\gamma}$ proteins (Zhang et al., 1996), particularly those regions encoded by exons 45 and 46 (Qin et al., 1997). G-proteins modulate the kinetics of channel activation and inactivation, the voltage-dependence of activation, and recovery from inactivation (Bean, 1989; Patil et al., 1998; Zamponi and Snutch, 1998). Polyglutamine tract expansions in exon 47 (Zhuchenko et al., 1997) shift the voltage-dependence of activation to more negative potentials, dramatically increase current

density (Piedras-Renteria et al., 1999), and alter activation and inactivation kinetics (Resituito et al., 1999). These latter effects appear to be dependent on co-expression of the β_4 subunit.

This study focuses on two naturally occurring splice variants of the α_{1A} subunit gene that differ in nucleotide sequences corresponding to the NP exon of the IVS3-IVS4 extracellular linker and C-terminal exons 37 and 44. One variant, $\alpha_{1A\text{-}C2}$, has been identified previously in human cerebellum but has not been expressed and characterized (Zhuchenko et al., 1997; Genbank U79663). It lacks the NP exon, but contains exons 37a and 44. The other variant, $\alpha_{1A\text{-}C16}$, which has not been identified previously, contains the NP exon and exon 37b but lacks exon 44. Neither $\alpha_{1A\text{-}C2}$ nor $\alpha_{1A\text{-}C16}$ contain exon 47, which is present in the well-characterized α_{1A} subunits, BI-1 and BI-2, isolated from rabbit brain (Mori et al., 1991; Sather et al., 1993). Given the central role of the α_{1A} C-terminus in defining channel gating characteristics, we hypothesized that the difference in splicing pattern between the two variants would be reflected by changes in their biophysical properties.

Expression in *Xenopus* oocytes demonstrated that $\alpha_{1A\text{-}C2}$ and $\alpha_{1A\text{-}C16}$ are similar with respect to current-voltage relationships and voltage-dependency of activation and inactivation. This is different from previously reported results. The presence of the NP exon shifted the voltage-dependence of activation and inactivation of a rat brain α_{1A} subunit (Bourinet et al., 1999). In a study conducted with a human α_{1A} subunit, the NP exon only shifted the voltage-dependence of inactivation (Hans et al., 1999). Taken together, these data suggest that regions in addition to NP are important for determining

the voltage-dependence of activation and inactivation. However, other differences, such as the isoform of Chβ subunit co-expressed with the α_{1A} subunit, differing expression systems, and the lack of complete inactivation at the end of the conditioning pulse, could shift the voltage-dependence of inactivation (Hans et al, 1999).

Further characterization reveals differences in the respective rates of activation, inactivation, deactivation, and recovery from inactivation of channels containing the $\alpha_{1A\text{-}C2}$ or $\alpha_{1A\text{-}C16}$ subunits. Complexes containing the $\alpha_{1A\text{-}C16}$ subunit activate more slowly than those that contain $\alpha_{1A\text{-}C2}$. This may be explained, in part, by the presence of the NP amino acids in the extracellular IVS3-IVS4 linker, which have been shown to decrease the rate of activation of α_{1A} and α_{1B} channel complexes by approximately 1.5-fold at +10 mV (Hans et al., 1999; Lin et al., 1999). The $\alpha_{1A\text{-}C2}$ complex has an apparent rate of activation that is similar to other α_{1A} subunits that lack NP (1.6 ± 0.2 msec vs. 1.2 ± 0.5 msec; Hans et al., 1999). The activation rate of $\alpha_{1A\text{-}C16}$ is considerably slower than other subunits that contain NP (4.8 ± 0.5 msec vs. 2.2 ± 1.1 msec; Hans et al., 1999), suggesting that other regions of the C-terminus also affect activation. Our results indicate that the region encoded by exon 44 appears to be acting in a modular fashion to enhance the rate of inactivation of α_{1A} complexes 2 – 3 fold. It is unclear whether this results from a direct conformational change, or whether the presence or absence of this charged sequence affects modulation by intracellular signaling molecules. Further experiments are required to resolve this issue. Interestingly, the regions encoded by exons 43 through 47 have been shown to bind β_4 and β_{2a} subunits, but not β_1 or β_3 subunits (Walker et al., 1998). Our results with the β_1 subunit suggest that changes in inactivation imparted by

exon 44 are independent of C-terminal β subunit binding. The deactivation rate of the $\alpha_{1A\text{-}C16}$ complex is slightly slower than that of $\alpha_{1A\text{-}C2}$. Since the settling time of the oocyte clamp is approximately 2 msec, these rates are likely to be faster than we report. Regardless, the $\alpha_{1A\text{-}C16}$ complexes are consistently slower over a wide voltage range, (-60 to -100 mV, data not shown). Thus, as is true for the α_{1C} subunit of L-type Ca^{2+}channels (Soldatov et al., 1997, 1998), C-terminal alternative splicing does affect the biophysical properties of channel complexes composed of α_{1A} subunits.

The slower activation, inactivation and deactivation of $\alpha_{1A\text{-}C16}$ splice variants relative to $\alpha_{1A\text{-}C2}$ could translate to differences in neurotransmitter release at subtype specific synapses. Though differences in channel number and density, second messenger effects, and Ca^{2+} buffering make it difficult to predict what the combined effects of C-terminal splicing on Ca^{2+} entry will be (Park and Dunlap, 1998; Lin et al., 1999), our results do allow for some generalizations to be made. The slower rate of activation of channels containing the $\alpha_{1A\text{-}C16}$ subunit should lead to a decrease in the initial rate of calcium influx. However, the slower inactivation rate of the $\alpha_{1A\text{-}C16}$ subunit would enhance later calcium entry, providing the channel does not recover from inactivation by passing through the open state (Slesinger and Lansman, 1991). The slower deactivation rate of $\alpha_{1A\text{-}C16}$ channel complexes would increase Ca^{2+} flux through these channels at a time when the driving force is relatively large. Therefore, it is likely that in response to a single action potential, the initial rate of Ca^{2+} entry would be slower through complexes containing the $\alpha_{1A\text{-}C16}$ subunit, but these channels would allow for a greater total Ca^{2+} influx.

The rate of recovery from inactivation at negative potentials plays an important role in determining Ca^{2+} influx and neurotransmitter release in response to a train of action potentials. The voltage dependence of the rate of recovery of channel complexes containing the $\alpha_{1A\text{-}C16}$ subunit differs from those containing $\alpha_{1A\text{-}C2}$. At less negative potentials, the two splice variants behave similarly. After 500 msec at -60 mV, approximately 30% of channels composed of either variant are fully recovered. However, at more negative potentials, complexes containing the $\alpha_{1A\text{-}C16}$ subunit recover more slowly. After 500 msec at -80 mV, approximately 73% of $\alpha_{1A\text{-}C2}$ complexes are recovered as compared to approximately 62% of $\alpha_{1A\text{-}C16}$ complexes. Thus, Ca^{2+} entry following a train of action potentials would be less in nerve terminals expressing the $\alpha_{1A\text{-}C16}$ subunit relative to those expressing the $\alpha_{1A\text{-}C2}$ subunit. These differences may be important from the standpoint of Ca^{2+}-mediated synaptic plasticity.

Our results add to a developing picture of neuronal calcium channels that suggests that α_1 subunit genes express channels with a wide array of structures and functions. These channels may have evolved to meet the specific needs of highly specialized synapses. Our results, combined with those of several laboratories (Bourinet et al., 1999; Hans et al., 1999) point to the fact that it is no longer sufficient to refer to α_{1A} channels as simply P- and Q-type. Minor splicing events in critical domains of the α_{1A} subunit alters both pharmacological and physiological properties in ways in which we are only beginning to understand. Determination of where specific α_{1A} subunit splice variants are expressed, how they respond to trains of action potentials, and how they interact with

various signaling molecules should greatly enhance our understanding of the physiology of the synapse.

References

Bean, BP (1989) Neurotransmitter inhibition of neuronal calcium currents by changes in channel voltage dependence. Nature 340: 153-156.

Bourinet E, Soong TW, Sutton K, Slaymaker S, Mathews E, Monteil A, Zamponi GW, Nargeot J, and Snutch TP (1999) Splicing of alpha 1A subunit gene generates phenotypic variants of P- and Q-type calcium channels. Nat Neurosci. 2:407-15.

Catterall WA (1995) Structure and function of voltage-gated ion channels. Annu. Rev. Biochem. 64:493-531.

de Leon M, Wang Y, Jones L, Perez-Reyes E, Wei X, Soong TW, Snutch TP, Yue DT (1995) Essential Ca^{2+}-binding motif for Ca^{2+}-sensitive inactivation of L-type Ca^{2+} channels. Science. 270:1502-6.

Dunlap K, Luebke JI, and Turner TJ (1995) Exocytotic Ca^{2+} channels in mammalian central neurons. Trends Neurosci. 18:89-98.

Hans M, Urrutia A, Deal C, Brust PF, Stauderman K, Ellis SB, Harpold MM, Johnson EC, and Williams ME (1999) Structural elements in domain IV that influence biophysical and pharmacological properties of human alpha1A-containing high-voltage-activated calcium channels. Biophys J. 76:1384-400.

Jun K, Piedras-Renteria ES, Smith SM, Wheeler DB, Lee SB, Lee TG, Chin H, Adams ME, Scheller RH, Tsien RW, and Shin HS (1999) Ablation of P/Q-type Ca^{2+} channel currents, altered synaptic transmission, and progressive ataxia in mice lacking the $alpha_{1A}$-subunit. Proc Natl Acad Sci. 96:15245-50.

Kozak M (1991) An analysis of vertebrate mRNA sequences: intimations of translational control. J Cell Biol. 115:887-903.

Lee A, Wong ST, Gallagher D, Li B, Storm DR, Scheuer T, and Catterall WA (1999) Ca^{2+}/calmodulin binds to and modulates P/Q-type calcium channels. Nature. 399:155-9.

Lin Z, Lin Y, Schorge S, Pan JQ, Beierlein M, and Lipscombe D (1999) Alternative splicing of a short cassette exon in alpha1B generates functionally distinct N-type calcium channels in central and peripheral neurons. J Neurosci. 19:5322-31.

Moreno H, Rudy B and Llinas R (1997) Beta subunits influence the biophysical and pharmacological differences between the P- and Q-type calcium currents expressed in a mammalian cell line. Proc. Natl. Acad.Sci. 94:14042-47.

Mori Y, Friedrich T, Kim MS, Mikami A, Nakai J, Ruth P, Bosse E, Hoffmann F, Flockerzi V, Furuichi T, Mikoshiba K, Imoto K, Tanabe T and Numa S (1991) Primary structure and functional expression from complementary DNA of a brain calcium channel. Nature. 350:398-402.

Murphy TH, Worley PF, and Baraban JM (1991) L-type voltage-sensitive Ca^{2+} channels mediate synaptic activation of immediate early genes. Neuron. 7:625–635.

Ophoff RA, Terwindt GM, Vergouwe MN, van Eijk R, Oefner PJ, Hoffman SMG, Lamerdin JE, Mohrenweiser HW, Bulman DE, Ferrari M, Haan J, Lindhout D, van Ommen G-J, Hofker MH, Ferrari MD, and Frants RR (1996) Familial hemiplegic migraine and episodic ataxia type-2 are caused by mutations in the Ca^{2+} channel gene CACNL1A4. Cell. 87:543-552.

Park D and Dunlap K (1998) Dynamic regulation of calcium influx by G-proteins, action potential waveform, and neuronal firing frequency. J Neurosci. 18:6757-66.

Patil PG, Brody DL, and Yue DT (1998) Preferential closed-state inactivation of neuronal calcium channels. Neuron. 20:1027-1038.

Peterson BZ, DeMaria CD, Adelman JP and Yue DT (1999) Calmodulin is the Ca^{2+} sensor for Ca^{2+} -dependent inactivation of L-type calcium channels. Neuron. 22:549-58.

Piedras-Rentería ES, Watase K, Zoghbi HY, Lee CC and Tsien RW (1999) Alteration of expressed alpha1A Ca^{2+} channel currents arising from expanded trinucleotide repeats in spinocerebellar ataxia type 6. Soc. Neurosci. Abstr. 431.1.

Qin N, Olcese R, Zhou J, Cabello OA, Birnbaumer L, and Stefani E (1996) Identification of a second region of the beta-subunit involved in regulation of calcium channel inactivation. Am J Physiol. 271(5 Pt 1):C1539-45.

Qin N, Platano D, Olcese R, Stefani E, and Birnbaumer L (1997) Direct interaction of Gbetagamma with a C-terminal Gbetagamma-binding domain of the Ca^{2+} channel alpha1 subunit is responsible for channel inhibition by G protein-coupled receptors. Proc Natl Acad Sci. 94:8866-71.

Resituito S, Thompson R, Charnet P, and Gomez C (1999): Multiple SCA6-associated & alpha1A splice forms may have altered activation/inactivation kinetics. Soc. Neurosci. Abstr. 431.2.

Sather WA, Tanabe T, Zhang JF, Mori Y, Adams ME, and Tsien RW (1993) Distinctive biophysical and pharmacological properties of class A(BI) calcium channel alpha 1 subunits. Neuron. 11:291-303.

Slesinger PA and Lansman JB (1991) Reopening of Ca^{2+} channels in mouse cerebellar neurons at resting membrane potentials during recovery from inactivation. Neuron. 7:755-62.

Soldatov NM, Oz M, O'Brien KA, Abernethy DR, and Morad M (1998) Molecular determinants of L-type Ca^{2+} channel inactivation. Segment exchange analysis of the carboxyl-terminal cytoplasmic motif encoded by exons 40-42 of the human alpha1C subunit gene. J Biol Chem. 273:957-963.

Soldatov NM, Zühlke RD, Bouron A and Reuter H (1997) Molecular structures involved in L-type calcium channel inactivation. Role of the carboxyl-terminal region encoded by exons 40-42 in alpha 1C in the kinetics and Ca^{2+} dependence of inactivation. J Biol Chem. 272: 3650 –3566.

Sutton KG, McRory JE, Guthrie H, Murphy TH, Snutch TP (1999) P/Q-type calcium channels mediate the activity-dependent feedback of syntaxin-1A. Nature. 401:800-4.

Sutton KG, Zamponi GW, Bourinet E, Soong TW, and Snutch TP (1998) Alternative splicing of the α1a gene generates distinct P- or Q-type sensitivity to omega-Agatoxin IVA. Soc. Neurosci. Abstr. 16.1.

Takahashi T and Momiyama A (1993) Different types of calcium channels mediate central synaptic transmission. Nature. 366:156-158.

Tsien RW, Ellinor PT, and Horne WA (1991) Molecular diversity of voltage-dependent Ca^{2+} channels. TIPS. 12:349-354.

Turner TJ, Adams ME, Dunlap K (1992) Calcium channels coupled to glutamate release identified by omega-Aga-IVA. Science. 258:310-3.

Walker D, Bichet D, Campbell KP, and De Waard M (1998) A beta 4 isoform-specific interaction site in the carboxyl-terminal region of the voltage-dependent Ca^{2+} channel alpha1A subunit. J Biol Chem. 273:2361-7.

Westenbroek RE, Ahlijanian MK, and Catterall WA (1990) Clustering of L-type Ca^{2+} channels at the base of major dendrites in hippocampal pyramidal neurons. Nature. 347:281-4.

Westenbroek RE, Hoskins L, and Catterall WA (1998) Localization of Ca^{2+} channel subtypes on rat spinal motor neurons, interneurons, and nerve terminals. J Neurosci. 18:6319-6330.

Wheeler DB, Randall A, Tsien RW (1994) Roles of N-type and Q-type Ca2+ channels in supporting hippocampal synaptic transmission. Science. 264:107-11

Yokoyama CT, Westenbroek RE, Hell JW, Soong TW, Snutch TP, and Catterall WA (1995) Biochemical properties and subcellular distribution of the neuronal class E calcium channel alpha 1 subunit. J Neurosci. 15:6419-32.

Zamponi GW, Bourinet E, Nelson D, Nargeot J, and Snutch TP (1997) Crosstalk between G proteins and protein kinase C mediated by the calcium channel α1 subunit. Nature. 385:442-446.

Zamponi GW and Snutch TP (1998) Modulation of voltage-dependent calcium channels by G proteins. Curr Opin Neurobiol. 8:351-6.

Zhang JF, Ellinor PT, Aldrich RW, Tsien RW (1996) Multiple structural elements in voltage-dependent Ca^{2+} channels support their inhibition by G proteins. Neuron. 17:991-1003.

Zhang JF, Randall AD, Ellinor PT, Horne WA, Sather RA, Tanabe T, Schwarz TL and Tsien RW (1993) Distinctive pharmacology and kinetics of cloned neuronal Ca^{2+} channels and their possible counterparts in mammalian cns neurons. Neuropharmacology. 32:1075-1088.

Zhuchenko O, Bailey J, Bonnen P, Ashizawa T, Stockton DW, Amos C, Dobyns WB, Subramony SH, Zoghbi HY, and Lee CC. (1997) Autosomal dominant cerebellar ataxia (SCA6) associated with small polyglutamine expansions in the alpha1A-voltage-dependent calcium channel. Nat Genet. 15:62-9.

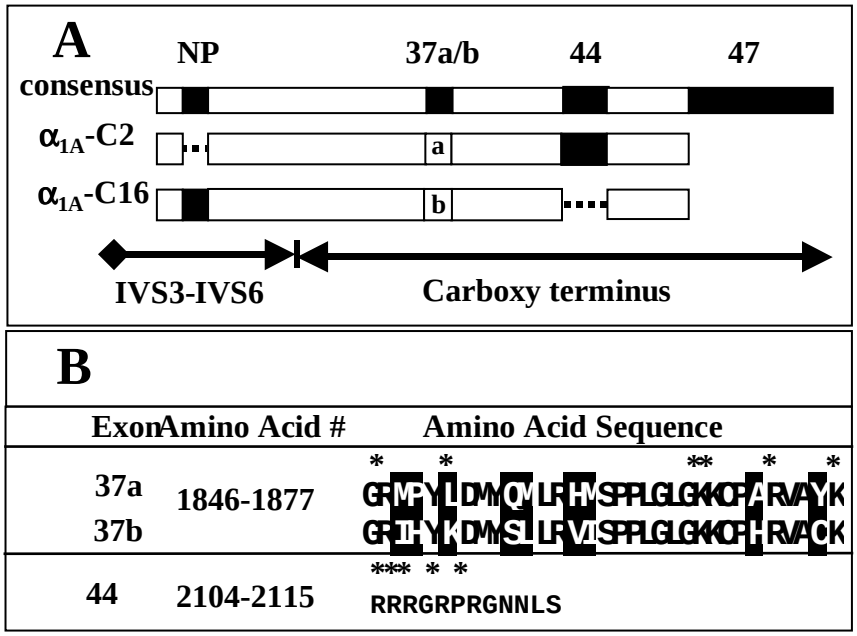

Figure 2.1. Alternative splicing of α_{1A} domain IV and C- terminal exons. A) Alternatively spliced exon patterns of $a_{1A\text{-}C2}$ and $a_{1A\text{-}C16}$ cDNAs relative to a consensus protein that is a composite of known exons (*upper bar*). This figure is drawn based on our data and that of others (Ophoff et al., 1996; Zhuchenko et al., 1997; Hans et al., 1999). Note that the NP sequence is located in the extracellular loop between transmembrane domains IVS3 and IVS4. B) The amino acid sequences of exons 37a, 37b and 44. Regions of variation are highlighted in black. Charged amino acids are denoted by an asterisk (*).

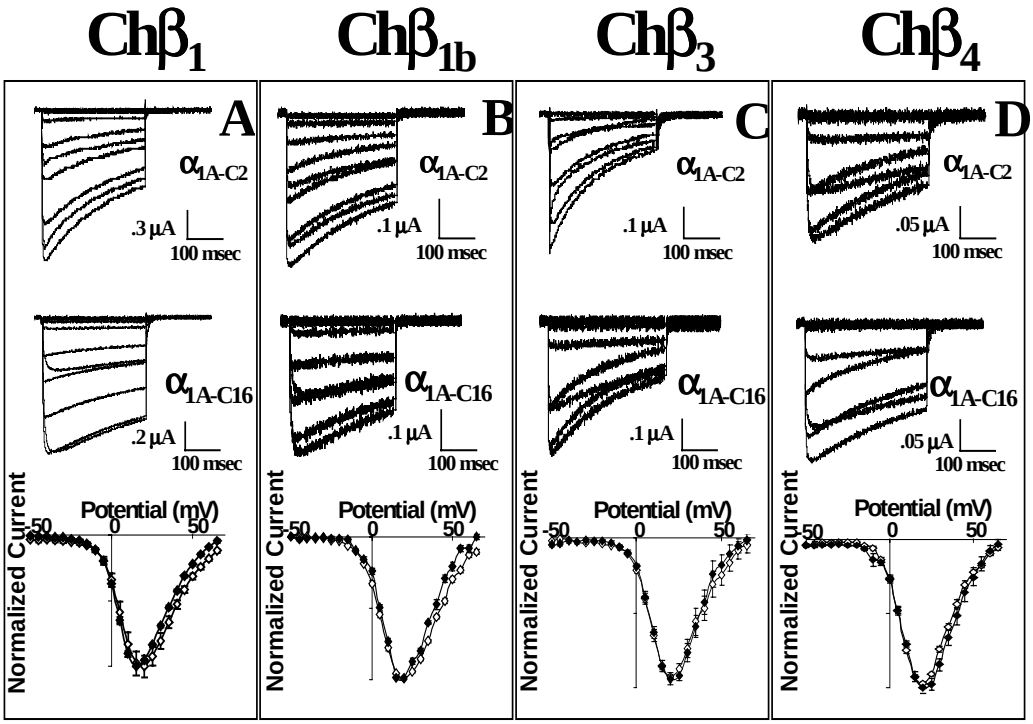

Figure 2.2. Biophysical properties of the $\alpha_{1A\text{-}C2}$ and $\alpha_{1A\text{-}C16}$ subunits co-expressed with rabbit α_2a/δ and $Ch\beta_{1a}$, $Ch\beta_{1b}$, $Ch\beta_3$, or $Ch\beta_4$ subunits. A-D) Representative current traces of $\alpha_{1A\text{-}C2}$ between -40 mV and +40 mV with the $Ch\beta_{1a}$(A), $Ch\beta_{1b}$(B), $Ch\beta_3$(C), or $Ch\beta_4$(D) subunit. Normalized current-voltage relationships of $\alpha_{1A\text{-}C2}$ (open diamonds) and $\alpha_{1A\text{-}C16}$ (filled diamonds) with the $Ch\beta_{1a}$ (n=14 and 20), $Ch\beta_{1b}$ (n=21 and 14), $Ch\beta_3$ (n=10 and 10), or $Ch\beta_4$ (n=26 and 22) subunit.

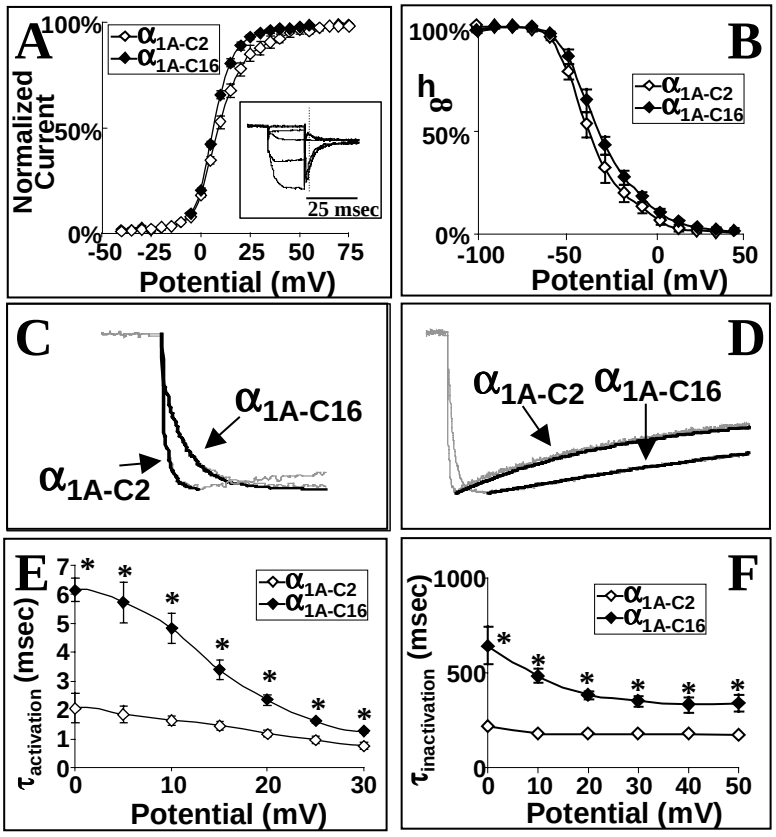

Figure 2.3. Voltage-dependencies and rates of inactivation and activation of $\alpha_{1A\text{-}C2}$ and $\alpha_{1A\text{-}C16}$ subunit complexes. A) Voltage-dependence of activation of $\alpha_{1A\text{-}C2}$ and $\alpha_{1A\text{-}C16}$ as measured from tail current measurements. As depicted in the inset, tail currents were measured following the capacitive current (dashed line) at 0 mV following a 20 msec depolarization to the test potential (-40 to +75 mV in 5 mV increments). Tail currents were normalized to the largest tail current in each series of test pulses. These data were fit with a Boltzmann equation: $\%I = 1/[1 + \exp(-(V_{test} - V_{1/2})/k)]$. B) Isochronal inactivation of $\alpha_{1A\text{-}C2}$ and $\alpha_{1A\text{-}C16}$. A 20 second conditioning pulse ranged from -100 mV to +40 mV in 10 mV increments. The conditioning pulse was followed by a test pulse to +20 mV for 300 msec. Data were fit with a Boltzmann equation: $\% I = 1/[1 + \exp((V_{test} - V_{1/2})/k)]$. C) Single exponential fits of activation of $\alpha_{1A\text{-}C2}$ and $\alpha_{1A\text{-}C16}$ at +20 mV. Fits are shown as solid black lines. D) Single exponential fits of inactivation of $\alpha_{1A\text{-}C2}$ and $\alpha_{1A\text{-}C16}$ at +20 mV. Fits are shown as solid black lines. E) Average $\tau_{activation}$ of $\alpha_{1A\text{-}C2}$ and $\alpha_{1A\text{-}C16}$ between the voltages 0 and +30 mV. Traces were fit with a single exponential from the onset of the inward current to the time of peak current. For this and all following figures, the asterisks (*) denote statistical significance ($P < 0.01$) using an ANOVA test. F) Average $\tau_{inactivation}$ between -10 and +50 mV for $\alpha_{1A\text{-}C2}$ and $\alpha_{1A\text{-}C16}$. Each point represents a minimum of 6 recordings. The standard error of the mean for each point is shown unless the values were smaller than the symbol. Traces were fit with a single exponential from the peak inward current to the end of the depolarization.

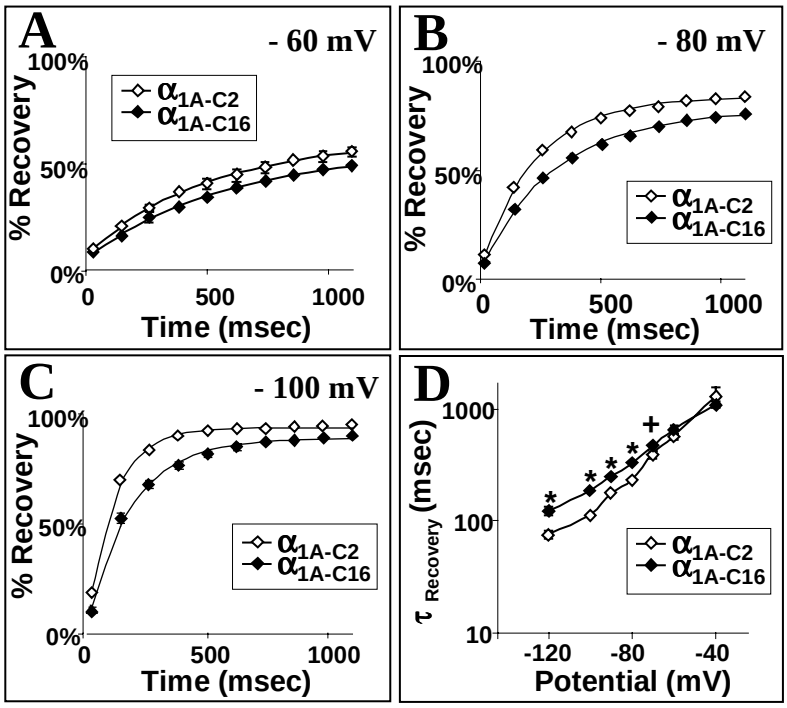

Figure 2.4. Voltage dependency of recovery from inactivation of the $\alpha_{1A\text{-}C2}$ and $\alpha_{1A\text{-}C16}$ subunit complexes. A-C) Average recoveries of $\alpha_{1A\text{-}C2}$ and $\alpha_{1A\text{-}C16}$ at -60 (Fig. 4A), -80 (Fig. 4B), and -100 mV (Fig. 4C). A two-pulse protocol was employed using an initial test pulse of 600 msec to +30 mV followed by a conditioning pulse (ranging from -40 mV to -120 mV) of intervals ranging from 20 to 1100 msec. This was followed by a second 200 msec test pulse to +30 mV, I_2. The percentage recovery was measured as % Recovery = $(I_2\text{-}I_{\text{end of pulse I1}})/(I_1\text{-}I_{\text{end of pulse I1}})$. Each point shown is the average of 6-9 different recordings. The standard error of the mean for each point is shown unless the values were smaller than the symbol. The solid lines are the single exponential fits of the % Recovery. D) Voltage dependency of the rate of recovery from inactivation of $\alpha_{1A\text{-}C2}$ and $\alpha_{1A\text{-}C16}$. τ_{recovery} is the average value derived from single exponential fits of individual experiments. The asterisks (* $p<0.01$) and crosses (+ $p<0.05$) denote statistical significance using an ANOVA test.

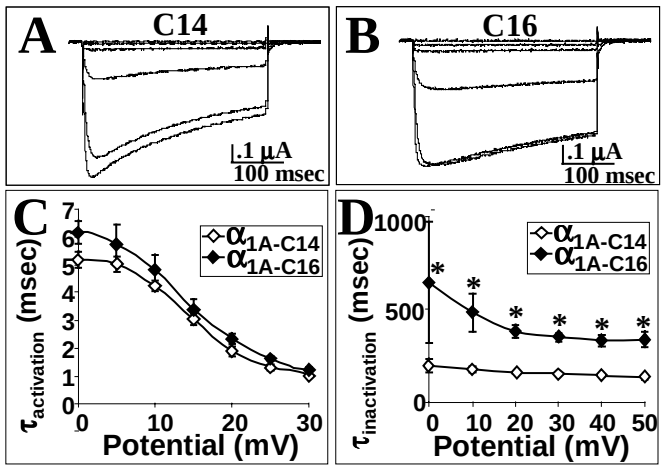

Figure 2.5. Exon 44 enhances the rate of inactivation. A) Current traces of α_{1A-C14}, a clone that contains the 12 amino acids encoded by exon 44, between -50 mV and +40 mV. B) Current traces of α_{1A-C16}, a clone that does not contain exon 44, between -50 mV and +40 mV. C) Average $\tau_{activation}$ of α_{1A-C14} and α_{1A-C16} between 0 and +30 mV. D) Average $\tau_{inactivation}$ between 0 and +50 mV for α_{1A-C14} and α_{1A-C16}. Each point represents a minimum of 5 recordings. The standard error of the mean for each point is shown unless the values were smaller than the symbol. Traces were fit with a single exponential from the peak inward current to the end of the depolarization.

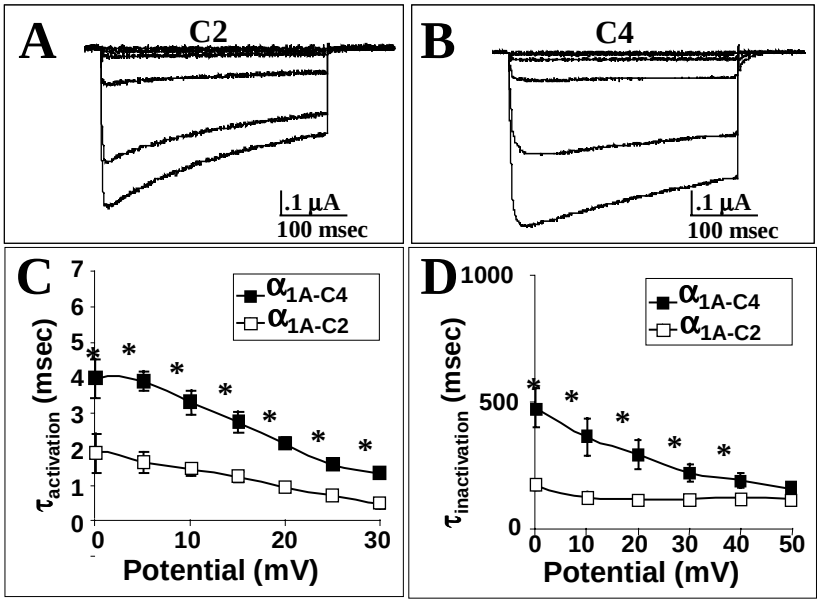

Figure 2.6. In a different C-terminal combination, the exon 44 slows the rate of activation but still enhances the rate of inactivation. A) Current traces of α_{1A-C2}, a clone that contains the 12 amino acids encoded by exon 44, between -50 mV and +40 mV. B) Current traces of α_{1A-C4}, a clone that does not contain exon 44, between -50 mV and +40 mV. C) Average $\tau_{activation}$ of α_{1A-C2} and α_{1A-C4} between 0 and +30 mV. D) Average $\tau_{inactivation}$ between 0 and +50 mV for α_{1A-C2} and α_{1A-C4}. Each point represents a minimum of 5 recordings. The standard error of the mean for each point is a shown unless the values were smaller than the symbol. Traces were fit with single exponential from the peak inward current to the end of the depolarization.

Chapter 3

ALTERNATIVE SPLICING OF THE β_4 SUBUNIT HAS α_1 SUBUNIT SUBTYPE-SPECIFIC EFFECTS ON CA^{2+} CHANNEL GATING

Abstract

Ca^{2+} channel β subunits are important molecular determinants of the kinetics and voltage dependence of Ca^{2+} channel gating. Through direct interactions with channel-forming α_1 subunits, β subunits enhance expression levels, accelerate activation, and have variable effects on inactivation. Four distinct β subunit genes each encode five homologous sequence domains (D1-5), three of which (D1, 3 and 5) undergo alternative splicing. We have isolated from human spinal cord a novel alternatively spliced β_4 subunit containing a short form of domain D1 (β_{4a}) that is highly homologous to N-termini of *Xenopus* and rat β_3 subunits. The purpose of this study was to compare the gating properties of various α_1 subunit complexes containing β_{4a} with those of complexes containing a β_4 subunit with a longer form of domain D1, β_{4b}. Expression in *Xenopus* oocytes revealed that, relative to α_{1A} and α_{1B} complexes containing β_{4b}, the voltage dependence of activation and inactivation of complexes containing β_{4a} were shifted to more depolarized potentials. Moreover, α_{1A} and α_{1B} complexes containing β_{4a} inactivated at a faster rate. Interestingly, β_4 subunit alternative splicing did not influence the gating properties of α_{1C} and α_{1E} subunits. Experiments with β_4 deletion mutants revealed that both the N- and C-termini of the β_4 subunit play critical roles in setting voltage dependent

gating parameters, and that their effects are α_1 subunit specific. Our data are best explained by a model in which distinct modes of activation and inactivation result from β-subunit splice variant-specific interactions with an α_1 subunit gating structure.

Introduction

Neuronal high voltage-activated Ca^{2+} channels (L, N, P/Q, and R) consist of at least four subunits, α_1, α_2/δ, and β (Liu et al., 1996), with a fifth subunit, γ, being recently described (Letts et al., 1998). Different Ca^{2+} channel phenotypes arise primarily from the expression of five unique α_1 subunit genes (α_{1A}- α_{1E}). These genes encode large pore-forming proteins (over 2200 amino acids) that are differentially distributed throughout the nervous system (Westenbroek et al., 1990, 1998). Synaptic N-, P/Q- and R-type channels, formed by α_{1B}, α_{1A}, and α_{1E} subunits, respectively, play a principal role in regulating neurotransmitter release (Turner et al., 1992; Takahashi and Momiyama, 1993; Wheeler et al., 1994; Wu et al., 1999).

Ca^{2+} channel β subunits (subtypes 1- 4) are highly homologous intracellular proteins with primary sequences ranging from 480-630 amino acids (reviewed by Birnbaumer et al., 1998). The sequence can be divided into 5 domains based on regions of amino acid identity between subtypes. All β subunits contain a highly conserved β interaction domain (BID) in domain 4, which has been shown to interact with high affinity to an α interaction domain (AID) on the I-II linker of α_1 subunits (Pragnell *et al*., 1994, De Waard *et al*., 1995). Structure prediction methods using the Prodom and Pfam protein databases have established a domain structure (A-E domains) for the β_{1b} subunit

(Hanlon et al., 1999) that largely overlaps with sequence domains 1- 5. The A domain (100 aa) shows some homology to PDZ domains, the B domain (61 aa) to SH3 domains, and the D domain (210 aa) to guanylate-kinase, though it lacks a functional ATP-binding P-loop motif. Domains C and E were without precedent in the Prodom and Pfam protein databases; however, Domain C is rich in serine residues, suggesting that it serves a linker function between Domains B and D. Thus, in many respects, Ca^{2+} channel β subunits resemble members of the MAGUK (membrane-associated guanylate kinase) protein family which are known to cluster ion channels, receptors, adhesion molecules, and cytosolic signaling proteins at synapses and cellular junctions (Fanning and Anderson, 1999).

Previous studies have shown that the kinetics and voltage sensitivity of α_1 subunit gating are affected profoundly by β subunits (Lacerda et al., 1991, Singer et al., 1991), and the extent to which these parameters are altered varies significantly with β subunit subtype (Ellinor et al., 1993; Olcese et al., 1994). For example, while β_1 and β_3 subunits shift the voltage dependence of α_{1E} subunit inactivation to more hyperpolarized potentials, β_2 subunits have a marked depolarizing effect (reviewed by Birnbaumer et al., 1998). Moreover, the responsiveness of α_1 subunits to β subunit modulation can be modified by alternative splicing of both β (Olcese et al., 1994; Qin et al., 1996) and α_1 subunits (Pan and Lipscombe, 2000; Krovetz, et al., 2000). In this study, we demonstrate for the first time that alternative splicing of the N-terminus of the β_4 subunit alters Ca^{2+} channel gating, and that this effect is specific to α_{1A} and α_{1B} subunits.

Materials and Methods

Human spinal cord library screening. Calcium channel β_4 subunits were isolated from an oligo-dT and random-primed human spinal cord λgt11 5'-Stretch Plus cDNA library (Clontech, Palo Alto, CA) using a non-radioactive digoxigenin-labeling and colorimetric detection system (Roche Molecular Biochemicals, Indianapolis, IN). The library was constructed from mRNA isolated from whole spinal cords pooled from 26 male and female Caucasians, ages 16 - 75, who died of sudden death syndrome. The insert size range of the library was 0.8 - 7.0 kb (average size 1.7 kb). Plaque-purified phage DNAs were isolated using a Lambda Prep Kit (Qiagen, Santa Clara, Ca) and digested with the restriction endonuclease EcoRI (Roche Molecular Biochemicals, supplier of all endonucleases used). All cDNA isolates were ligated into pBluescriptII (Stratagene, La Jolla, CA) for PCR-based cycle sequencing (FS chemistry; PE Biosystems, Foster City, CA) with universal and custom internal primers (Genosys, The Woodlands, TX). Sequences were obtained using an ABI Prism 310 Genetic DNA analyzer, and data were analyzed using ABI Prism DNA Sequencing Software (Version 2.12; PE Biosystems). Sequence comparisons, alignments, and restriction maps were performed using Lasergene Software (DNA Star, Madison, WI).

The library-screening process was initiated with a human brain β_4 cDNA probe obtained from the NCBI dbEST database (1.5 kb human fetal brain β_4 fragment; GenBank number R15035). Of 9 first round β_4 cDNAs isolated, the 1.6 kb β_4-7 clone was the largest, extending from nucleotide 216 to beyond an in-frame stop codon (the human brain β_4 cDNA, GenBank number U95020, was used as a reference for all β_4 nucleotide and amino acid positions). The β_4-7 clone contained 134 nucleotides of 5' untranslated

sequence. A second round of screening, using a probe consisting of the N-terminal portion of β_4-7 from an internal *Bam*HI site (550) to the 5' untranslated region, yielded 7 additional β_4 cDNAs, β_4-15 to β_4-22. Clone β_4-17 possessed an in-frame start codon and novel exon 1 sequence but lacked the last 33 nucleotides of the human brain β_4 C-terminal coding sequence. Therefore, to create a full-length β_4 cDNA, the N-terminus of the β_4-17 clone from the *Bam*HI site at nucleotide position 550 to the *Bam*HI site in the pBluescript II was ligated into a *Bam*HI prepared β_4-7 clone. Sequence analysis was used to confirm that the β_4-17/7 ligation occurred in the proper orientation. This full-length β_4 cDNA was referred to as β_{4a} (Genbank number AY054985). We used RT-PCR to isolate the previously published human brain β_4 N-terminus (U95020). An 800 bp fragment was obtained using a commercially available RT-PCR kit (Stratagene), custom oligonucleotide primers (β_4 25F: 5' CTCCGCCCACCGCACACG, and β_4 719R: 5' CTAACACCACCGGACGCAT), and human spinal cord poly- A^+ RNA (Clontech). Complete sequence analysis determined that the 800bp fragment was identical to the U95020 N-terminus, that it contained a start codon, and that it extended beyond the *Bam*HI restriction site at position 550. Therefore, to make a second full-length β_4 subunit, this fragment was cloned into a *Bam*HI prepared pBluescriptII SK+ vector containing β_4-7. Sequence analysis was used to confirm correct reading frame and proper N-terminal orientation. This full-length β_4 cDNA was referred to as β_{4b}.

Construction of $\beta_4\Delta N$, $\beta_{4a}\Delta C$, $\beta_{4b}\Delta C$, and $\beta_4\Delta N/\Delta C$ deletion mutants. A β_4 cDNA lacking exon 1 ($\beta_4\Delta N$) was obtained by using PCR to replace exon 1 of β_{4a} with an idealized Kozak sequence (Kozak M., 1991) and start codon. Custom oligonucleotide

primers $\beta_4\Delta$NF (5' GCCACCATGGGTTCAGCGGATTCC) containing the Kozak sequence and start codon, and beginning at nucleotide 215, and β_4 719R were used in a PCR reaction with the β_4-17 clone as template to generate the fragment, β_4NT(-). This fragment was then cloned into the *Bam*HI prepared β_4-7 cDNA and sequenced to confirm correct reading frame and proper N-terminal orientation. The $\beta_{4a}\Delta$C, $\beta_{4b}\Delta$C, and $\beta_4\Delta$N/ΔC cDNAs were obtained by using PCR to remove the C-terminal nucleotide sequence 3' to nucleotide 1286 (corresponding to amino acid position 404). Custom oligonucleotide primers β_4 849F (5' GCTGACATTTCTCTTGCTAA upstream of a unique *Bgl*II site) and $\beta_4\Delta$CR (5' TCAGGTTGTGTGGGTGGCAC which ended at β_4 nucleotide 1286 and included an in-frame stop codon) were used in a PCR reaction with the β_4-17 clone as template to generate the truncated fragment, β_4C(-). This fragment was then cloned into the pT-Advantage vector (Clonetch Palo Alto, CA) and sequenced to determine correct orientation. The β_4C(-) fragment was then cut with *Bgl*II and *Xho*I (from pT-Advantage poly-linker) and cloned into *Bgl*II and *Xho*I prepared β_{4a}, β_{4b}, and $\beta_4\Delta$N cDNAs. The resulting cDNAs were then sequenced with internal primers flanking the C-terminal deletion to confirm sequence orientation and fidelity.

The BI-2 (α_{1A}) and α_{2a}/δ-1 clones used in this study were provided by T. Tanabe (Tokyo Medical and Dental University, Tokyo, Japan). The rat α_{1B} and rabbit α_{1C} clones were kindly provided by D. Lipscombe (Brown University, Providence, RI) and E. Perez-Reyes (University of Virginia, Charlottesville, VA), respectively.

Electrophysiology and Data Analysis. Complementary RNAs (cRNAs) were synthesized in vitro using Ambion's mMessage mMachine® RNA transcription kit (T3 or

T7 depending on clone orientation in pBluescript II S/K+ or pBSTA (α_{1B})). Standard Xenopus laevis oocyte expression methods were used to characterize β subunit splice variants. Briefly, full-length α_1, α_2/δ, and β cRNA's were injected in equimolar ratios (5.6 ng $\alpha_{1A\ or}\ \alpha_{1B}$, 2.4 ng α_{2a}/δ, and 1.6 ng β in 46 nl; 17ng $\alpha_{1C\ or}\ \alpha_{1E}$, 7 ng α_{2a}/δ, and 5 ng β in 50nl) into defolliculated oocytes (stage V-VI). Calcium channel currents were recorded 2-8 days after oocyte injection by standard two-electrode voltage clamp using a Warner amplifier (OC-725B) at 20-22°C, and data were collected using pCLAMP6 software (Axon Instruments, Foster City, CA). Microelectrodes were filled with 3M KCl, and the resistances of the current and voltage electrodes were 0.3-1.5 MΩ. Data were filtered at 2 kHz and sampled at 10 kHz. Currents were recorded in a chloride-free bath containing 5 mM $Ba(OH)_2$, 5 mM HEPES, 85 mM TEA-OH, and 2 mM KOH, pH adjusted to 7.4 with methansulfonic acid (α_{1A} and α_{1B}) or 40 mM $Ba(OH)_2$, 5 mM HEPES, 85 mM TEA-OH, and 2 mM KOH, pH adjusted to 7.4 with methansulfonic acid (α_{1C} and α_{1E}). Currents used to generate the data in this study ranged from 0.5 μA to 2.9 μA. For activation and inactivation experiments, the average current sizes for α_{1A} and α_{1B} complexes containing either β_{4a} or β_{4b} were 1.2μA and 1.6μA, respectively. Leak currents were between 20 nA and 100 nA. Only recordings with minimal tail currents were used for each data set (see representative traces in Figure 3.5). Data were analyzed using pCLAMP6 software (Axon Instruments) and Excel 7.0 (Microsoft Corp., Redmond WA). The leak and capacitive currents were subtracted on line using a standard P/4 protocol. Boltzmann fits to the activation and inactivation data were performed using Sigma Plot version 5.0 (SSPS Inc., Chicago IL) with the equations $\%I_{Ba} = 1/[1 + \exp(-$

$(V_{test} - V_{1/2})/k)]$ and $\%I_{Ba} = 1/[1 + \exp((V_{pre} - V_{1/2})/k)]$, respectively, where V_{test} = I-V test potential, V_{pre} = prepulse potential, $V_{1/2}$ = midpoint of activation or inactivation, and k = slope factor. An estimate of gating charge, z, was calculated by dividing 25 (approximate value for RT/F at room temperature, where R = gas constant, T = temperature, and F = Faraday constant) by the slope factor. Statistical analysis was performed with a students two-sample equal variance t-test with a two-tailed distribution (Microsoft®Excel 97 SR-2). Data are presented as mean ± SEM.

Results

Cloning of a Ca^{2+} channel β_4 subunit with an N-terminus similar to that of β_3 subunits

Two β_4 subunit N-terminal splice variants, β_{4a} and β_{4b} (Figure 3.1) are the focus of this study. Both were isolated from a human spinal cord cDNA library using routine screening techniques. The amino acid sequence of the β_{4b} variant is identical to a previously published sequence (GenBank- U95020), whereas this is the first reporting of the β_{4a} sequence. The difference in the two variants lies solely in the nucleotide sequence of exon 1, the translated region of which is referred to as domain D1 (Birnbaumer et al., 1998). The remaining sequence of both β_{4a} and β_{4b} is composed of 1410 nucleotides that encode the 470 amino acids of domains 2-5 (data not shown). As shown in Figure 3.1, exon 1 of β_{4a} encodes a 15 amino acid sequence that is highly homologous to the N-terminal sequences of several previously identified Ca^{2+} channel β_3 subunits. This indicates that β_{4a} exon 1 must have been present in the genome prior to the time that an

ancestral gene duplicated to form distinct β_3 and β_4 genes. Interestingly, amino acids 5 – 11 (LYLHGIE) are identical to those found in the *Xenopus* β subunit, xβ_{32}, but quite divergent from the same region of the human β_3 subunit. This could imply that a particular function of this sequence has been purposely conserved throughout evolution. Also of note in the human β_{4a} sequence are two D to N conversions at positions 4 and 12 (*asterisks*) that eliminate two negative charges that appear to be highly conserved among β_3 subunits. Figure 3.1 also demonstrates that D1 of β_{4a} is not at all homologous to D1 of β_{4b}. It can be seen, however, that D1 of β_{1b} and β_{4b} are more closely related than D1 of β_{4a} and β_{4b}. Domain 1 of β_{4b} contains 49 amino acids, 2 of which are negatively charged, and 8 of which are positively charged. Six of these positive charges are clustered in the center of the sequence close to consensus sites (TTR and TRR) for phosphorylation by protein kinase C. No further Prosite-listed consensus sites were found in the D1 sequences of either β_{4a} or β_{4b}.

Alternative splicing of the β_4 subunit N-terminus affects Ca^{2+} channel expression

Critical to the interpretation of our expression data is the fact that some populations of *Xenopus* oocytes have been shown to express low levels of an endogenous β_3-like subunit that is capable of binding to and altering the gating properties of injected α_1 subunits (Tareilus et al., 1997). To test for this possibility in our oocytes, we conducted experiments in which we measured the time required for $\alpha_{1A}/\alpha_2\delta$, $\alpha_{1A}/\alpha_2\delta$ + β_{4a}, and $\alpha_{1A}/\alpha_2\delta$ + β_{4b} complexes to reach levels of expression that we thought suitable for electrophysiological recording (1 μA of peak current). Figure 3.2 shows that channel

complexes containing β_{4b} expressed at a much faster rate than those containing β_{4a}, reaching adequate levels within 1-2 days. Complexes containing β_{4a} took 3-4 days to reach similar levels, whereas complexes that did not contain a β subunit required 7 – 8 days to express 1 μA of current. Similarly, $\alpha_{1B}/\alpha_2\delta + \beta_{4b}$ complexes reached adequate levels in 1-2 days, while $\alpha_{1B}/\alpha_2\delta + \beta_{4a}$ complexes took 3-4 days to reach similar levels. Alpha 1B complexes expressed without β_4 subunits did not reach suitable current size until day 7-8 (data not shown). Alpha $_{1C}/\alpha_2\delta$ and $\alpha_{1E}/\alpha_2\delta$ expressed with either β_{4a} or β_{4b} reached adequate current size in 6-8 days while complexes without β_4 subunits showed no appreciable current even after 8 days. Expression rates and levels for $\alpha_{1C}/\alpha_2\delta$ and $\alpha_{1E}/\alpha_2\delta + \beta_{4a}$ and β_{4b} were essentially identical (data not shown). As shown in Figure 3.2, a 6-fold increase in the amount of β subunit cRNA injected into oocytes relative to that of α_{1A} did not affect expression rates or levels, suggesting that β subunit binding sites on α_{1A} are saturated even when the two subunits are co-injected at a 1:1 ratio. This is consistent with the findings of Qin et al. (1996). We concluded from these experiments that the endogenous *Xenopus* β_3-like subunit would not significantly influence the examination of exogenous currents measured in the 2-6 day time period.

Alternatively spliced β_4 subunits have α_1-subunit subtype-specific effects on voltage-dependent activation and inactivation

To determine whether β_4 N-terminal splicing affected Ca^{2+} channel gating properties, we expressed either β_{4a} or β_{4b} with rabbit $\alpha_2\delta -1$ and either rabbit α_{1A} (BI-2, Mori et al., 1991), rat α_{1B} (Δ21 α_{1B}, Pan and Lipscombe, 2000), rabbit α_{1C} (Mikami et al.,

1989) or marine ray α_{1E} (doe-1, Horne et al., 1993) in *Xenopus* oocytes. (The $\alpha_2\delta$-1 subunit is included in all experiments in this study). Figure 3.3 *A, B, E* and *F* show comparisons of normalized current-voltage (*I-V*) curves for the four different α_1 subunits expressed with either β_{4a} or β_{4b}. Figure 3.3*A* and *B* illustrate that the peaks of the current-voltage curves for α_{1A} and α_{1B} complexes containing β_{4b} were shifted to more hyperpolarized potentials relative to complexes containing β_{4a}. In contrast, Figure 3.3*E* and *F* show that the *I-V* curves for α_{1C} and α_{1E} complexes containing either β_{4a} or β_{4b} were essentially superimposed. The difference in α_1 subunit responsiveness was not due to differences in charge carrier concentrations used in the experiments (5 mM Ba^{2+} for α_{1A} and α_{1B}; 40 mM Ba^{2+} for α_{1C} and α_{1E}), as we observed identical hyperpolarizing shifts for both α_{1A} and α_{1B} with β_{4b} even in 40 mM Ba^{2+} (data not shown). We concluded from these first experiments that alternative splicing of the β_4 subunit N-terminus affects activation of Ca^{2+} channel complexes containing α_{1A} and α_{1B} subunits, but not those containing α_{1C} or α_{1E}. To estimate the $V_{1/2}$ of activation for the different α_{1A} and α_{1B} combinations, we averaged Boltzmann fits to the *I-V* data generated over the range of -40 to + 10 mV for α_{1A} complexes and – 40 to + 20 mV for α_{1B} complexes containing either β_{4a} or β_{4b} (Figure 3.3*C* and *D*). The results show that the $V_{1/2}$ of activation for both α_{1A} and α_{1B} complexes containing β_{4b} were shifted to the left relative to complexes containing β_{4a} by ~ 5 mV and ~ 7 mV, respectively (Table 3.1). The results also show that the slopes of the β_{4b} fits were somewhat steeper than for β_{4a}.

We next examined whether alternative splicing of the β_4 subunit affected steady-state inactivation. We used a 20-second conditioning prepulse over a wide range of

potentials followed by a 300 msec test pulse to near-peak potentials to generate the data. We found that extending the prepulse duration to 60 seconds had no effect on the results (data not shown), indicating that steady-state was achieved for all subunit combinations within 20 seconds. Figure 3.4 *A-D* shows that, as was the case for activation, alternative splicing of the β_4 subunit N-terminus affects inactivation of Ca^{2+} channel complexes containing α_{1A} and α_{1B} subunits, but not those containing α_{1C} or α_{1E}. The figure illustrates that the voltage-dependence of inactivation of both α_{1A} (Figure 3.4*A*) and α_{1B} (Figure 3.4*B*) complexes containing β_{4b} was shifted to more hyperpolarized potentials relative to complexes containing β_{4a}. In contrast, inactivation curves for α_{1C} (Figure 3.4*C*) and α_{1E} (Figure 3.4D) complexes containing β_{4a} or β_{4b} were essentially identical. The Boltzmann-derived $V_{1/2}$ for inactivation of both α_{1A} and α_{1B} complexes containing β_{4b} were shifted to the left relative to complexes containing β_{4a} by ~ 10 – 11 mV (Table 3.1). Interestingly, the hyperpolarizing shift in $V_{1/2}$ for α_{1A} complexes (Figure 3.4*A*) occured as the result of a parallel shift in the voltage-dependence of inactivation, whereas for α_{1B} complexes (Figure 3.4*B*), the shift in $V_{1/2}$ occurred primarily as the result of a change in slope. Slope factors for α_{1B} complexes containing β_{4a} and β_{4b} complexes were ~ 14mV and 7 mV, respectively (Table 3.1).

Since α_{1C} and α_{1E} subunits were not affected by alternative splicing of β_4 subunits, we next directed our experiments toward characterizing the α_{1A} and α_{1B} responses in more detail. Figure 3.5 shows representative current *traces* of α_{1A} (Figure 3.5*A*) and α_{1B} (Figure 3.5*B*) complexes containing either β_{4a} (*top*) or β_{4b} (*bottom*) expressed in *Xenopus* oocytes. *Traces* shown were generated by step depolarization to –10, 0, 10, 20 and 30

mV. The *arrows* indicate that the potentials at which peak currents were reached varied with each complex. Regardless of the α_1 subunit subtype, however, complexes containing β_{4a} inactivated faster than those containing $\beta_{4b,}$ with a difference in rates being more apparent for complexes containing α_{1B}. Figures 3.5*C* and *D* show the averaged currents remaining after 300 msec (R300) step depolarizations to each potential for α_{1A} and α_{1B}, respectively. The results indicate that the rate of inactivation for all four complexes is voltage dependent, and that the differences in rates between complexes containing β_{4a} versus β_{4b} becomes apparent primarily with depolarizations beyond 0 mV.

α_1 subunit-specific responses to β_4 subunit N- and C- terminal deletions

The results to this point indicated that the N-terminus of the β_4 subunit plays an important role in setting the kinetics and voltage-dependence of Ca^{2+} channel gating, with some differences in responsiveness noted between α_{1A} and α_{1B} subunits. We next sought to determine whether the β_4 N-terminus could be acting in concert with the β_4 C-terminus to exert its effects on gating. Since previous studies had shown that the β_4 C-terminus binds directly to the α_{1A} subunit (Walker et al., 1998, 1999), it was of particular interest to determine whether the gating properties of α_{1A} would change in comparison to α_{1B} if the β_4 C-terminus were deleted. To address this issue, we made four β_4 subunit deletion constructs that along with β_{4a} and β_{4b} provided us with all the possible +/- combinations of β_4 N- and C-termini (Figure 3.6*A*). We found that all four constructs augmented Ca^{2+} channel expression to a level that was comparable to or exceeded (i.e. $\beta_4\Delta N\Delta C$) the expression levels we observed with β_{4b}. The effects of these constructs on activation and

inactivation of α_{1A} and α_{1B} subunits are shown in Figure 3.6*B* and *C* and Figure 3.7*A* and *B*, respectively. (Our initial results with β_{4a} and β_{4b} are included as dashed lines for reference in Figure 3.6 and 3.7). Interestingly, it was readily apparent from both the activation and inactivation results shown in Figure 3.6 and 3.7, that despite testing six different β_4 subunit constructs, our data could be grouped into two activation modes, A_1 and A_2 (α_{1A} and α_{1B}), and two (α_{1B}) or three (α_{1A}) inactivation modes, I_1 - I_3, based on curve position alone. As can be seen from the data, the distinction between activation and inactivation modes was most clearly delineated in experiments involving α_{1B} (Figure 3.6*C* and 3.7*B*). Table 3.1 shows that the distinction between modes is quite evident when comparing Boltzmann-derived values for $V_{1/2}$ and slope factor, and along with Figure 3.6 and 3.7 reveals that the β_4 subunit constructs responsible for setting each mode differ between α_{1A} and α_{1B} subunits.

The details of the deletion results are best understood by examining in sequence the data we obtained with individual β subunit constructs. Our first experiments were directed toward determining what effect deletion of both the β_4 N- and C- terminus ($\beta_4\Delta N\Delta C$) would have on α_{1A} and α_{1B} gating properties. Unexpectedly, both α_{1A} and α_{1B} complexes containing the $\beta_4\Delta N\Delta C$ subunit had activation properties very similar to complexes containing full-length β_{4b} (mode A_1, Figure 3.6*B* and 3.6*C*). This indicated that α_1 subunits could not distinguish β_4 subunits without an N- or C-terminus from β_4 subunits with the longer form of N-terminus and the C-terminus present. Relative to α_1 complexes containing $\beta_{4a,}$ however, $\beta_4\Delta N\Delta C$ caused a 6-7 mV hyperpolarizing shift and a slight increase in slope of activation of both α_{1A} and α_{1B} (Table 3.1). Figure 3.7*A* and *B*

show that, while the inactivation curve for α_{1A} complexes containing $\beta_4\Delta N\Delta C$ fell between those for complexes containing β_{4a} and β_{4b}, the inactivation properties of α_{1B} complexes containing $\beta_4\Delta N\Delta C$ and β_{4b} were also indistinguishable. For both α_{1A} and $\alpha_{1B,}$ it can be seen that relative to complexes containing β_{4a}, $\beta_4\Delta N\Delta C$ caused a qualitatively similar hyperpolarizing shift in the voltage dependence of inactivation and decrease in slope (shift from mode I_2 to mode I_1). As shown in Figure 3.7*B*, this effect was most dramatic for α_{1B} complexes, where relative to β_{4a}, $\beta_4\Delta N\Delta C$ caused a ~ 10 mV hyperpolarizing shift in inactivation and a nearly 50% decrease in slope (Table 3.1).

We next characterized the effects of the construct $\beta_4\Delta N$ ($\beta_4\Delta N\Delta C$ plus the β_4 C-terminus) on the gating properties of α_{1A} and α_{1B} subunits. Interestingly, as shown in Figure 3.6*A* and *B*, the $\beta_4\Delta N$ construct had different effects on activation of α_{1A} as compared to α_{1B}. Whereas addition of the C-terminus had a depolarizing effect on α_{1A} activation relative to β_{4b} and $\beta_4\Delta N\Delta C$, there was no change in the activation properties of α_{1B}. Moreover, as can be seen in Figure 3.6*B* and Table 3.1, the activation properties of α_{1A} complexes containing $\beta_4\Delta N$ were essentially identical to those containing β_{4a} (mode A_2). Similarly, as shown in Figure 3.7*A* and *B*, $\beta_4\Delta N$, like β_{4a}, had a noticeable depolarizing effect on α_{1A} inactivation (mode I_2) relative to complexes containing $\beta_4\Delta N\Delta C$, but caused no change in the inactivation properties of α_{1B}. These results indicated that, at least in the absence of the N-terminus, the β_4 C-terminus has α_{1A} subunit-specific effects on the voltage dependence of both activation and inactivation.

To define further the role of the β_4 N-termini in gating, we next characterized the effects of two constructs, $\beta_{4a}\Delta C$ and $\beta_{4b}\Delta C$, that lacked the β_4 C-terminus but contained

the N-termini of β_{4a} and β_{4b}, respectively ($\beta_4\Delta N\Delta C$ plus β_{4a} or β_{4b} N-terminus). Interestingly, the pattern of results that we obtained with these constructs was, in many respects, just the opposite of what we saw with $\beta_4\Delta N$. While $\beta_4\Delta N$ had α_{1A} subunit-specific effects on gating, $\beta_{4a}\Delta C$ and $\beta_{4b}\Delta C$ had, for the most part, α_{1B} subunit-specific effects. Figure 3.6*A* shows that relative to $\beta_4\Delta N\Delta C$, $\beta_{4b}\Delta C$, like β_{4a}, caused a depolarizing shift in activation of α_{1A} subunits, but $\beta_{4a}\Delta C$ was without effect. Figure 3.7*A* shows that relative to $\beta_4\Delta N\Delta C$, neither $\beta_{4a}\Delta C$ nor $\beta_{4b}\Delta C$ had effects on inactivation of α_{1A} subunits. In contrast, Figure 3.6*B* and 7*B* show that relative to $\beta_4\Delta N\Delta C$ both $\beta_{4a}\Delta C$ and $\beta_{4b}\Delta C$ caused a depolarizing shift in activation and inactivation of α_{1B}. Moreover, the gating properties of α_{1B} complexes containing $\beta_{4a}\Delta C$ or $\beta_{4b}\Delta C$ were essentially identical to those containing β_{4a} (modes A_2 and I_2). The results of these experiments indicate that, at least in the absence of the C-terminus, the β_{4b} but not the β_{4a} N-terminus has effects on α_{1A} activation, while neither affects α_{1A} inactivation. In contrast, both the β_{4a} and β_{4b} N-termini have effects on α_{1B} activation and inactivation.

With the results from the deletion experiments, it was informative to reexamine the data from our initial experiments (dashed lines in Figure 3.6 and 7) with the idea that full-length β_{4a} and β_{4b} subunits were constructed by adding back the β_{4a} and β_{4b} N-termini to $\beta_4\Delta N$. As the data reveals, this also had α_1 subunit-specific effects on both activation and inactivation. With respect to activation, Figure 3.6*A* shows that, relative to $\beta_4\Delta N$, adding back the β_{4a} N-terminus had no effect on α_{1A} activation, suggesting that the short form of the N-terminus could not overcome the α_{1A}-specific β_4 C-terminal effect noted with $\beta_4\Delta N$ previously. Adding back the β_{4b} N-terminus, however, did supercede the C-

terminal effect and caused a hyperpolarizing shift in α_{1A} activation relative to $\beta_4\Delta N$ (back to mode A_1). In contrast, Figure 3.6*B* shows that adding back the β_{4a} N-terminus to $\beta_4\Delta N$ caused a depolarizing shift in the activation of α_{1B} (back to mode A_2), but adding back the β_{4b} N-terminus had no effect. This goes along with the $\beta_4\Delta N$ data showing that with α_{1B} there is no β_4 C-terminal effect to overcome, and that the β_{4a} N-terminus alone causes an α_{1B}-specific depolarizing shift in activation. With respect to inactivation, Figure 3.7*B* shows that, as was the case for activation, adding back the β_{4a} N-terminus to $\beta_4\Delta N$ had little effect on α_{1A} inactivation, but adding back the β_{4b} N-terminus caused a significant hyperpolarizing, and in this case, parallel shift in the curve for α_{1A} inactivation (mode I_3). It is worth noting that this shift is different from, and goes beyond the curve for $\beta_4\Delta N\Delta C$, and that this effect on α_{1A} gating is unique to β_{4b}. Figure 3.7*B* shows that, as expected from the $\beta_{4a}\Delta C$ results with α_{1B}, without a C-terminal effect to overcome, adding back the β_{4a} N-terminus to $\beta_4\Delta N$ caused a depolarizing shift in α_{1B} inactivation (back to mode I_2). Not expected, however, was the result that adding back the β_{4b} N-terminus had no effect, recalling that the β_{4b} N-terminus alone causes a depolarizing shift in α_{1B} inactivation. This suggests that the presence of the β_4 C-terminus, though not having effects on its own, interferes in some way with the ability of the β_{4b} N-terminus to influence α_{1B} channel gating.

Discussion

Our results provide the first evidence that alternative splicing of the β_4 subunit alters Ca^{2+} channel gating, and that this effect is specific to α_{1A} and α_{1B} subunits. The

physiological relevance of our findings lies in the fact that α_{1A}, α_{1B} (Westenbroek et al., 1998), and β_4 subunits (Wittemann et al., 2000) colocalize in nerve terminals, and that α_{1A} and β_4 (Liu et al., 1996) and α_{1B} and β_4 subunits (Scott et al., 1996) are directly associated. In many respects, our experiments were similar to those of Olcese et al. (1994) and Qin et al. (1996), which characterized the effects of a variety of β subunit splice variants, chimeras, and deletion mutants on human α_{1E} subunit gating. Their studies yielded five results pertinent to our findings. 1) Relative to α_{1E} alone, all β subunit constructs tested caused a nearly identical hyperpolarizing shift in the $V_{1/2}$ of activation and decrease in slope factor. (See also Jones et al., 1998). 2) Deletion of the N-terminus of the β_{1b}, β_{2a} and β_3 subunits had no effect on the fast component of activation. 3) Alternative splicing of the N-terminus, C-terminus and/or internal domain 3 of β_1 and β_2 subunits had opposing effects on the $V_{1/2}$ of steady-state inactivation, but did not affect slope. 4) Deletion of the N-terminus of the β_{1b} and β_3 subunits caused a depolarizing shift in the $V_{1/2}$ of inactivation without affecting slope, while deletion of the N-terminus of the β_{2a} subunit caused a hyperpolarizing shift. 5) C–terminal alternative splicing did not affect gating properties. The principal conclusion of these experiments was that, independent of effects on activation, the N-terminus of the β subunit plays a dominant role in governing the voltage sensitivity of α_{1E} subunit inactivation. This suggested to the authors that there were two separate α_1 and β subunit interaction sites regulating activation and inactivation.

Our results point similarly to the N-terminus of the β_4 subunit as a key determinant of α_{1A} and α_{1B} gating properties, but show some dissimilarity to the five α_{1E}

results listed above. 1) Unlike α_{1E} with β_1- β_3 subunits, alternatively spliced β_4 subunits had differential effects on activation of both α_{1A} and α_{1B}. Relative to the short β_{4a} N-terminus, the longer β_{4b} form caused a hyperpolarizing shift in activation of both α_{1A} and α_{1B} subunits (but not α_{1C} or α_{1E}). 2) Relative to β_{4b}, deletion of the N-terminus of the β_4 subunit caused a depolarizing shift in activation of α_{1A} but not α_{1B}. 3) Alternative splicing of the β_4 subunit affected both the $V_{1/2}$ and slope of inactivation of α_{1B}, while only shifting the $V_{1/2}$ of α_{1A} inactivation without a change in slope. Alternative splicing of the β_4 subunit did not affect inactivation of α_{1C} or α_{1E}. 4) Relative to β_{4b}, deletion of the N-terminus of the β_4 subunit caused a depolarizing shift in inactivation of α_{1A} but not α_{1B}. 5) C-terminal deletion experiments revealed that the β_4 N- and C-termini work in concert to set gating parameters of α_{1A} and α_{1B} subunits. Taken together, these results indicate that alternatively spliced β subunits can affect both activation and inactivation of Ca^{2+} channels, and the responsiveness of Ca^{2+} channels to β subunit splicing varies with α_1 subunit subtype.

To explain our results, we devised a structural model for potential α_1-β_4 subunit domain interactions based on a β subunit modular structure (Domains A-E, Hanlon et al., 1999) and actual molecular weights of the potential α_{1A} and β subunit domains involved (Figure 3.8). Though highly speculative, the model integrates related structure-function results from a number of different laboratories that point to the β subunit D domain interaction with the α_1 subunit I-II linker as a key determinant of Ca^{2+} channel gating properties (Herlitze et al., 1997; Bourinet et al., 1999; Stotz et al., 2000; Berrou et al., 2001). Moreover, it incorporates results showing that regulation of activation and

inactivation are separable functions of β subunits (Olcese et al., 1994). Of particular relevance to our model are studies showing that the β_1 subunit D domain was all that was required to reproduce the inactivation rate of L-type channels coexpressed with full-length β_1 (Cens et al., 1999). And that a single point mutation (R378E) in the β subunit binding site of the α_1 I-II linker (AID domain) had a depolarizing effect on the voltage dependence of both activation and inactivation of an α_{1E} subunit (Berrou et al., 2001).

Previous studies have shown that the D domain of the β_4 subunit binds with high affinity to the α_{1A} I - II linker (Pragnell et al., 1994), and that the E domain of the β_4 subunit binds to both the N- and C-terminus of the α_{1A} subunit (Walker et al., 1998 & 1999). As shown in Figure 3.8, this indicates that the D and E domains likely establish the N- to C-terminal orientation of the β_4 subunit relative to the α_{1A} subunit. Though little is known about β subunit N-terminus interactions with the α_1 subunit, a modular structure for the β subunit A, B, and C domains suggests that the interactions could occur over a wide range. As suggested in Fig 3.8, a change in the size and/or sequence of the β subunit A domain could have an effect on the way the β subunit D domain interacts with the α_1 I-II linker. Such a change might be responsible for the different gating properties observed between Ca^{2+} channel complexes containing β_{4a} versus β_{4b}.

The salient feature of the model is that a core β subunit structure encoded by exons 2-12 ($\beta_4\Delta N\Delta C$), through interactions with the α_1 subunit I - II linker, sets separate default parameters for α_1 activation and inactivation (mode A_1I_1, Table 3.2). This mode likely represents a specific α_1 I-II linker conformation that, through its connection to the α_1 IS6 transmembrane domain, influences the mobility of the gating charges within α_1

IS4 (Zhang et al., 1994). (The effects of β_4 N-terminal alternative splicing on apparent gating charge (z value) are shown in Table 3.1. Note the significant difference in calculated *z* values during inactivation of α_{1B} complexes containing β_{4a} versus β_{4b}). As shown in Table 3.2, in mode A_1I_1 the two presumed α_1 and β subunit interaction domains are in alignment (α_1, filled symbols; β, open symbols). Changes from default parameters occur when either the β subunit N- or C- terminus, or both, interact with, or are acted upon by, other regions of the α_1 subunit such that the I-II linker changes mode conformations. For example, in mode A_2I_2 (Row 2), the two presumed α_1 and β subunit interaction domains would be out of alignment. Displacing the β subunit D-domain in either the C-terminal or N-terminal direction would enable mode 2 conformation, while a balance of these two forces favors mode 1.

Describing our data in terms of the model (Table 3.2), the default activation and inactivation parameters of α_{1A} and α_{1B} complexes containing $\beta_4\Delta N\Delta C$ are denoted as mode A_1I_1 (Row 1). Steep activation and shallow inactivation typify this mode. Row 2 shows that adding back the C-terminus to $\beta_4\Delta N\Delta C$ ($\beta_4\Delta N$) shifts α_{1A} complexes to mode A_2I_2, while α_{1B} complexes remain in mode A_1I_1. This could be explained by the α_{1A} - β_4 C-terminal binding event described by Walker et al., (1998 and 1999) causing the β_4 D-domain to be displaced in the C-terminal direction. Relative to mode A_1I_1, activation in mode A_2I_2 is shallower and inactivation is steeper. Rows 3 and 4 show that by adding back the N-terminus, α_{1B} complexes containing either the $\beta_{4a}\Delta C$ or $\beta_{4b}\Delta C$ construct shift to mode A_2I_2. This shift might be explained by β_4 N-terminal-α_{1B} interactions causing the β_4 D-domain to be displaced in the N-terminal direction. Alternatively, steric changes

resulting from the presence of the N-terminus may shift the β_4 D-domain in the C-terminal direction (Row 4, $\beta_{4b}\Delta C(\alpha_{1B})$). Whatever the cause, it is likely to be different for α_{1B} complexes containing $\beta_{4a}\Delta C$ versus $\beta_{4b}\Delta C$. Adding back the C-terminus to $\beta_{4a}\Delta C$ has no effect on α_{1B} mode A_2I_2 (Row 5), whereas addition of the C-terminus to $\beta_{4b}\Delta C$ causes a shift to mode A_1I_1 (Row 6). Row 4 also shows that $\beta_{4b}\Delta C$ causes an α_{1A} subunit mode change that is limited to activation (A_2I_1). This was the one instance in our experiments in which regulation of activation and inactivation were separable functions. The addition of the C-terminus to $\beta_{4a}\Delta C$ shifts α_{1A} to mode A_2I_2 (Row 5), which again, is likely the result of a β_4 C-terminal binding event. The addition of the C-terminus to $\beta_{4b}\Delta C$ creates a distinct α_{1A} mode, A_1I_3 characterized by steep activation and inactivation.

In conclusion, our results add to the developing picture of the intracellular domains surrounding the Ca^{2+} channel pore being composed of modular "hot spots" for channel regulation by β-subunits, protein kinases, G-proteins, syntaxin, and calmodulin (reviewed by Walker and DeWaard, 1998 and Levitan, 1999). Our future experiments will be directed toward understanding how interactions between these diverse regulatory components might contribute to the dynamic molecular events giving rise to synaptic plasticity.

References

Berrou L, Bernatchez G, Parent L (2001) Molecular determinants of inactivation within the I-II linker of α_{1E} (CaV2.3) calcium channels. Biophys J 215-228.

Birnbaumer L, Qin N, Olcese R, Tareilus E, Platano D, Costantin J, Stefani E (1998) Structures and functions of calcium channel β subunits. J Bioenerg Biomembr 30:357-375.

Bourinet E, Soong TW, Sutton K, Slaymaker S, Mathews E, Monteil A, Zamponi GW, Nargeot J, Snutch TP (1999) Splicing of α_{1A} subunit gene generates phenotypic variants of P- and Q-type calcium channels. Nat Neurosci 2:407-415.

Cens T, Restituito S, Charnet P (1999) Regulation of Ca-sensitive inactivation of a L-type Ca^{2+} channel by specific domains of β subunits. FEBS Lett 450:17-22.

De Waard M, Campbell KP (1995) Subunit regulation of the neuronal α_{1A} Ca^{2+} channel expressed in Xenopus oocytes. J Physiol 485:619-34.

Ellinor PT PT, Zhang JF, Randall AD, Zhou M, Schwarz TL, Tsien RW, Horne WA (1993) Functional expression of a rapidly inactivating neuronal calcium channel. Nature 363:455-458.

Fanning AS, Anderson JM (1999) Protein modules as organizers of membrane structure. Curr Opin Cell Biol 11:432-439.

Hanlon MR, Berrow NS, Dolphin AC, Wallace BA (1999) Modelling of a voltage-dependent Ca^{2+} channel β subunit as a basis for understanding its functional properties. FEBS Lett 445:366-370.

Herlitze S, Hockerman GH, Scheuer T, Catterall WA (1997) Molecular determinants of inactivation and G protein modulation in the intracellular loop connecting domains I and II of the calcium channel α_{1A} subunit. Proc Natl Acad Sci USA 94:1512-1516.

Horne WA, Ellinor PT, Inman I, Zhou M, Tsien RW, Schwarz TL (1993) Molecular diversity of Ca^{2+} channel α_1 subunits from the marine ray *Discopyge ommata*. Proc Natl Acad Sci USA 90:3787-3791.

Jones LP, Wei SK, Yue DT (1998) Mechanism of auxiliary subunit modulation of neuronal α_{1E} calcium channels. J Gen Physiol 112:125-143.

Kozak M (1991) An analysis of vertebrate mRNA sequences: intimations of translational control. J Cell Biol 115:887-903.

Krovetz HS, Helton TD, Crews AL, Horne WA (2000) C-Terminal alternative splicing changes the gating properties of a human spinal cord calcium channel α_{1A} subunit. J Neurosci 20:7564-7570.

Lacerda AE, Kim HS, Ruth P, Perez-Reyes E, Flockerzi V, Hofmann F, Birnbaumer L, Brown AM (1991) Normalization of current kinetics by interaction between the α_1 and β subunits of the Nature 352:527-530.

Letts VA, Felix R, Biddlecome GH, Arikkath J, Mahaffey CL, Valenzuela A, Bartlett FS 2nd, Mori Y, Campbell KP, Frankel WN (1998) The mouse stargazer gene encodes a neuronal Ca^{2+} channel γ subunit. Nat Genet 19:340-347.

Levitan IB (1999) It is calmodulin after all! Mediator of the calcium modulation of multiple ion channels. Neuron 22:645-648.

Liu H, De Waard M, Scott VE, Gurnett CA, Lennon VA, Campbell KP (1996) Identification of three subunits of the high affinity omega-conotoxin MVIIC-sensitive Ca^{2+} channel. J Biol Chem 271:13804-13810.

Mikami A, Imoto K, Tanabe T, Niidome T, Mori Y, Takeshima H, Narumiya S, Numa S (1989) Primary structure and functional expression of the cardiac dihydropyridine-sensitive calcium channel. Nature 340:230-233.

Mori Y, Friedrich T, Kim MS, Mikami A, Nakai J, Ruth P, Bosse E, Hofmann F, Flockerzi V, Furuichi T, Mikoshiba K, Imoto K, Tanabe T and Numa S (1991) Primary structure and functional expression from complementary DNA of a brain calcium channel. Nature 350:398-402.

Olcese R, Qin N, Schneider T, Neely A, Wei X, Stefani E, Birnbaumer L (1994) The amino terminus of a calcium channel β subunit sets rates of channel inactivation independently of the subunit's effect on activation. Neuron 13:1433-1438.

Pan JQ, Lipscombe D (2000) Alternative splicing in the cytoplasmic II-III loop of the N-type Ca^{2+} channel α_{1B} subunit: functional differences are β subunit-specific. J Neurosci 20:4769-4775.

Pragnell M, De Waard M, Mori Y, Tanabe T, Snutch TP, Campbell KP (1994) Calcium channel β-subunit binds to a conserved motif in the I-II cytoplasmic linker of the α_1-subunit. Nature 368:67-70.

Qin N, Olcese R, Zhou J, Cabello OA, Birnbaumer L, Stefani E (1996) Identification of a second region of the β subunit involved in regulation of calcium channel inactivation. Am J Physiol 271:C1539-1545.

Singer D, Biel M, Lotan I, Flockerzi V, Hofmann F, Dascal N (1991) The roles of the subunits in the function of the calcium channel. Science 253:1553-1557.

Scott VE, De Waard M, Liu H, Gurnett CA, Venzke DP, Lennon VA, Campbell KP (1996) β subunit heterogeneity in N-type Ca^{2+} channels. J Biol Chem 271:3207-3212.

Stotz SC, Hamid J, Spaetgens RL, Jarvis SE, Zamponi GW (2000) Fast inactivation of voltage-dependent calcium channels. A hinged-lid mechanism? J Biol Chem 275:24575-24582.

Takahashi T, Momiyama A (1993) Different types of calcium channels mediate central synaptic transmission. Nature 366:156-158.

Tareilus E, Roux M, Qin N, Olcese R, Zhou J, Stefani E, Birnbaumer L (1997) A *Xenopus* oocyte β subunit: evidence for a role in the assembly/expression of voltage-gated calcium channels that is separate from its role as a regulatory subunit. Proc Natl Acad Sci USA 94:1703-1708.

Turner TJ, Adams ME, Dunlap K (1992) Calcium channels coupled to glutamate release identified by omega-Aga-IVA. Science 258:310-313.

Walker D, Bichet D, Campbell KP, De Waard M (1998) A β_4 isoform-specific interaction site in the carboxyl-terminal region of the voltage-dependent Ca^{2+} channel α_{1A} subunit. J Biol Chem 273:2361-2367.

Walker D, Bichet D, Geib S, Mori E, Cornet V, Snutch TP, Mori Y, De Waard M (1999) A new β subtype-specific interaction in α_{1A} subunit controls P/Q-type Ca^{2+} channel activation. J Biol Chem. 274:12383-12390.

Walker D, De Waard M (1998) Subunit interaction sites in voltage-dependent Ca^{2+} channels: role in channel function. Trends Neurosci 21:148-154.

Westenbroek RE, Ahlijanian MK, Catterall WA (1990) Clustering of L-type Ca^{2+} channels at the base of major dendrites in hippocampal pyramidal neurons. Nature 347:281-284.

Westenbroek RE, Hoskins L, Catterall WA (1998) Localization of Ca^{2+} channel subtypes on rat spinal motor neurons, interneurons, and nerve terminals. J Neurosci 18:6319-6330.

Wheeler DB, Randall A, Tsien RW (1994) Roles of N-type and Q-type Ca^{2+} channels in supporting hippocampal synaptic transmission. Science 264:107-111.

Wittemann S, Mark MD, Rettig J, Herlitze S (2000) Synaptic localization and presynaptic function of calcium channel β_4 subunits in cultured hippocampal neurons. J Biol Chem 275:37807-37814.

Wu LG, Westenbroek RE, Borst JG, Catterall WA, Sakmann B (1999) Calcium channel types with distinct presynaptic localization couple differentially to release in single calyx-type synapses. J Neurosci 19:726-736.

Zhang JF, Ellinor PT, Aldrich RW, Tsien RW (1994) Molecular determinants of voltage-dependent inactivation in calcium channels. Nature 372:97-100.

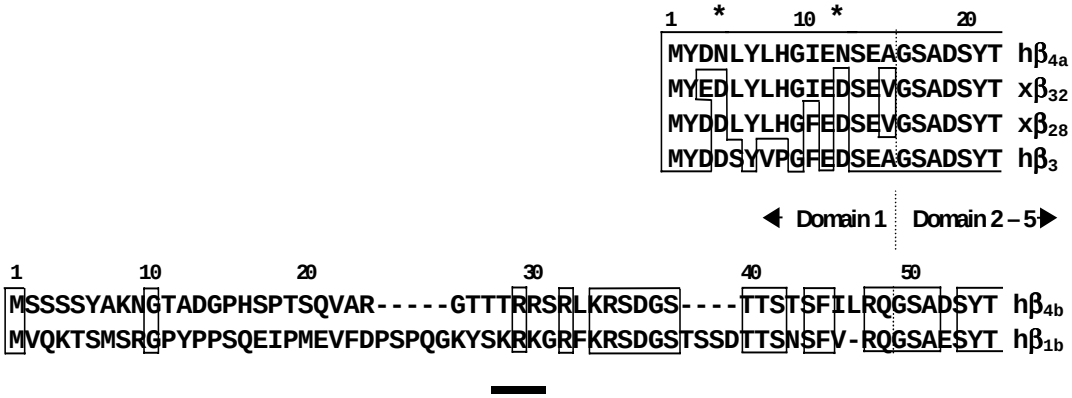

Figure 3.1. Sequence comparisons of human spinal cord Ca^{2+} channel β_{4a} and β_{4b} subunits and other β subunit subtypes. ***Top,*** **The amino acid sequence of domain 1 and a short segment of domain 2 of the human β_{4a} subunit ($h\beta_{4a}$) is shown aligned with comparable domains of two *Xenopus* β_3 subunits ($x\beta_{32}$ and $x\beta_{28}$; Tareilus et al., 1997) and a human β_3 subunit ($h\beta_3$). Amino acids identical to the $h\beta_{4a}$ sequence are *boxed*. *Asterisks* denote D to N amino acid conversions in the human β_{4a} sequence.** ***Bottom,*** **The amino acid sequence of domain 1 and a short segment of domain 2 of the human β_{4b} subunit ($h\beta_{4b}$) is shown aligned with comparable domains of the human β_{1b} subunit. Identical amino acids are *boxed*. *Dashed lines* indicate gaps in the sequence. The *bar* denotes consensus sites for phosphorylation by protein kinase C.**

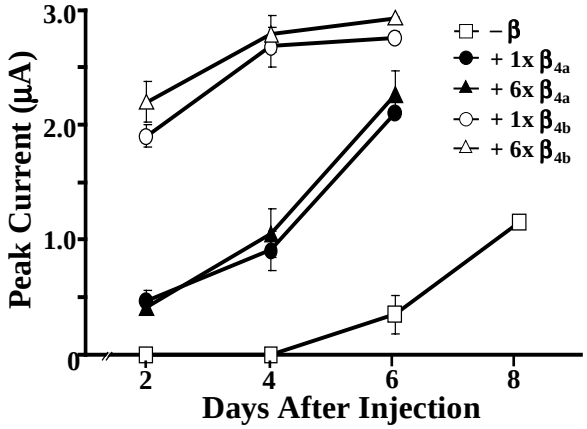

Figure 3.2. Expression rates of α_{1A} Ca^{2+} channel complexes with different β subunit compositions. Peak currents elicited by depolarization to + 10 mV ($\alpha_{1A}/\alpha_{2a}\delta$), + 5 mV ($\alpha_{1A}/\alpha_{2a}\delta + \beta_{4a}$), or 0 mV ($\alpha_{1A}/\alpha_{2a}\delta + \beta_{4b}$) from a holding potential of – 80 mV are plotted against days post-injection. Barium (5 mM) was the charge carrier. Oocytes were maintained in ND96 culture media at 18 °C. Comparisons between experiments in which the β_{4a} or β_{4b} subunits were injected at 1:1 (1X) or 6:1 (6X) ratios relative to the α_{1A} are shown. Each data *point* represents a minimum of six recordings. The SEM for each *point* is shown unless the values were smaller than the *symbol*.

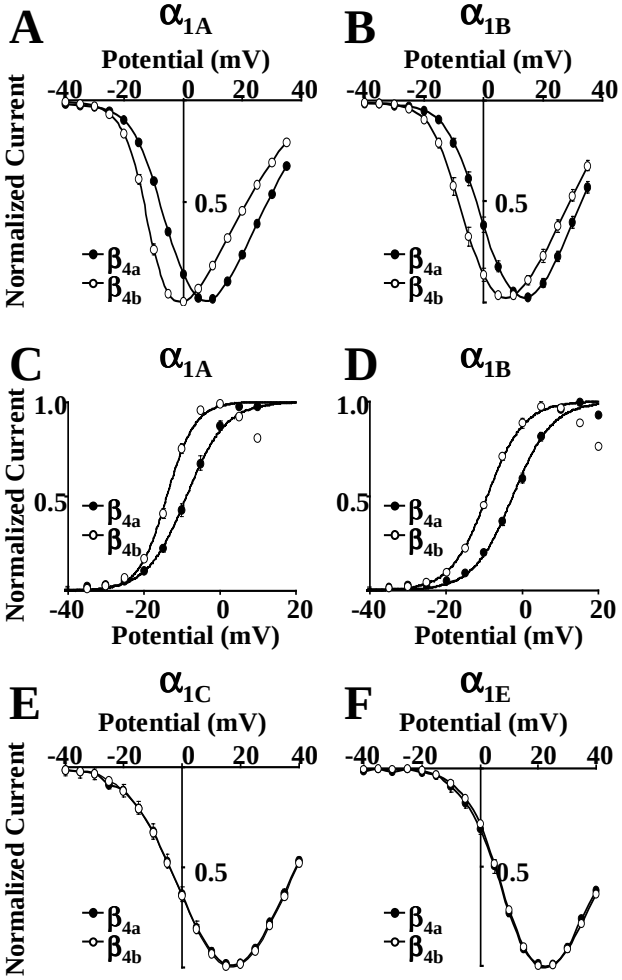

Figure 3.3. β_{4a} **and** β_{4b} **subunits have** α_1 **subunit subtype-specific effects on the voltage dependence of activation.** ***A***, ***B***, **Normalized, averaged peak current-voltage (*I-V*) plots for** α_{1A} **(*A*) and** α_{1B} **(*B*) coexpressed with** $\alpha_{2a}\delta$ **and either** β_{4a} **or** β_{4b}**. The** α_{1A} **(BI-2) and** α_{1B} **(Δ21) subunits used in these and subsequent experiments are those described by Mori et al.(1991), and Pan and Lipscombe (2000), respectively. Currents were activated by 300 msec depolarizations to various test potentials (- 40 mV to + 40 mV in 5 mV increments) from a holding potential of – 80 mV. Barium (5 mM) was the charge carrier for both** α_{1A} **and** α_{1B}**.** ***C*** **and** ***D*****, Voltage-dependence of activation up to + 10 mV for** α_{1A} **(*C*) and + 20 mV for** α_{1B} **(*D*) as determined from averaged *I-V* data in *A* and *B*. *Data points* represent the means of the normalized data at a given membrane potential. The SEM for each *point* is shown unless the values were smaller than the *symbol*. *Smooth curves* represent a single Boltzmann fit to the averaged data. Values for $V_{1/2}$ and *k* for** α_{1A} **and** α_{1B} **plus** α_2/δ **and either** β_{4a} **or** β_{4b} **are listed in Table 1. The** α_{1C} **(cardiac) and** α_{1E} **(doe-1) subunits used in these and subsequent experiments are those described by Mikami et al. (1989), and Horne et al.(1993), respectively. Currents were activated by 300 msec depolarizations to various test potentials (- 40 mV to + 40 mV in 5 mV increments) from a holding potential of – 80 mV (**α_{1C} **+** β_{4a}**, n = 12;** α_{1C} **+** β_{4b}**, n = 13;** α_{1E} **+** β_{4a}**, n = 9;** α_{1E} **+** β_{4b}**, n = 9). Barium (40 mM) was the charge carrier.**

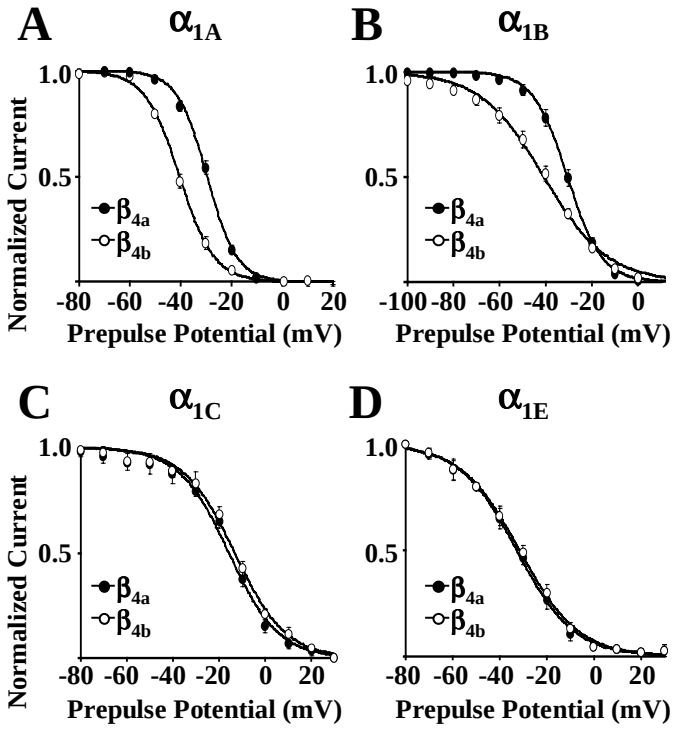

Figure 3.4. β_{4a} and β_{4b} subunits have α_1 subunit subtype-specific effects on the voltage dependence of inactivation. ***A-D*** **Normalized, averaged steady-state inactivation curves for α_{1A} (*A*), α_{1B} (*B*), α_{1C} (*C*) and α_{1E} (*D*) coexpressed with $\alpha_{2a}\delta$ and either β_{4a} or β_{4b}. Curves were generated from peak currents elicited by a 300 msec test depolarization to + 5 mV (α_{1A}+ β_{4a}), 0 mV (α_{1A} + β_{4b}), + 10 mV (α_{1B} + β_{4a}), + 5 mV (α_{1B} + β_{4b}), or + 20 mV (α_{1C} and α_{1E} with β_{4a} and β_{4b}) after a 20 second conditioning prepulse to voltages ranging from – 80 to + 30 mV (*A*, *C* and *D*) or – 100 to + 10 mV (*B*). Barium (5 mM for α_{1A} and α_{1B}, 40 mM for α_{1C} and α_{1E}) was the charge carrier.** ***Data points*** **represent the means of the normalized data at a given membrane potential. The SEM for each** ***point*** **is shown unless the values were smaller than the** ***symbol*****.** ***Smooth curves*** **represent a single Boltzmann fit to the averaged data. Values for $V_{1/2}$ and *k* for inactivation of α_{1A} and α_{1B} plus $\alpha_{2a}\delta$ and either β_{4a} or β_{4b} are listed in Table 1.**

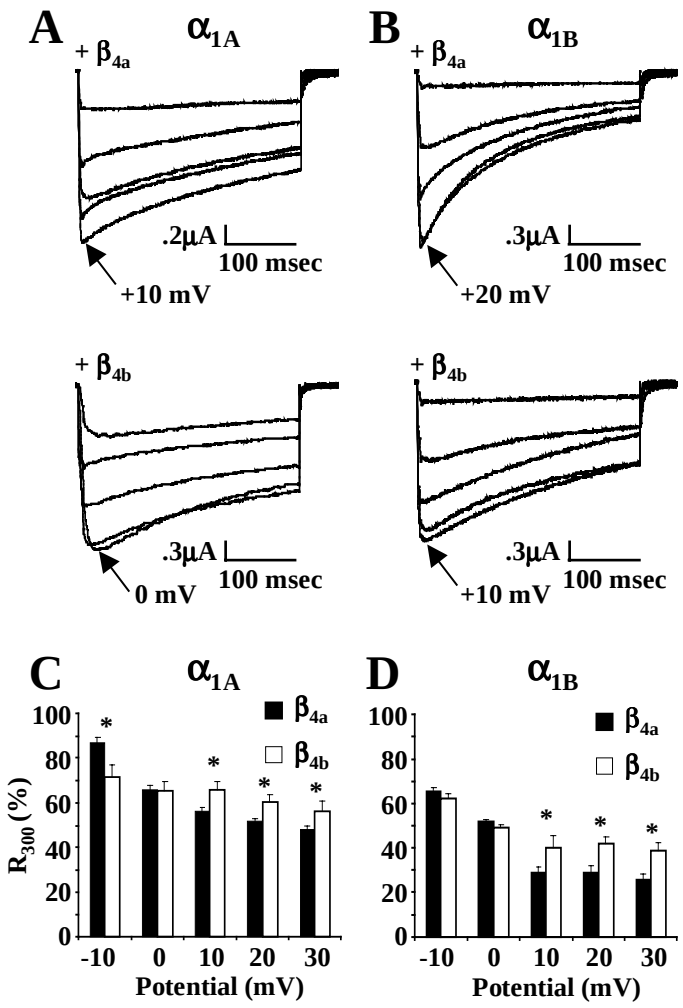

Figure 3.5. α_{1A} and α_{1B} complexes containing β_{4a} inactivate faster than those containing β_{4b}. *A*, *B*, Representative current *traces* of α_{1A} (*A*) and α_{1B} (*B*) plus $\alpha_{2a}\delta$ and either β_{4a} (*top*) or β_{4b} (*bottom*). Currents were elicited by step depolarizations to a range of test potentials (- 10 to + 30 mV in 10 mV increments) from a holding potential of – 80 mV. Barium (5 mM) was used as the charge carrier. *Traces* were fit with a single exponential from 25 msec beyond the peak inward current to the end of the depolarization. Averages of $\tau_{inactivation}$ at the peak current potential were: α_{1A} + β_{4a}, 226.6 ± 12.5 msec (n = 12); α_{1A} + β_{4b}, 307.2 ± 19.2 msec (n = 10); α_{1B} + β_{4a}, 160.1 ± 20.0 msec (n = 10); α_{1A} + β_{4b}, 213.9 ± 15.6 msec (n = 10). *C*, *D*, Current remaining at the end of a 300 msec test pulse (R_{300}), elicited as in the protocol above, for α_{1A} (*C*) and α_{1B} (*D*) plus $\alpha_{2a}\delta$ and either β_{4a} or β_{4b}. The SEM for each *bar* is shown. *Asterisks* denote statistical significance ($p < 0.05$) as determined by a student's two-sample equal variance *t*-test.

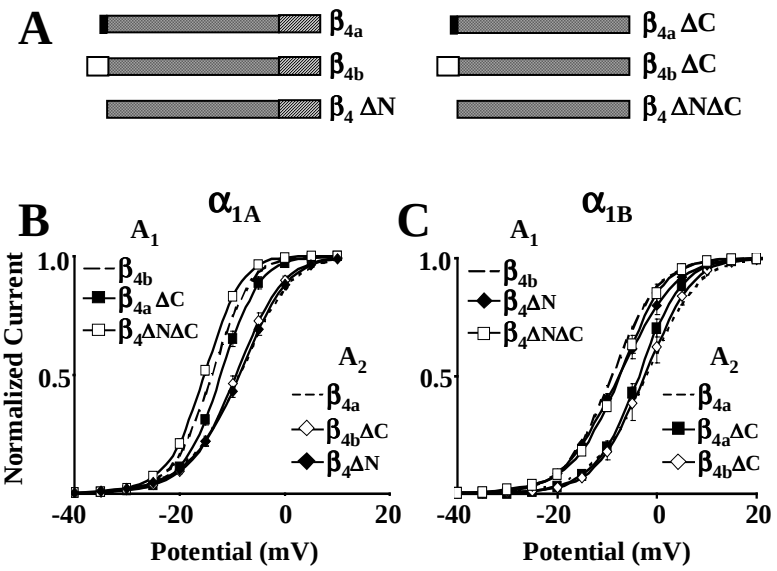

Figure 3.6. Effects of β_4 subunit N- and C-terminal deletions on the voltage dependence of activation of α_{1A} and α_{1B} Ca^{2+} channels. *A*, Schematic diagrams of the wild-type and artificial β_4 subunits used in this series of experiments. The 15 amino acid β_{4a} and 49 amino acid β_{4b} N-termini (alternatively spliced forms of domain 1) are denoted by *filled* and *open bars*, respectively. Domains 2 - 4 are represented by a single *cross-hatched bar*. The C-terminus (domain 5) is denoted by a *diagonally striped bar*. *B* and *C*, Voltage-dependence of activation up to + 10 mV for α_{1A} (*C*) and + 20 mV for α_{1B} (*D*) as determined from averaged *I-V* data. *Data points* represent the means of the normalized data at a given membrane potential. The SEM for each *point* is shown unless the values were smaller than the *symbol*. *Smooth curves* represent a single-Boltzmann fit to the averaged data. *Broken curves* represent activation data shown in Fig. 3*C* and *D* and are included in this figure for reference. Values for *V*1/2 and *k* for α_{1A} and α_{1B} plus α_2/δ and each of the six β_4 constructs are grouped according to curve similarities in Table 1.

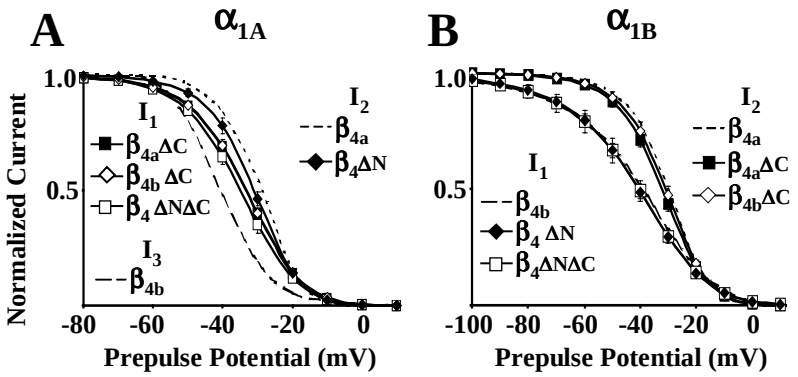

Figure 3.7. Effects of β_4 subunit N- and C-terminal deletions on the voltage dependence of inactivation of α_{1A} and α_{1B} Ca^{2+} channels. *A*, *B*, Normalized, averaged steady-state inactivation curves for α_{1A} (*A*) and α_{1B} (*B*) coexpressed with $\alpha_{2a}\delta$ and one of the six β_4 constructs shown in Fig. 6*A*. Curves were generated from peak currents elicited by a 300 msec test depolarization to - 5 mV (α_{1A}+ $\beta_4\Delta N\Delta C$), 0 mV (α_{1A} + β_{4b}, $\beta_{4a}\Delta C$), + 5 mV (α_{1A} + β_{4a}, $\beta_4\Delta N$, and $\beta_{4b}\Delta C$; α_{1B} + β_{4b} and $\beta_4\Delta N$), + 10 mV(α_{1B} + β_{4a}, $\beta_4\Delta N\Delta C$), or + 15 mV (α_{1B} + $\beta_{4a}\Delta C$ and $\beta_{4b}\Delta C$) after a 20 second conditioning prepulse to voltages ranging from – 80 to + 10 mV (*A*) or – 100 to + 10 mV (*B*). Barium (5 mM) was the charge carrier for both α_{1A} and α_{1B}. *Data points* represent the means of the normalized data at a given membrane potential. The SEM for each *point* is shown unless the values were smaller than the *symbol*. *Smooth curves* represent a single Boltzmann fit to the averaged data. *A, B* Values for $V_{1/2}$ and *k* for inactivation of α_{1A} and α_{1B} plus $\alpha_{2a}\delta$ and each of the six β_4 constructs are grouped according to curve similarities in Table 1.

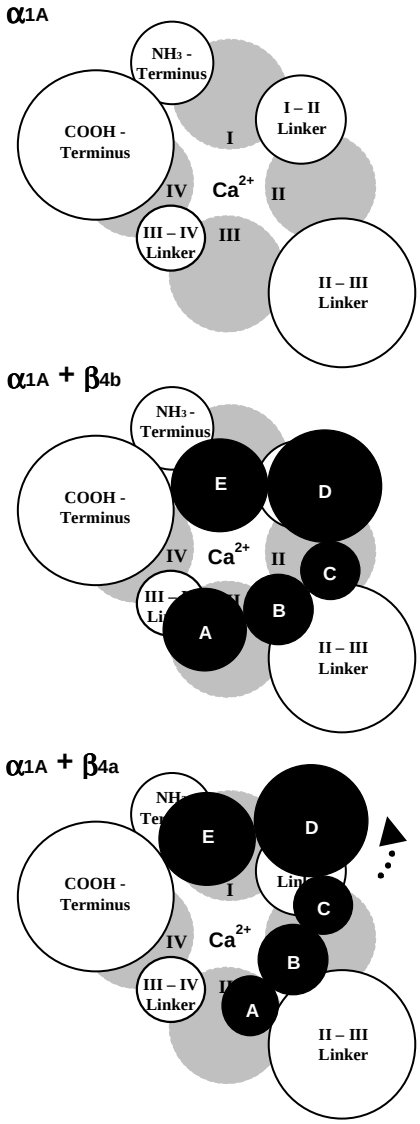

Figure 3.8. Potential α_{1A} and β subunit domain interactions as viewed from inside the cell looking out through the pore. *Top*, α_{1A} alone. Transmembrane domains I - IV are represented as *gray circles* and intracellular domains as *white circles*. *Middle*, α_{1A} + β_{4b}. The β_{4b} subunit A-E domains are shown as *black circles* superimposed on α_{1A}. Bottom, α_{1A} + β_{4a}. The radius of each circle was calculated from the spherical volume ($V = 4/3\ \pi r^3$) of each subunit domain, where V = [(0.73 cm^3/gm x $10^{24}Å^3/cm^3$ x molecular weight)/6.02x10^{23}] and the average molecular weight of an amino acid (aa) is 120 Da. For α_{1A} (BI-2): N-terminus, 98 aa; transmembrane domains I - IV, 229-268 aa; I -II linker, 127 aa, II - III linker, 537 aa; III - IV linker, 54 aa; C-terminus, 604 aa. For β_{4b} (nomenclature as in Hanlon et al., 1999): A domain, 92 aa; B domain, 61 aa; C domain, 37 aa; D, 210 aa; E, 144 aa. For β_{4a}: A domain, 44 aa. Interactions of the β_4 D domain with the α_{1A} I-II linker (Pragnell et al., 1994) and β_4 E domain with α_{1A} N- and C-termini have been well documented (Walker et al., 1998 & 1999). *Dashed arrow* in the *bottom* diagram indicates the potential for a conformational change when the β_{4a} N-terminus is

Activation

	α_{1A}						α_{1B}				
	β	$V_{1/2}$ *mV*	*k* *mV*	*z*	n		β	$V_{1/2}$ *mV*	*k* *mV*	*z*	n
A_1	β_{4b}	-14.1 ± 0.4	3.5 ± 0.1	7.1	15	A_1	β_{4b}	-9.9 ± 0.6	4.2 ± 0.1	5.9	15
	$\beta_{4a}\Delta C$	-12.0 ± 0.5	3.6 ± 0.2	6.9	13		$\beta_4\Delta N$	-9.3 ± 1.2	4.8 ± 0.3	5.2	11
	$\beta_4\Delta N\Delta C$	-15.3 ± 0.6	3.7 ± 0.5	6.8	11		$\beta_4\Delta N\Delta C$	-8.0 ± 0.5	4.6 ± 0.2	5.4	14
A_2	β_{4a}	-8.4 ± 0.6	4.8 ± 0.1	5.2	12	A_2	β_{4a}	-2.3 ± 0.6	5.0 ± 0.1	5.0	16
	$\beta_{4b}\Delta C$	-8.8 ± 0.4	4.1 ± 0.2	6.0	16		$\beta_{4a}\Delta C$	-3.3 ± 0.5	4.2 ± 0.2	6.0	11
	$\beta_4\Delta N$	-8.9 ± 0.5	4.6 ± 0.1	5.4	14		$\beta_{4b}\Delta C$	-2.6 ± 1.0	4.0 ± 0.4	6.2	11

Inactivation

	α_{1A}						α_{1B}				
	β	$V_{1/2}$ *mV*	*k* *mV*	*z*	n		β	$V_{1/2}$ *mV*	*k* *mV*	*z*	n
I_1	$\beta_{4a}\Delta C$	-34.0 ± 0.8	8.0 ± 0.3	3.1	13	I_1	β_{4b}	-40.0 ± 2.6	13.0 ± 1.1	1.9	9
	$\beta_{4b}\Delta C$	-34.7 ± 0.9	8.2 ± 0.3	3.0	14		$\beta_4\Delta N$	-44.1 ± 1.3	14.2 ± 0.6	1.8	9
	$\beta_4\Delta N\Delta C$	-35.9 ± 0.9	7.9 ± 0.3	3.2	12		$\beta_4\Delta N\Delta C$	-41.6 ± 1.6	12.9 ± 0.8	1.9	10
I_2	β_{4a}	-29.7 ± 0.7	5.9 ± 0.3	4.3	10	I_2	β_{4a}	-31.4 ± 0.6	8.0 ±0.9	3.1	8
	$\beta_4\Delta N$	-31.1 ± 0.7	6.3 ± 0.4	4.0	8		$\beta_{4a}\Delta C$	-32.1 ± 0.9	7.5 ± 0.3	3.3	10
I_3	β_{4b}	-40.3 ± 0.8	6.6 ± 0.4	3.8	9		$\beta_{4b}\Delta C$	-31.9 ± 1.1	7.3 ± 0.4	3.4	8

Table 3.1. Values for activation and inactivation parameters ($V_{1/2}$= midpoint, *k*= slope factor) derived from averaged Boltzmann fits to the data. Charge, *z*, was calculated by dividing 24 (approximate value for RT/F at room terperature, where R= gas constant, T=temperature, and F=Faraday constant) by the slope factor. Similar values are grouped into distinct modes, A_1, A_2, and I_1-I_3.

	β Subunit	Mode	Activation	Inactivation
1	ΔN ΔC (α_{1A}) ΔN ΔC (α_{1B})	$A_1 I_1$ $A_1 I_1$		
2	ΔN (α_{1A}) ΔN (α_{1B})	$A_2 I_2$ $A_1 I_1$	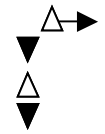	
3	β_{4a} ΔC (α_{1A}) β_{4a} ΔC (α_{1B})	$A_1 I_1$ $A_2 I_2$	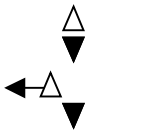	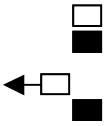
4	β_{4b} ΔC (α_{1A}) β_{4b} ΔC (α_{1B})	$A_2 I_1$ $A_2 I_2$	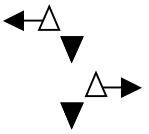	
5	β_{4a} (α_{1A}) β_{4a} (α_{1B})	$A_2 I_2$ $A_2 I_2$	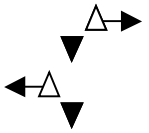	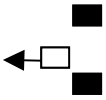
6	β_{4b} (α_{1A}) β_{4b} (α_{1B})	$A_1 I_3$ $A_1 I_1$		

Table 3.2. Gating mode model describing the effects of β_4 subunit constructs on α_{1A} and α_{1B} subunit activation and inactivation. Gating modes induced by each β subunit described in terms of separate α_1-β interaction points for activation and inactivation (α_1, filled symbols, β, open symbols). Arrows indicate potential displacement of the β subunit in either N- or C-terminal direction.

Chapter 4

ALTERNATIVE SPLICING OF A β_4 SUBUNIT PROLINE-RICH MOTIF REGULATES VOLTAGE-DEPENDENT GATING AND TOXIN BLOCK OF $CA_V2.1$ Ca^{2+} CHANNELS

Abstract

Ca^{2+} channel β subunits modify α_1 subunit gating properties through direct interactions with intracellular linker domains. In a previous report (Helton and Horne, 2002), we showed that alternative splicing of the β_4 subunit had α_1 subunit subtype-specific effects on Ca^{2+} channel activation and fast inactivation. We extend these findings in the present report to include effects on slow inactivation and block by the peptide toxin, ω–CgTx-MVIIC. N-terminal deletion and site-directed mutagenesis experiments revealed that the effects of alternative splicing on toxin block and all aspects of gating could be attributed to a proline- rich motif found within N-terminal β_{4b} amino acids 10 – 20. Interestingly, this motif is conserved within the third PDZ domain of the distantly related MAGUK homologue, PSD-95. Sequence identity of ~ 30% made possible the building of β_{4a} and β_{4b} 3D structural models using PSD-95 as the target sequence. The models reveal that alternative splicing of the β_4 N-terminus results in dramatic differences in surface charge distribution, and localize the proline-rich motif of β_{4b} to an extended arm structure that flanks what would be the equivalent of a highly modified PSD-95 carboxylate binding loop. Northern analysis revealed a markedly different pattern of distribution for β_{4a} versus β_{4b} in the human CNS. Whereas β_{4a} is distributed throughout evolutionarily older regions of the CNS, β_{4b} is concentrated

heavily in the forebrain. These results raise interesting questions about the functional role that alternative splicing of the β_4 subunit has played in the evolution of complex neural networks.

Introduction

Voltage-gated Ca^{2+} channels participate in an extensive array of cellular activities including excitation-contraction coupling, transcription, and neurotransmitter release. Neuronal Ca_v2 channels are assemblies of up to five subunits, α_1, α_2/δ, β, and γ. The α_1 subunit consists of four homologous repeats (I-IV) of six helices (S1-S6) that arrange to form the selectivity filter and pore. The 24 transmembrane helices are connected by a series of alternating intra- and extracellular loops. These loops are targets for a host of modifying proteins, including β subunits, G-proteins, calmodulin, and syntaxin, as well as the peptide toxins of venomous spiders and marine snails (Catterall, 2000). Interaction of these proteins with α_1 subunits typically alters the voltage-dependency and kinetics of channel gating, which in turn modifies Ca^{2+} entry into neurons.

Ultimately, gating behavior is determined by the interactions of individual amino acid side chains with the electrostatic forces within their microenvironments. This is especially true for the positively charged S4 helical segments that constitute the voltage sensors in Na^+, Ca^{2+}, and K^+ channels. Biophysical studies have shown that depolarization disrupts S4 side chain interactions of Shaker K^+ channels to the extent that S4 helices rotate 180º along their axes (Cha *et al*., 1999; Glauner *et al*.,1999). This motion likely triggers a cascade of side chain disruptions that ultimately leads to rotation and separation of the intracellular S6 segments that form the K^+ channel gate (Bezanilla, 2000). Such a mechanism is supported by recent studies delineating the conformational

changes associated with open and closed states of bacterial two membrane spanning K^+ channels (Jiang *et al*., 2002a), and is generally applicable to Na^+ and Ca^{2+} channel gating.

Attempts have been made to assign specific gating functions to individual Ca^{2+} channel homology domains. Early chimera studies indicated that the IS6 segment was critical for setting the rate of fast inactivation (Zhang *et al*., 1994); however, substitution of IIS6 and IIIS6 of the $Ca_v2.3$ channel into the slow inactivating $Ca_v1.2$ channel caused a left-shift in the voltage dependence of inactivation and increased the rate of $Ca_v1.2$ channel inactivation to near $Ca_v2.3$ rates. (Stotz *et al*., 2000). Effects on gating have been reported for amino acid substitutions in IS3 (Zhong *et al*., 2001), the I-II linker (Berrou *et al*., 2001), IIS6 (Stotz and Zamponi, 2001), extracellular linkers IIIS3-S4 (Lin *et al*., 1999) and IVS3-S4 (Hans *et al*., 1999), and IVS6 (Berjukow *et al*., 2001). Additive effects on $Ca_v1.2$ channel inactivation were recently reported for individual IS6, IIS6, IIIS6, and IVS6 substitutions (Shi and Soldatov, 2002). Taken together, these data support a structural model of α_1 subunits in which individual transmembrane segments are interdependently entwined (Horn, 2000).

Our results indicate that this model also applies to β subunit interactions with α_1 subunit intracellular linkers. We showed previously that alternative splicing of the β_4 subunit had α_1 subtype specific effects on voltage dependent activation and inactivation (Helton and Horne, 2002). In this report we extend these findings to include effects on slow inactivation and block by ω-CgTx MVIIC, and identify a proline-rich motif in β_{4b} that is responsible for the observed differences in effects.

Materials and Methods

Deletion Mutants. Truncation of the β_{4b} N-terminus in 10 amino acid increments was carried out using PCR and custom oligonucleotide primers (Integrated DNA Technologies (IDT), Coralville, IA). All nucleotide and amino acid positions for primers and restriction enzymes correspond to the β_{4b} sequence (Genbank # U95020). Each forward primer sequence contained an idealized Kozak (Kozak, 1991) sequence and start codon corresponding to the beginning of each of the deleted 10 amino acids as follows: β_{4b} Δ1-10F (5' GCCACCATGACCGCGGACGGGCCG); and β_{4b} Δ1-20F (GCCACCATGCAGGTGGCCCGAGGC). Both reactions included a common β_4 reverse primer β_{4b} 732R (5' TGACGGCCCCACTAACACC). Full-length β_{4b} was used as the template for these reactions. The β_{4b} Δ10-20 deletion mutant was generated with the primer, β_{4b} Δ10-20F (5' GCCACCATGTCCTCCTCCTCCTACGCCAAGAACTCG) paired with β_{4b} 732R using the β_{4b} Δ1-20 mutant as the template. Annealing temperature for PCR reaction was 56ºC with Gene Choice Taq® DNA polymerase (PGC Scientific, Durham, NC). Correct-sized PCR fragments were cloned into the pT-Advantage vector (Clontech, Palo Alto, CA). PCR-based cycle sequencing (FS chemistry; Applied Biosystems, Foster City, CA) was used with an ABI Prism 310 Genetic Analyzer. The data were analyzed using ABI Prism DNA sequencing software (version 2.12: PE Biosystems) and sequence alignments and restriction maps were generated using Lasergene Software (DNA Star, Madison, WI). Correct clones were digested with *Bam*HI (Roche Molecular Biochemicals, Indianapolis, IN) and the corresponding approximately 530bp fragments were ligated into *Bam*HI (nucleotide position 550)

digested β_{4b} in pBluescriptII S/K+ (Stratagene, La Jolla, CA) containing β_{4b}. Each β_{4b} deletion mutant was sequenced to confirm correct reading frame and proper N-terminal orientation.

Site Directed Mutagenesis. For all β_{4b} site directed mutants, full-length β_{4b} cDNA (U95020) was used as the template unless otherwise indicated. All site directed mutagenesis reactions were carried out using a QuikChange® site-directed mutagenesis kit (Stratagene) and custom forward and reverse compliment oligonucleotide primers (IDT): β_{4b}G10A,D13A(5' ACGCCAAGAACGCGACCGCGGCCGGGCCGCAC); β_{4b}P15A,P18A (5'GCGGACGGGGCGCACTCCGCCACCTCGCAGGTG);β_{4b}G10A,D13A,P15A,P18A (5' ACGCCAAGAACGCGACCGCGGCCGGGGCGCAC; β_{4b} P15A, P18A used as template); β_{4b}G10A,P15A(5'TACGCCAAGAACGCGACCGCGGACGGGGCGCACTCCCCCAC CTCGCAGGTG); β_{4b}H16A (5'-ACCGCGGACGGGCCGGCCTCCCCCACCTC); β_{4b}G10A,P18A(5'TACGCCAAGAACGCGACCGCGGACGGGCCGCACTCCGCCAC CTCGCAGGTG);β_{4b}D13A,P15A(5'TACGCCAAGAACGGGACCGCGGCCGGGGCG CACTCCCCCACCTCGCAGGTG);β_{4b}D13A,P18A(5'TACGCCAAGAACGGGACCG CGGCCGGGCCGCACTCCGCCACCTCGCAGGTG);β_{4b}H16A (5'ACCGCGGACGGGCCGGCCTCCCCCACCCTCG); β_{4b}T11A,S17A,T19A,S20A(5'CAAGAACGGGGCCGCGGACGGGCCGCACGCCCC CGCCGCGCAGGTGGCC). Each of the mutant clones was sequenced to confirm reaction fidelity.

Electrophysiology. Complementary RNA's (cRNA's) were synthesized *in vitro* using Ambion's mMessage mMachine® RNA transcription kit (T3 or T7 depending on clone orientation in pBluescript II S/K+). Standard *Xenopus laevis* oocyte expression methods were used to characterize β deletion and site-directed mutants. Briefly, full-length α_1, α_2/δ-1, and β cRNA's were injected in equimolar ratios (5.6 ng α_{1A}, 2.4 ng α_2/δ-1, and 1.6 ng β_4 in 46 nl) into defolliculated oocytes (stage V-VI). The BI-2 (α_{1A}) and α_2/δ-1 clones used in this study were provided by T-Tanabe (Tokyo Medical and Dental University, Tokyo, Japan). Calcium channel currents were recorded 2-4 days after oocyte injection by standard two-electrode voltage clamp using a Warner amplifier (OC-725B) at 20-22°C, and data were collected using pCLAMP6 software (Axon Instruments, Foster City, CA). Microelectrodes were filled with 3M KCl, and the resistances of the current and voltage electrodes were 0.3-1.5 MΩ. Data were filtered at 2 kHz and sampled at 10 kHz. Currents were recorded in a chloride-free bath containing 5 mM $Ba(OH)_2$, 5 mM HEPES, 85 mM TEA-OH, and 2 mM KOH, pH adjusted to 7.4 with methansulfonic acid. In experiments with the peptide toxin ω-CTx-MVIIC (Peptide Institute Inc. Osaka, Japan) the 5mM Ba^{2+} solution was supplemented with 0.1mg/ml cytochrome c to saturate nonspecific peptide binding sites. Cytochrome c at 0.1 mg/ml had no noticeable effect on recorded Ba^{2+} currents. Peptides were reconstituted according to manufacturer's instructions (100μM stock solutions in sterile, deionized water). Fresh dilutions of the peptide were made immediately before use. Currents typically ranged between 0.8-2.5μA, and leak currents were between 20 ηA to 100 ηA. Data were analyzed using pCLAMP6 software (Axon Instruments) and Excel 7.0 (Microsoft Corp.,

Redmond WA). The leak and capacitive currents were subtracted on line using a standard P/4 protocol. Curve fitting was performed with SigmaPlot Version 5.0 (SSPS Inc., Chicago IL)

Slow Inactivation. Oocytes were held at –80 mV for approximately 2 minutes prior to a 300 msec reference pulse (I_R) to 0 mV (β_{4b}) or +10mV (β_{4a}). Following I_R, the membrane potential was stepped immediately to a conditioning pulse potential ranging from –100 mV to –20 mV (20 mV increments) and held for 5 min. During the conditioning pulse, a 300 msec test pulse (I_T) to 0 mV (β_{4b}) or +10mV (β_{4a}) was applied every 15 seconds. Data were normalized as the ratio of the maximum current at time T (I_T) divided by the maximum reference current (I_R). Data were fit to the double-exponential equation $I_T/I_R=A_1e^{-x/\tau1}+A_2e^{-x/\tau2}$ where I_T = current at time T, I_R = max reference current, x = time in seconds, and A_1 and A_2 are components for the time constants τ_1 and τ_2 respectively. The SEM is shown for each data point unless the values are smaller than the symbol.

Recovery from Slow Inactivation. Currents were stabilized at -80 mV or -100 mV for approximately 2 minutes prior to a 300 msec reference pulse (I_R) to 0 mV (β_{4b}) or +10mV (β_{4a}). Following a 100 msec step to either –80 mV or –100 mV, the oocytes were held at a conditioning pulse potential of –30 mV for 5 min. Immediately following the conditioning pulse, a 300 msec test pulse was applied (I_1), then the holding potential was stepped back to either –80 mV or –100 mV and 300 msec test pulses ($I_{2\text{-}12}$) were applied at 15 second intervals starting at time 0 for a total of 3 minutes. Data were normalized as the ratio of the maximum current at time T (I_T) divided by the maximum reference current (I_R). Data were fit to the single exponential equation $I_T/I_R= I_\infty+ Ae^{-x/\tau}$ where I_T=

current at time point T, I_R= max reference current, I_∞= current remaining at end of protocol, x = time in seconds, and A is the component for the time constant τ.

Voltage-dependence of activation and inactivation. Voltage-dependency of activation data were generated from I-V curves. Maximal currents were obtained from 300 msec depolarizations from a holding potential of – 80 mV to various test potentials (-40 to +10 mV in 5 mV increments). Each individual recording was then normalized, inverted, and fit to the Boltzmann equation $\%I_{Ba} = 1/[1 + \exp(-(V_{test} - V_{1/2})/k)]$ where V_{test} = *I-V* test potential, V_{pre} = prepulse potential, $V_{1/2}$ = midpoint of activation or inactivation, and k = slope factor. The fit curves, $V_{1/2}$, and k values were then averaged and plotted as a function of membrane voltage.

Voltage-dependency of inactivation data were obtained from peak currents elicited by a 300 msec maximal current test depolarization after a 20 second conditioning prepulse to voltages ranging from –80 to +20 mV. Each individual recording was then normalized and fit to the Boltzmann equation $\%I_{Ba} = 1/[1 + \exp((V_{pre} - V_{1/2})/k)]$ where V_{test} = *I-V* test potential, V_{pre} = prepulse potential, $V_{1/2}$ = midpoint of activation or inactivation, and k = slope factor. The fit curves, $V_{1/2}$, and k values were then averaged and plotted as a function of prepulse potential.

Pharmacology. Oocytes were held at a potential of –80mV with maximal currents elicited by 150ms test pulses to 0 mV (β_{4b}) or +10mV (β_{4a}) every 15 seconds for a total of 10 minutes. During recordings, oocytes were perfused at a constant rate of approximately 0.5 ml/min. The data were fit to the single-exponential equation $I_T/I_R=I_\infty+Ae^{-x/\tau}$ where I_T= max current at time point T, I_R= max current at time point 0, I_∞= residual current at end of protocol , x = time in seconds, and A is the component for

the time constant, τ. The averaged rate constants (1/τ) for the four ω-CTx-MVIIC concentrations (0.2μM, 0.6μM, 2μM, and 6μM) were plotted as a log function of their concentration and were fit well by the equation $(\tau)^{-1} = k_{on}[Tx] + k_{off}$.

Northern Blot Analysis. A commercially available human neuronal tissue northern blot (MTN Blot brain II, Clontech) was probed with a non-specific β_4 subunit probe ($\beta_4\Delta N$, nucleotides 215-1628 plus approximately 300bp of 3'untranslated). A ^{32}P labeled β_4 subunit probe was made with a nick translation kit (Promega) using the β_4 ΔN mutant as the template. The β_4 ΔN mutant is missing the first coding 147 bp corresponding to the 49 amino acid N-terminus of β_4 (clone from Helton and Horne, 2002). The MTN blot was hybridized overnight at 42°C in hybridization buffer (5XSSC, 5% w/v blocking reagent (Roche), 0.1% N-lauroylsarcosine, 0.02% w/v SDS, 50% w/v formamide) plus 100 μg/ml herring sperm DNA (Promega). The probe concentration was 1 million counts/ ml. The blot was washed with successive stringency washes (4 washes, 15 minutes each at 37°C) ranging from 2XSSC/0.1% SDS to 0.1XSSC/0.1% SDS. The blot was then exposed to radiographic film for 12 hours at -80°C. One microgram of cRNA for both β_{4a} and β_{4b} were run out on a 1% denaturing formaldehyde gel along with a poly-A tailed cRNA mass ladder (RNA Molecular Weight Marker 1, Roche). The β_{4a} cRNA is longer than the β_{4b} cRNA due to the additional approximately 400 nucleotides of 5' untranslated sequence.

Molecular Modeling. The sequences for rat PSD-95 (DLG4_rat) and human β_4 (CACNB4) were obtained (accession numbers P31016 and U95020) from the Swiss-prot database (Appel *et al*., 1994). Amino acids 10 – 96 of β_{4b} were aligned to residues 307-

390 of PSD-95 based on secondary structure prediction (nnPredict) and visual inspection. For β_{4a}, amino acids 50 – 96 of β_{4b} were aligned to residues 345-390 of PSD-95. Using default parameters, the program MODELLER 6 (Sali and Blundell, 1993) was utilized to produce 50 models each of β_{4b} and β_{4a} structure based on the solved structure of the third PDZ domain of PSD-95 (1BEF). Five models each were chosen for further analysis based on the molecular probability density function (PDF) output from MODELLER and stereochemical analysis obtained through Ramachandran output from PROCHECK-NMR (Laskowski *et al*., 1993). The interactions between different atom types within these models and Cα RMSD comparisons between the models and 1BEF were characterized with ERRAT (Colovos and Yeates, 1993). The β_{4a} and β_{4b} models chosen for comparison had the fewest disallowed residues (Ramachandran), lowest molecular PDF and RMSD values, and highest percentage of residues in acceptable conformations based on ERRAT and PROCHECK-NMR analysis. Models were visualized with the program MOLMOL (Koradi *et al*., 1996).

Results

Alternative splicing of the β_4 subunit affects slow inactivation of $Ca_v2.1$ Ca^{2+} channels

In a previous study (Helton and Horne, 2002) we showed that $Ca_v2.1$ complexes containing the longer form of an alternatively spliced β_4 subunit N-terminus, β_{4b} (49 amino acids), inactivated at more negative potentials in response to 20 sec conditioning pre-pulses than complexes containing a shorter form, β_{4a} (15 amino acids). To determine

whether this response extended to slower types of inactivation, we examined in the present study the effects of β_{4a} and β_{4b} on $Ca_v2.1$ cumulative inactivation elicited by 5 min conditioning pre-pulses combined with stimulation at 0.25 Hz. Oocytes were stabilized at - 80 mV prior to a 300 msec reference pulse (I_R) to potentials that were predetermined to give peak inward currents (β_{4b}, 0 mV; β_{4a}, +10 mV). The membrane potential was then stepped to and held at the conditioning pre-pulse potential (ranging from -100 to -20 mV) for 5 min. A 300 msec test pulse (I_T) was elicited from the conditioning pre-pulse potential every 15 sec (I_5 = test pulse at 5 min). The kinetics of entry to slow inactivation for $Ca_v2.1$ complexes containing either β_{4a} or β_{4b} at - 40 mV are shown in Figure 4.1*A*. For comparison purposes, we fit the data points for both β_{4a} and β_{4b} to two exponentials (smooth curves in the figure). The time constants for the fast component of entry (τ_1) for β_{4a} and β_{4b} were 28.6 ± 2.6 sec and 18.9 ± 1.2 sec, respectively, and for the slow component of entry (τ_2) 769 ± 23.6 and 384 ± 14.8 sec, respectively. Overall, the I_T/I_R ratio for $Ca_v2.1$ complexes containing β_{4b} decreased to 0.5 in ~ 70 sec, whereas those containing β_{4a} required ~ 380 sec (not shown). This indicated that β_{4b} caused a more than five-fold acceleration of the kinetics of slow inactivation. Representative current traces for reference and 5 min test pulses from a conditioning potential of – 40 mV for $Ca_v2.1$ complexes containing β_{4a} (top) and β_{4b} (bottom) are shown in Figure 4.1*B*. As seen in the figure and as described in our previous study, $Ca_v2.1$ complexes containing β_{4a} underwent open-state fast inactivation faster than did complexes containing β_{4b}. After 5 min at -40 mV, the rate of fast inactivation was unaltered for complexes containing β_{4a}, and slowed only somewhat for complexes

containing β_{4b}. The absence of any appreciable tail-current indicated that deactivation was not affected by prolonged depolarization. The I_5/I_R ratio is plotted against the range of conditioning potentials (-100 to -20 mV) in Figure 4.1*C*. The figure illustrates that the voltage dependence of $Ca_v2.1$ slow inactivation is shifted to the left for complexes containing β_{4b} relative to those containing β_{4a}. Half-maximal inactivation occurred at approximately -50 mV for complexes containing β_{4b} and -35 mV for β_{4a}. These values are approximately 10 mV (β_{4b}) and 5 mV (β_{4a}) more negative than were determined for inactivation in response to 20 sec conditioning pre-pulses (Helton and Horne, 2002). Figure 4.1*D* shows that recovery from 5 min of slow inactivation at – 30 mV is nearly complete when the membrane potential is stepped back to – 80 mV, and that there is no difference in the time course of recovery for $Ca_v2.1$ complexes containing either β_{4a} or β_{4b}. Recovery was somewhat faster and more complete when the membrane potential was stepped back to -100 mV. The recovery data at both potentials fit well to single exponentials. The time constants for recovery for β_{4a} and β_{4b} at -80 mV were 28.6 ± 2.0 and 27.8 ± 1.6 sec, respectively, and at -100 mV, 18.9 ± 0.5 and 17.2 ± 0.4 sec, respectively.

Alternative splicing of the β_4 subunit affects ω-CTx MVIIC block of $Ca_v2.1$ Ca^{2+} channels

The results to this point indicate that changes in the structure of the β_4 subunit N-terminus impact α_{1A} subunit structures that are important for many aspects of gating, including activation, open-state inactivation, and fast and slow closed-state inactivation.

Given that recent evidence indicates that cytosolic determinants of two-membrane spanning K^+ channel gating are coupled to changes in outer vestibule structure (Perozo *et al*., 1999; Jiang *et al*., 2002a, b), we next sought to determine whether alternative splicing of the β_4 subunit would affect the block of $Ca_v2.1$ channels by a marine snail peptide conotoxin, ω-CTx-MVIIC. Conotoxin interactions with voltage-gated Ca^{2+} channels are entirely extracellular and occur through binding sites located near H5 (P) helices in several of the six helix transmembrane-spanning motifs (Ellinor *et al*., 1994). Figure 4.2*A* shows the effects of 2 μM ω-CTx-MVIIC on $Ca_v2.1$ Ca^{2+} channel complexes expressed in *Xenopus* oocytes in the presence of either β_{4a} or β_{4b}. The oocytes were held at -80 mV for 10 min and stimulated every 15 sec. Under these conditions, ω-CTx-MVIIC associated with $Ca_v2.1$ complexes containing β_{4b} at a faster rate (τ = 50 ± 0.75 sec) than complexes containing β_{4a} (τ = 200 ± 16 sec). The loss of Ca^{2+} current resulting from slow inactivation over ten minutes at -80 mV (<15%) was subtracted from the data plotted in the figure. Figure 4.2*B* demonstrates that as expected for a first-order reaction, the rate constants (τ^{-1}) for toxin block were linearly dependent on toxin concentration as described by the equation, $(\tau)^{-1} = k_{on}$ [Tx] + k_{off}. Slopes of linear fits to the data for $Ca_v2.1$ complexes containing either β_{4a} and β_{4b} were 3.7 X 10^{-6} $M^{-1}\cdot$ sec^{-1} and 1.1 X 10^{-5} $M^{-1}\cdot$ sec^{-1}, respectively. This indicated that the on-rate (k_{on}) for toxin block was approximately three-fold faster for $Ca_v2.1$ complexes containing β_{4b} than for those containing β_{4a}.

The molecular determinants of alternatively spliced β_4 subunit differential effects on gating and pharmacology are located within amino acids 10 - 20 of β_{4b}

Having characterized many of the functional consequences of alternative splicing of the β_4 A domain, we focused next on identifying the key structural determinants underlying the observed differences in effects. It was of particular interest to determine whether or not the effects of alternative splicing on gating and pharmacology could be assigned to separate structural entities. To accomplish this, we first created a series of β_{4b} deletion mutants in which the N-terminus was shortened by multiples of 10 amino acids (β_{4b} Δ1- 10 through β_{4b} Δ1- 49), and characterized their effects on gating and pharmacology of $Ca_v2.1$ complexes. Figure 4.3, *A-D* shows that, relative to full-length β_{4b}, deletion of the first 10 amino acids (β_{4b} Δ1- 10) had no effect on the voltage dependence of activation (*A*), isochronal (20 sec prepulse) inactivation (*B*), onset into slow inactivation (*C*), or susceptibility to block by 2 μM ω-CTx-MVIIC (*D*). However, when amino acids 1-20 were removed (β_{4b} Δ1- 20), both the voltage dependence of activation (Figure 4.3 *A*) and inactivation (Figure 4.3*B*) of $Ca_v2.1$ complexes shifted to more depolarized potentials. As shown in the figure, the acquired gating properties were essentially identical those for $Ca_v2.1$ complexes containing β_{4a}. $Ca_v2.1$ complexes containing β_{4b} Δ1-20 also had a slower onset into slow inactivation (Figure 4.3*C*) and were less susceptible to block by 2 μM ω-CTx-MVIIC (Figure 4.3*D*). The effects of constructs β_{4b} Δ1-30, β_{4b} Δ1-40, and β_{4b} Δ1-49 were identical to those of β_{4b} Δ1-20 (data not shown). As a first attempt at determining whether the effects of β_{4b} Δ1-20 were simply the result of a decreased size of the β_{4b} N-terminus, we reintroduced amino acids

1- 10 to the N-terminus of β_{4b} Δ1-20 to create the construct β_{4b} Δ10-20. As shown in Figure 4.3 *A* and 4.3*B*, this did not restore the $V_{1/2}$ of either activation or inactivation to the hyperpolarized potentials characteristic of $Ca_v2.1$ complexes containing β_{4b}. Taken together, these results indicated that the molecular determinants responsible for the observed differences between $Ca_v2.1$ complexes containing β_{4a} versus β_{4b} were located in amino acids 10-20 of $\beta_{4b.}$ Moreover, it was apparent that their influence extended to changes both in gating and pharmacology.

The β_4 A Domain is a distant homologue of the third PDZ domain of PSD-95

With the results of the deletion experiments highlighting a specific location for the molecular determinants of β_{4b} gating and pharmacology effects, and with the observation that the β_{1b} A domain resembles PDZ domains (Hanlon *et al*., 1999), we began a systematic comparison of the β_{4b} sequence with similar regions of a number of PDZ domains. Unexpectedly, we found that the entire β_{4b} A domain was weakly homologous to the third PDZ domain of PSD-95 (Figure 4.4*A*). Of the 87 amino acids that have been shown by X-ray crystallography to form the modular PDZ structure of PSD-95 (Doyle *et al*., 1996), twenty-six of these (~ 30%) are conserved in the β_{4b} sequence. Most importantly, these identities are conserved within key secondary structural elements, such as β-strand C and α-helix 2 of PSD-95. Also of note is the conservation of a RG(S/T)T motif in what would be the equivalent of the carboxylate binding loop (CBL) between β-strands A and B of PSD-95, and the loss of the GLGF motif that is extremely common among PDZ domain subtypes (Harris and Lim, 2001;

Bezprozvanny and Maximov, 2001). Four of β_{4b} amino acids 10–20 (G10, D13, P15, and P18) were found in PSD-95. We used these as a starting point for further defining key β_{4b} residues involved in setting $Ca_v2.1$ gating parameters.

Figure 4.4*B* lists a series of site-directed mutants (*left)*, along with their effects on the voltage-dependence ($V_{1/2}$) of activation (*middle*) and inactivation (*right*) of $Ca_v2.1$ complexes. The $V_{1/2}$'s for complexes containing β_{4a} and β_{4b} are included for comparison. Interestingly, the first site-directed β_{4b} mutant tested, G10A, D13A, P15A, P18A, in which all four of the amino acids in common with PSD-95 were altered, displayed activation and inactivation properties similar to that of β_{4a}. To determine whether this was a specific effect, we altered four different amino acids in the β_{4b} 10–20 sequence to create the mutant, T11A, S17A, T19A, S20A. As shown in Figure 4.4B, $Ca_v2.1$ gating properties changed little in response to these mutations. $Ca_v2.1$ complexes containing the G10A, D13A, P15A, P18A mutant also had β_{4a}-like slow inactivation and pharmacological properties (data not shown). This indicates that the conserved amino acids are playing a defining role in the gating motif. To delineate the structure in more detail, we next characterized six of the possible G10, D13, P15, P18 amino acid pairs for their effects on gating. Surprisingly, none of the pairs were absolutely essential for maintaining wild-type β_{4b} gating behavior, although small but statistically significant hyperpolarizing effects on activation were noted for 5 of the 6 pairs. To complete the alanine substitution study, we created the mutant, H16A, which had a small but statistically significant effect on inactivation, but not activation.

One interpretation of these results is that β_{4b} amino acids 10–20 form a ligand motif that interacts with a binding pocket located somewhere either on the α_{1A} subunit or on the β_4 subunit itself. The affinity of the ligand motif for its receptor site could be defined, for example, by the sum of the interactions of amino acids G10, D13, P15, and P18 with their individual targets. Any given pair may be capable of maintaining a binding interaction under the conditions of our experiments. As a first step toward addressing this possibility, we created three-dimensional structural models of the β_{4a} and β_{4b} A domains (Figure 4.5, *A* and *B*) using the real-space optimization method employed in the computer program MODELLER (Sali and Blundell, 1993). The models were initiated using the distance and dihedral angle restraints derived from alignments with portions of the sequence of the third PDZ domain of PSD-95. For β_{4b}, amino acids 10-96 were aligned with amino acids 307-390 of PSD-95. There is 30% sequence identity over this region, which is considered minimally acceptable for this type of comparative modeling (Martí-Renom *et al*., 2000). For β_{4a}, amino acids 10 – 49 of β_{4b} were deleted from the alignment. Thus, the models do not include the first 15 amino acids of β_{4a} and the first 9 amino acids of β_{4b}. Figure 4.5 *A* (*left*) shows that β_{4a} models as a compact structure containing three β sheets and 2 α helices. Stereochemical quality assessment of the model using PROCHECK-NMR (Laskowski *et al*., 1993) identified 41 residues (87.7%) in most favored regions, 5 (10.6 %) in additional and generously allowed, and 1 (2.1%) in a disallowed region. Calculation of the electrostatic surface potential using MolMol (Koradi *et al*., 1996) reveals that the face of the molecule as oriented in Figure 1.5*A*, *left,* contains a pocket of negative charge (red residues) between the two α helices (Figure

4.5*A*, *right*). Figure 4.5*B, right and left,* illustrates that the overall effect of alternative splicing to form β_{4b} is to bury the charged pocket beneath 3 additional β sheets. Interestingly, the molecule acquires as the result of splicing a positively charged binding pocket (blue residues) in what would be the equivalent of the CBL in PSD-95 (Figure 4.4*A*). The stereochemical quality of the β_{4b} model as shown is not quite as good as that for β_{4a}. PROCHECK-NMR identified 64 residues (79%) in most favored regions, 11 residues (13.6%) in additional allowed regions, and 3 residues (3.7%) each in generously allowed and disallowed regions. Two of the three disallowed residues (R30 and K34) flank what would be the equivalent PSD-95 β sheet B. Together with the loss of the highly conserved PDZ GLGF sequence, these results are consistent with the notion that through evolution this region of the β_{4b} structure has evolved away from the capacity to bind C-terminal peptide motifs. Of most importance to our present results, however, is the observation that β_{4b} amino acids 10-20 model as an extended arm (pointing to the left in Figure 4.5 *B*, *right* and *left*) that may serve as a ligand motif. Interestingly, the orientation of the arm appears to be dictated by the isomerization state of proline18 (not shown).

Differential distribution of alternatively spliced β_4 subunit mRNA

We noted in our previous study (Helton and Horne, 2002) that, based on extensive cDNA library screening, β_{4a} was the predominant alternatively spliced variant of the β_4 subunit expressed in human spinal cord. To confirm this observation, we performed a comparative Northern analysis using a commercially available multiple tissue Northern

blot (Human Brain II, Clonetech) and a β_4 cDNA probe containing sequence common to both β_{4a} and β_{4b}. The mRNA's for β_{4a} and β_{4b} can be readily distinguished by their distinct migration pattern in agarose-formaldehyde gels (Figure 4.6*A*). The results of the Northern analysis, shown in Figure 4.6*B,* were striking, revealing that not only was β_{4a} the predominant form of β_4 subunit in the spinal cord, but also in other "reptilian" portions of the human CNS such as the medulla and putamen. Moreover, β_{4a} was the predominant form of β_4 subunit expressed in evolutionarily older regions of the cerebrum, the temporal lobe and occipital pole. In marked contrast, β_{4b} was highly expressed in the most recent and most highly integrative region of the cerebrum, the frontal lobe. The two forms of the β_4 subunit were equally expressed in cerebellum.

A BLAST search of the human genome (Altschul *et al*., 1990) with β_4 sequences revealed that the exons coding for alternatively spliced forms of the β_4 subunit A domain are distributed widely on human chromosome 2. Figure 4.6C shows that, depending on the splice variant, the coding sequence for the β_4 PDZ domain is contained within 3 (β_{4a}) or 4 (β_{4b}) exons spread out over ~ 218,000 bases. The coding sequence for the GXXDXPXXP motif is included in the 5'-most exon of a pair of short exons that code for β_{4b} amino acids 1 – 49. Assembly of the β_{4b} mRNA requires that 3 RNA segments (536 bases, 214,959 bases, and 2,329 bases) be spliced out. The short exon coding for the first 15 amino acids of β_{4a} lies between the β_{4b} N-terminal exons and the exon coding amino acids 50–89 and 16–55 of β_{4b} and β_{4a}, respectively. By comparison, the third PDZ domain of PSD-95 is encoded by 2 exons separated by a 200 bp intron (not shown).

Discussion

We have identified an alternatively spliced proline-rich motif in the Ca^{2+} channel β_4 subunit that has considerable influence over gating of neuronal $Ca_v2.1$ Ca^{2+} channels. Given that the motif also affects extracellular toxin binding, it is likely that the interaction of this motif with its binding site has wide-reaching impact on resting and open-state Ca^{2+} channel conformations. This notion is supported by recent images of the conformational changes that occur with gating of bacterial two membrane-spanning K^+ channels (Liu *et al*., 2001; Jiang *et al*., 2002a, b). Like eukaryotic six membrane-spanning K^+ channels, KcsA and MthK channels are tetramers that pack with four-fold symmetry around a central pore (Doyle *et al*., 1998; Jiang *et al*., 2002b). The principal structural elements of KcsA and MthK from N to C terminus include an outer transmembrane helix (M1), a pore helix (P), and an inner transmembrane helix (M2). These correspond to S5, H5, and S6 segments of voltage-gated Ca^{2+} channels, respectively. In the closed conformation of the KcsA structure, the four M2 helices are straight and arranged such that they form the walls of an inverted teepee that narrows from a 12 Å diameter at its center to a 4 Å pore at its tip (Doyle *et al*., 1998). Upon opening, the KcsA M2 helices tilt away from the permeation pathway and rotate about their helical axis (Liu *et al*. 2001). In MthK bending and splaying of the inner helices upon opening expands the diameter of the pore three fold (Jiang *et al*., 2002a,b). The nearly 30º bend occurs at a "gating hinge" corresponding to a glycine residue just below the selectivity filter. Applying a radial-outward force on the intracellular aspects of the inner helices places a torque on the gating hinge such that a conformational change is transmitted the full length of the M2 helix. (This can be viewed as a movie in the Supplementary Information to Jiang *et al*.,

2002a). It has been hypothesized that similar mechanical forces are at work in the gating of voltage-gated Ca^{2+} channels (Jiang *et al*., 2002a).

Considered in the context of this mechanical framework, our results suggest that an interaction of the β_{4b} ligand motif with an inner aspect of the $Ca_v2.1$ complex either directly or indirectly fine-tunes the torque experienced by α_{1A} S6 segments. In so doing, the interaction alters the conformation of the voltage sensor or gate (or both) as well as the outer vestibule. Given the potential for the interaction to occur over a wide reach (Helton and Horne, 2002) it is not possible to pinpoint which S6 helices might be most affected. A case can be made for an indirect effect on the IS6 helix, since the primary α_1-β_4 subunit interaction occurs on the intracellular loop between homology domains I and II (I-II loop; Pragnell *et al*., 1994). This is consistent with an earlier study showing that IS6 is a critical determinant of voltage-dependent inactivation in $Ca_v2.1$ and $Ca_v2.3$ channels (Zhang *et al*., 1994). However, site-directed mutagenesis and domain swapping studies have highlighted the equal importance of IIS6, IIIS6, and IVS6 in Ca^{2+} channel gating (reviewed by Stotz and Zamponi, 2001; Shi and Soldatov, 2002), making the case for direct effects on these S6 helices equally plausible. It is interesting that many of the proteins that have evolved to modulate Ca^{2+} channel gating target α_1 I-II (β subunits, $G_{\beta\gamma}$ subunits, protein kinase C) and II - III loops (syntaxin, synaptotagmin, SNAP-25). The IS6 and IIS6 (but not IIIS6 or IVS6) helices of $Ca_v2.1$, 2.1 and 2.3 Ca^{2+} channels have glycines in hinge positions comparable to those present in KcsA and MthK (see alignments in Horne *et al*., 1993).

Despite extensive binding studies with β_4 subunits, there is currently no evidence to support the idea that the β_{4b} N-terminus binds directly to α_{1A} subunits (Walker *et al*.,

1998; Walker *et al*.,1999). One possible explanation for this is that the interaction may be too weak to be detected in solution binding assays. The other possibility is that the α_{1A} subunit is not the primary target. The sequence of the ligand motif (GXXDXPXXP) may provide an important clue as to the nature of its binding site. Proline-rich motifs are common within the primary structures of many ligands important for protein-protein interactions (for reviews see Kay *et al*., 2000 and Macias *et al*., 2002). SH3 and WW domains, for example, recognize proline-rich sequences containing a core PXXP, where X denotes any amino acid. These sequences adopt a PPII helix conformation which presents a hydrophobic surface as well as backbone carbonyls that are ideal for hydrogen bonding. Proline-rich ligands bind with low affinity, allowing for rapid modulation and added versatility in signaling pathways. In many respects, the β_{4b} ligand motif resembles the serine/threonine proline motifs recognized by group IV WW domains (Sudol and Hunter, 2000). As is the case for the β_{4b} motif, the structural basis for recognition of these motifs is based on the summed contributions of a series of side chain interactions, none of which is absolutely essential for ligand binding (Verdecia *et al*., 2000).

It is possible that the β_{4b} proline-rich motif binds to its own B domain, which is structurally similar to SH3 and WW domains (Hanlon *et al*., 1999). This possibility is supported by what is known about related MAGUK family proteins in which intramolecular interactions are a key aspect of their functional diversity (Dimitratos *et al*., 1999). In support of such an interaction, molecular modeling of SAP97 revealed that it is capable of forming a compact structure in which its third PDZ domain and SH3 are in close opposition (Wu *et al*. 2000). Binding of the β_{4b} proline-rich motif with its own SH3 could in turn affect a β_4 SH3-GK domain interaction. Disruption of the β_4 SH3-GK

interaction, may affect the conformation of the α_{1A} I-II loop, and alter the torque applied to IS6. In comparison, disruption of the SH3-GK interaction in PSD-95 inhibits clustering of the K+ channel $K_v1.4$ (Shin *et al*., 2000). Though speculative, such a sequence of binding events would readily account for the differences in gating observed between $Ca_v2.1$ complexes containing β_{4a} and β_{4b}. Proof of such a model will require considerably more biochemical characterization of the β_4 subunit.

To date, the GXXDXPXXP motif of PSD-95 has been somewhat overlooked and no specific function has been assigned to it. Most attention has been paid to the structure of the third PDZ domain and has focused on the peptide binding functions of the carboxylate binding loop to which it is immediately adjacent (Doyle *et al*., 1996; CBL in Figure 4.4). A partial list of the proteins that interact specifically with the third PDZ domain of PSD-95 include the cell-surface neuroligins (Irie *et al*., 1997), the microtubule binding protein, CRIPT (Niethammer *et al*., 1998), the Rho effector protein, citron (Zhang *et al*., 1999), and the β_1 adrenergic receptor (Hu *et al*., 2000). It would be interesting to determine whether the GXXDXPXXP motif of PSD-95 plays a role maintaining the structure of the CBL. Such a role could also be considered for the GXXDXPXXP motif of β_{4b}. As is apparent in the β_{4b} A domain model structure (Figure 4.4B), the sequences of β_{4b} corresponding to the hydrophobic CBL and β- strand B of PSD-95 are highly positively charged. It is possible, as is true for some PDZ domains (Cuppen *et al*., 1998), that this region binds to an internal negatively charged domain. Interestingly, the immediate 5' sequence of the II-III loop of $Ca_v2.1$ and 2.2 Ca^{2+} channels fits this description, as it is densely packed with glutamate residues. Similar to the effects of β_{4b} on α_{1A}, binding of syntaxin to a "synprint site" just downstream from

this region in the II-III loop of α_{1B} shifts the $V_{1/2}$ of inactivation to more hyperpolarized potentials (Bezprozvanny *et al*., 2000) and accelerates entry into slow inactivation (Degtiar *et al*., 2000).

Viewed from the perspective of changing Ca^{2+} channel function, the differential distribution of β_{4a} and β_{4b} subunit mRNA displayed in Figure 4.6*B* provides an unexpected snapshot of the evolution of forebrain synapses. It raises the possibility that with the introduction of β_{4b} to the genome, synapses acquired properties that fit better with the overall demand to organize complex neural networks. It could be that with the advent of $Ca_v2.1$ complexes that entered more readily into closed inactivation states (Figure 4.1, *A*, *C*) without perceptible gain in time required for recovery (Figure 4.1, *D*), synapses inherited an enhanced mechanism for synaptic plasticity. In this regard, short-term synaptic depression has been linked to Ca^{2+} channel inactivation (Forsythe *et al*., 1998) through mechanisms shown to be β subunit dependent (Patil et. al, 1998). This form of short term synaptic plasticity has been implicated in cortical gain control (Abbott *et al*., 1997) and low-pass temporal filtering (Fortune and Rose, 2001). Accordingly, our future studies will be directed toward characterizing the responsiveness of Ca_v2 Ca^{2+} channels containing alternatively spliced β_4 subunits to changes in more dynamic regulatory inputs, such as neuronal firing frequency and action potential waveform.

References

Abbott LF, Varela JA, Sen K, Nelson SB (1997) Synaptic depression and cortical gain control. Science. 275: 220-224.

Appell RD, Bairoch A, Hochstrasser DF (1994) A new generation of information retrieval tools for biologists: the example of the ExPASy WWW server. Trends Biochem Sci. 19: 258-260.

Altschul SF, Gish W, Miller W, Myers EW, Lipman DJ (1990) Basic local alignment search tool. J Mol Biol. 215: 403-410.

Bezanilla F, The voltage sensor in voltage-dependent ion channels. (2000) Physiol Rev. 80:555-592.

Berjukow S, Marksteiner R, Sokolov S, Weiss RG, Margreiter E, Hering S (2001) Amino acids in segment IVS6 and β-subunit interaction support distinct conformational changes during $Ca_v2.1$ inactivation. J Biol Chem. 276: 17076-17082

Berrou L, Bernatchez G, Parent L (2001) Molecular determinants of inactivation within the I-II linker of α_{1E} ($Ca_V2.3$) calcium channels. Biophys J. 80: 215-228.

Bezprozvanny I, Maximov A (2001) PDZ domains: More than just a glue. Proc Natl Acad Sci. 98: 787-789.

Bezprozvanny I, Zhong P, Scheller RH, Tsien RW (2000) Molecular determinants of the functional interaction between syntaxin and N-type Ca^{2+} channel gating. Proc Natl Acad Sci. 97:13943-13948.

Cha A, Snyder GE, Selvin PR, Bezanilla F (1999) Atomic scale movement of the voltage-sensing region in a potassium channel measured via spectroscopy. Nature. 402:809-813.

Catterall WA (2000) Structure and regulation of voltage-gated Ca^{2+} channels. Ann Rev Cell Dev Biol. 16:521-555.

Colovos C, Yeates TO (1993) Verification of protein structures: patterns of nonbonded atomic interactions. Protein Sci. 2: 1511-1519.

Cuppen E, Gerrits H, Pepers B, Wieringa B, Hendriks W (1998) PDZ motifs in PTP-BL and RIL bind to internal protein segments in the LIM domain protein RIL. Mol Biol Cell. 9:671-683.

Degtiar VE, Scheller RH, Tsien RW (2000) Syntaxin modulation of slow inactivation of N-type calcium channels. J Neurosci. 20:4355-4367.

Dimitratos SD, Woods DF, Stathakis DG, Bryant PJ (1999) Signaling pathways are focused at specialized regions of the plasma membrane by scaffolding proteins of the MAGUK family. Bioessays. 21:912-921.

Doyle DA, Lee A, Lewis J, Kim E, Sheng M, MacKinnon R (1996) Crystal structures of a complexed and peptide-free membrane protein-binding domain: molecular basis of peptide recognition by PDZ. Cell. 85: 1067-1076.

Doyle DA, Morais-Cabral J, Pfuetzner RA, Kuo A, Gulbis JM, Cohen SL, Chait BT, MacKinnon R (1998) The structure of the potassium channel: molecular basis of K^+ conduction and selectivity. Science. 280:69-77.

Ellinor PT, Zhang JF, Horne WA, TsienRW (1994) Structural determinants of the blockade of N-type calcium channels by a peptide neurotoxin. Nature. 372:272-275.

Forsythe ID, Tsujimoto T, Barnes-Davies M, Cuttle MF, Takahashi T (1998) Inactivation of presynaptic calcium current contributes to synaptic depression at a fast central synapse. Neuron. 20:797-807.

Fortune ES, Rose GJ (2001) Short-term synaptic plasticity as a temporal filter. Trends Neurosci. 24:381-5.

Glauner KS, Mannuzzu LM, Gandhi CS, Isacoff EY (1999) Spectroscopic mapping of voltage sensor movement in the Shaker potassium channel. Nature. 402:813-817.

Hanlon MR, Berrow NS, Dolphin AC, Wallace BA (1999) Modeling of a voltage-dependent Ca^{2+} channel β subunit as a basis for understanding its functional properties. FEBS Lett. 445:366-370.

Hans M, Urrutia A, Deal C, Brust PF, Stauderman K, Ellis SB, Harpold MM, Johnson EC, Williams ME (1999) Structural elements in domain IV that influence biophysical and pharmacological properties of human α_{1A}-containing high-voltage-activated calcium channels. Biophys J. 76:1384-1400.

Harris BZ, Lim WA (2001) Mechanism and role of PDZ domains in signaling complex assembly. J Cell Sci. 114:3219-3231.

Helton TD, Horne WA (2002) Alternative splicing of the β_4 subunit has α_1 subunit subtype-specific effects on Ca^{2+} channel gating. J Neurosci. 22:1573-1582.

Horn R (2000) A new twist in the saga of charge movement in voltage-dependent ion channels. Neuron. 25:511-514.

Horne WA, Ellinor PT, Inman I, Zhou M, Tsien RW, and Schwarz TL (1993) Molecular diversity of Ca^{2+} channel α_1 subunits from the marine ray Discopyge ommata. Proc Natl Acad Sci. 90:3787-3791.

Hu LA, Tang Y, Miller WE, Cong M, Lau AG, Lefkowitz RJ, Hall RA (2000) β_1-adrenergic receptor association with PSD-95: Inhibition of receptor internalization and facilitation of β_1-adrenergic receptor interaction with N-methyl-D-aspartate receptors. J Biol Chem. 275:38659-38666.

Irie M, Hata Y, Takeuchi M, Ichtchenko K, Toyoda A, Hirao K, Takai Y, Rosahl TW, Sudhof TC (1997) Binding of neuroligins to PSD-95. Science. 277:1511-1515.

Jiang Y, Lee A, Chen J, Cadene M, Chait BT, MacKinnon R (2002a) The open pore conformation of potassium channels. Nature. 417:523-526.

Jiang Y, Lee A, Chen J, Cadene M, Chait BT, MacKinnon R (2002b) Crystal structure and mechanism of a calcium-gated potassium channel. Nature. 417:515-522.

Kay BK, Williamson MP, Sudol M (2000) The importance of being proline: the interaction of proline-rich motifs in signaling proteins with their cognate domains. FASEB J. 14:231-241.

Koradi R, Billeter M, Wuthrich K (1996) MOLMOL: a program for display and analysis of macromolecular structures. J Mol Graph. 14:51-55, 29-32.

Kozak M (1991) An analysis of vertebrate mRNA sequences: intimations of translational control. J Cell Biol. 115:887-903.

Laskowski RA, Moss DS, Thornton JM (1993) Main-chain bond lengths and bond angles in protein structures. J Mol Biol. 231:1049-1067.

Lin Z, Haus S, Edgerton J, Lipscombe D (1997) Identification of functionally distinct isoforms of the N-type Ca^{2+} channel in rat sympathetic ganglia and brain. Neuron. 18:153-166.

Liu YS, Sompornpisut P, Perozo E (2001) Structure of the KcsA channel intracellular gate in the open state. Nat Struct Biol. 8:883-887.

Macias MJ, Wiesner S, Sudol M (2002) WW and SH3 domains, two different scaffolds to recognize proline-rich ligands. FEBS Lett. 513:30-37.

Martí-Renom MA, Stuart AC, Fiser A, Sanchez R, Melo F, Sali A (2000) Comparative protein structure modeling of genes and genomes. Annu Rev Biophys Biomol Struct. 29:291-325.

Niethammer M, Valtschanoff JG, Kapoor TM, Allison DW, Weinberg TM, Craig AM, Sheng M (1998) CRIPT, a novel postsynaptic protein that binds to the third PDZ domain of PSD-95/SAP90. Neuron. 20:693-707.

Patil PG, Brody DL, Yue DT (1998) Preferential closed-state inactivation of neuronal calcium channels. Neuron. 20:1027-1038.

Perozo E, Cortes DM, Cuello LG (1999) Structural rearrangements underlying K+-channel activation gating. Science. 285:73-78.

Pragnell M, De Waard M, Mori Y, Tanabe T, Snutch TP, Campbell KP (1994) Calcium channel β-subunit binds to a conserved motif in the I-II cytoplasmic linker of the α_1-subunit. Nature. 368:67-70.

Sali A, Blundell TL (1993) Comparative protein modelling by satisfaction of spatial restraints. J Mol Biol. 234:779-815.

Shi C, Soldatov NM (2002) Molecular determinants of voltage-dependent slow inactivation of the Ca^{2+} channel. J Biol Chem. 277:6813-6821.

Shin H, Hsueh YP, Yang FC, Kim E, Sheng M (2000) An intramolecular interaction between Src homology 3 domain and guanylate kinase-like domain required for channel clustering by postsynaptic density-95/SAP90. J Neurosci. 20:3580-3587.

Stotz SC, Hamid J, Spaetgens RL, Jarvis SE, Zamponi GW (2000) Fast inactivation of voltage-dependent calcium channels. A hinged-lid mechanism? J Biol Chem. 275:24575-24582.

Stotz SC, Zamponi GW (2001) Identification of inactivation determinants in the domain IIS6 region of high voltage-activated calcium channels. J Biol Chem. 276:33001-33010.

Sudol M, Hunter T (2000) NeW wrinkles for an old domain. Cell. 103:1001-1004.

Verdecia MA, Bowman ME, Lu KP, Hunter T, Noel JP (2000) Structural basis for phosphoserine-proline recognition by group IV WW domains. Nat Struct Biol. 7:639-643.

Walker D, Bichet D, Campbell KP, De Waard M (1998) A β4 isoform-specific interaction site in the carboxyl-terminal region of the voltage-dependent Ca^{2+} channel α_{1A} subunit. J Biol Chem. 273:2361-2367.

Walker D, Bichet D, Geib S, Mori E, Cornet V, Snutch TP, Mori Y, De Waard M (1999) A new β subtype-specific interaction in α_{1A} subunit controls P/Q-type Ca^{2+} channel activation. J Biol Chem. 274:12383-12390.

Wu H, Reissner C, Kuhlendahl S, Coblentz B, Reuver S, Kindler S, Gundelfinger ED, Garner CC (2000) Intramolecular interactions regulate SAP97 binding to GKAP. EMBO J. 19:5740-5751.

Zhang JF, Ellinor PT, Aldrich RW, Tsien RW (1994) Molecular determinants of voltage-dependent inactivation in calcium channels. Nature. 372:97-100.

Zhang W, Vazquez L, Apperson M, Kennedy MB (1999) Citron binds to PSD-95 at glutamatergic synapses on inhibitory neurons in the hippocampus. J Neurosci. 19:96-108.

Zhong H, Li B, Scheuer T, Catterall WA (2001) Control of gating mode by a single amino acid residue in transmembrane segment IS3 of the N-type Ca^{2+} channel. Proc Natl Acad Sci. 98:4705-4709.

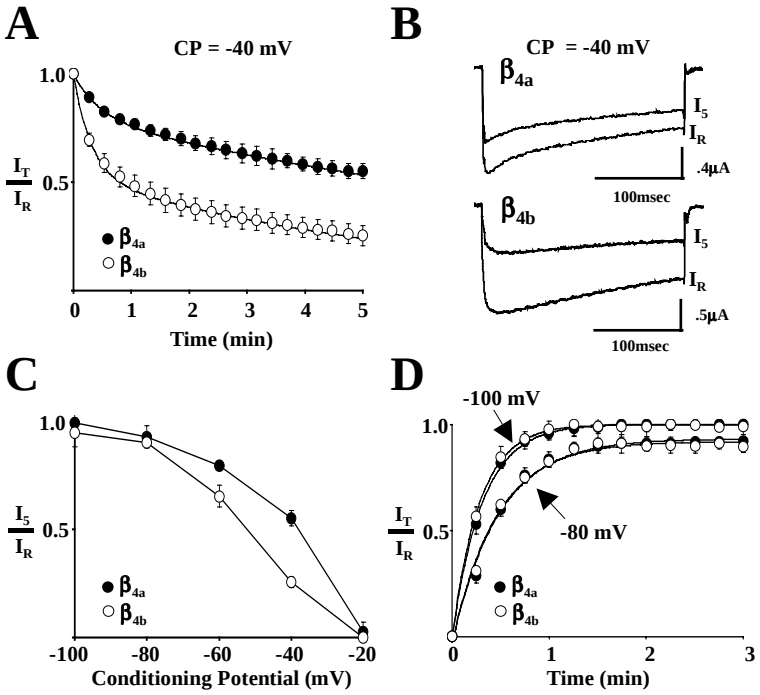

Figure 4.1. Effects of β_{4a} and β_{4b} on slow inactivation and recovery from slow inactivation of $Ca_v2.1$ Ca^{2+} channels. Studies were performed with *Xenopus* oocytes expressing α_{1A}, α_2/δ-1, and either β_{4a} or β_{4b}. Reference (I_R) and test current (I_T) traces were generated by 300 msec step depolarizations from various holding potentials to either 0 mV (β_{4b}) or +10mV (β_{4a}). Maximum values from 300 msec I_R and I_T current traces were used to calculate I_T/I_R where indicated. Barium (5 mM) was used as the charge carrier. *A*, Influence of β_{4a} and β_{4b} on the development of slow inactivation at a conditioning potential (CP) of -40 mV. Following a reference pulse (I_R) measured from a holding potential of –80 mV, oocytes were held at -40 mV for 5 min. During this time, 300 ms test pulses (I_T) were applied every 15 sec. Each *point* represents the mean value of I_T/I_R from 11 (β_{4a}) or 10 (β_{4b}) different recordings. The SEM is shown for each *point* unless the values were smaller than the *symbol*. The *solid lines* represent double-exponential fits to the data. *B*, Representative reference (I_R) and 5 min (I_5) current traces from $Ca_v2.1$ complexes containing either β_{4a} (*top*) or β_{4b} (*bottom*) generated as described in *A*. *C*, Voltage dependence of slow inactivation. The ratio of I_5 to I_R generated as in *A*, plotted as a function of conditioning potential for $Ca_v2.1$ complexes containing either β_{4a} or β_{4b}. Data *points* represent the means of at least 6 determinations at a given membrane potential. *Lines* serve only to connect the data points. *D*, Influence of β_{4a} and β_{4b} on the time course of recovery from slow inactivation. Following a 300 msec reference pulse (I_R) measured from a holding potential of either -80 or -100 mV, oocytes were held at -30 mV for 5 min. The membrane potential was then returned to either -80 or -100 mV, and sequential test pulses (I_T) were applied at 15 second intervals for a total of 3 minutes. Each *point* represents the mean of at least 7 different recordings. *Solid lines* represent the single-exponential fits of the data.

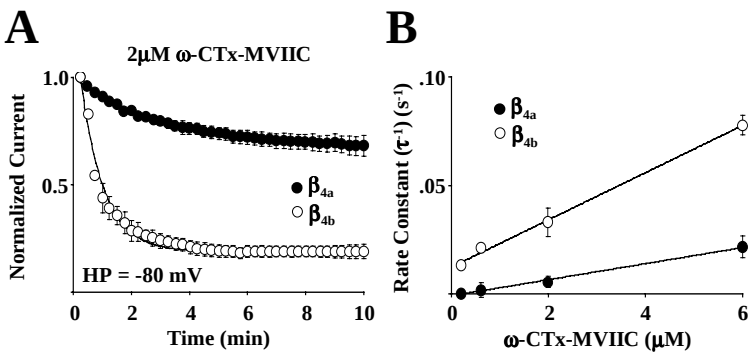

Figure 4.2. Effects of β_{4a} and β_{4b} on the blockade of $Ca_v2.1$ channels by ω-CTx-MVIIC. Studies were performed with *Xenopus* oocytes expressing α_{1A}, α_2/δ-1, and either β_{4a} or β_{4b}. *A*, Onset and degree of block by a 10 minute exposure to 2 μM ω-CTx-MVIIC for $Ca_v2.1$ subunit combinations at a holding potential (HP) of -80 mV. Each *point* represents the mean of 7 (β_{4a}) or 8 (β_{4b}) different recordings. The SEM is shown for each data *point* unless smaller than *symbol*. Onset of block for both subunit combinations fit well (*line*) to a single-exponential time course plus a constant. *B*, The rate constants for the time course of the onset on toxin block were determined from steady-state degree of block from single exponential fits at 4 different toxin concentrations (0.2 μM, 0.6 μM, 2 μM, and 6 μM) for $Ca_v2.1$ complexes containing either β_{4a} or β_{4b}. The averaged rate constants were plotted as a function of toxin concentration (minimum n = 7, ± SEM). The *line* represents a linear fit to the data.

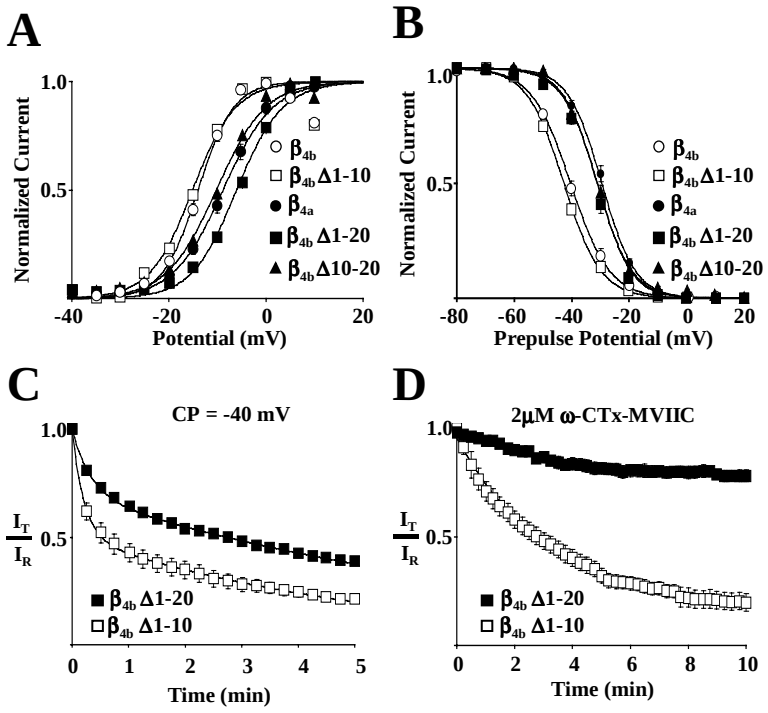

Figure 4.3. Localization of differential effects on $Ca_v2.1$ gating and pharmacology to β_{4b} N-terminal amino acids 10-20. The first 10 (β_{4b} Δ1-10), first 20 (β_{4b} Δ1-20) or second 10 (β_{4b} Δ10-20) amino acids of the N-terminus of the β_{4b} subunit were removed using PCR. The deletion mutants as well as β_{4a} or β_{4b} were expressed with α_{1A} and $\alpha_2\delta$-1 in *Xenopus* oocytes. *A*, Effects of the N-terminal deletion mutants on the voltage-dependency of activation of $Ca_v2.1$ channels. Plots were derived from averaged I-V data up to +10 mV for each β_4 subunit combination. Data *points* represent the means of the normalized data at a given membrane potential for a minimum of 9 different recordings. *Smooth lines* represent single Boltzmann fits to the averaged data. *B*, Normalized, averaged isochronal inactivation curves for $Ca_v2.1$ complexes containing the various β_4 subunits. *Points* represent the means of the normalized data at a given membrane potential for a minimum of 9 different recordings. *Smooth lines* represent single Boltzman fits to the averaged data. *C*, Effects of β_4 N-terminal deletion mutants on the development of slow inactivation at a conditioning potential (CP) of -40 mV. Reference (I_R) and test (I_T) currents were generated as in Figure 1*A*. Each *point* represents the mean value of I_T/I_R from 13 (β_{4b} Δ1-10) or 9 (β_{4b} Δ1-20) different recordings. The solid lines represent double-exponential fits to the data. *D*, Onset and degree of block by a 10 minute exposure to 2μM ω-CTx-MVIIC for $Ca_v2.1$ complexes containing β_{4b} Δ1-10 or β_{4b} Δ1-20. Data were generated as in Figure 2*A*. Each *point* represents the average of a minimum of 7 recordings. The solid lines represent single-exponential fits to the data.

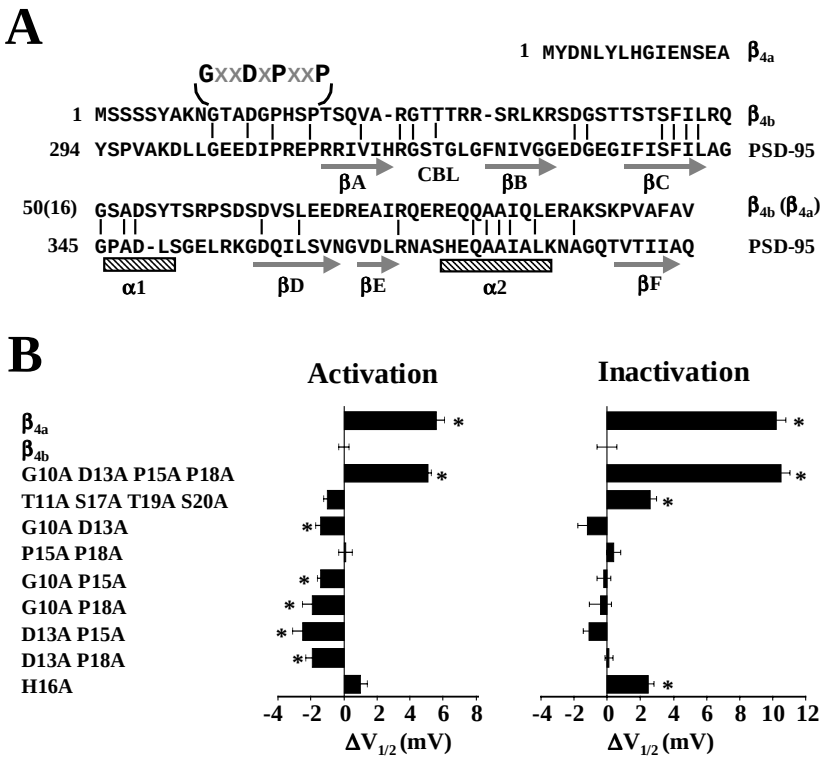

Figure 4.4. The β_4 subunit is a distant homologue of PSD-95. Identification of a conserved GXXDXPXXP motif critical to $Ca_v2.1$ gating. *A*, Amino acid alignment of the A domains of the human spinal cord β_{4a} (amino acids 1-64) and β_{4b} (amino acids 1-94) subunits with the third PDZ domain (amino acids 294-442) of PSD-95. *Vertical bars* denote identical amino acids between β_{4b} and PSD-95. Important amino acids involved in modulating the leftward shift in the voltage-dependence of activation and inactivation of β_{4b} (GXXDXPXXP) are highlighted. *Arrows* and *hatched bars* and represent predicted α-helices and β-strands of the third PDZ domain of PSD-95, respectively. *B*, Differences in the $V_{1/2}$'s of activation and inactivation of β_{4a} and β_{4b} N-terminal amino acid mutants versus β_{4b}. *Solid bars* represent average $V_{1/2}$'s of a minimum of 9 different recordings for each β_4 subunit variant. Positive or negative shifts, in mV, in the $V_{1/2}$'s of activation and inactivation of β_{4a} and β_{4b} mutants are compared to the $V_{1/2}$'s of activation and inactivation of β_{4b}. Currents were generated as described in Figure 3*A* and 3*B*. The SEM for each bar is shown. Asterisks denote statistical significance ($p<0.05$) by a Student's two-sample equal variance *t* test.

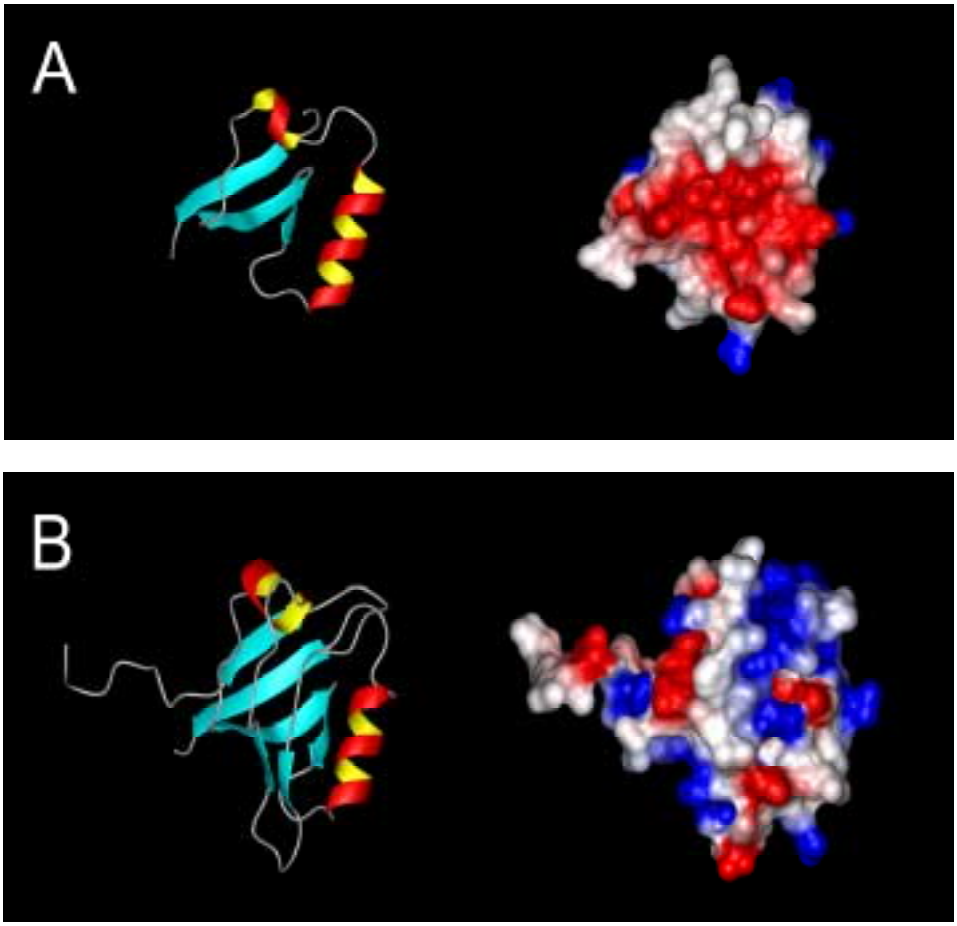

Figure 4.5. Real-space optimization structural models of the A domains of β_{4a} (*A*) and β_{4b} (*B*) based on sequence identities with the third PDZ domain of PSD-95. Ribbon (*left*) and electrostatic surface potential (*right*) diagrams were created using MOLMOL (Koradi et al., 1996). For ribbon diagrams, *arrows* indicate β-strands, and *helices*, α helices. For surface potential diagrams, *red*, *white*, and *blue* regions indicate negatively charged, hydrophobic and positively charged amino acids, respectively.

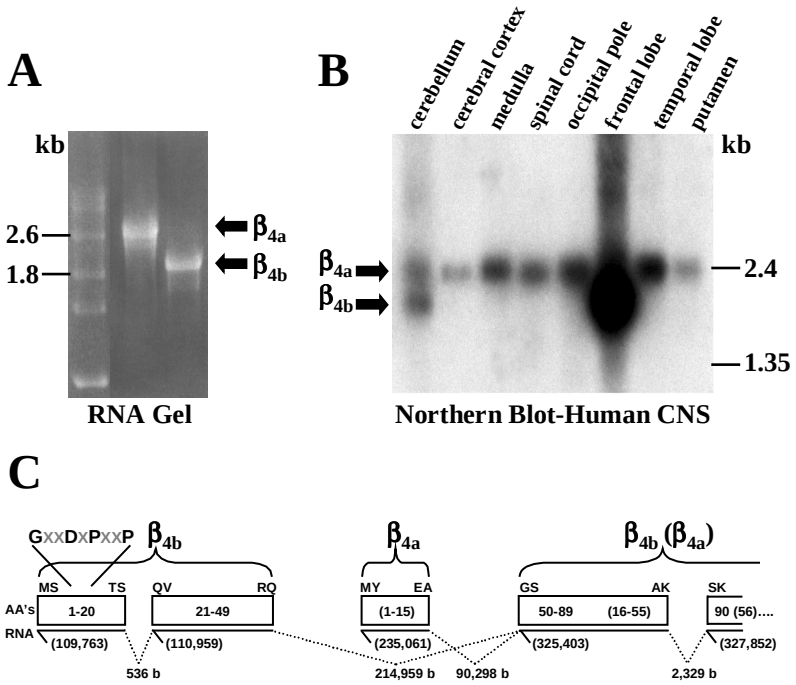

Figure 4.6. Differential distribution of β_{4a} and β_{4b} mRNA in the human central nervous system (CNS). *A*, Electrophoresis of full-length β_{4a} (*left*) and β_{4b} (*right*) cRNA's (includes 5' and 3' untranslated) in a 1% agarose formaldehyde denaturing gel. RNA markers (kb) are indicated on the left. *B*, Northern analysis performed with human multiple tissue blot (Human Brain II, Clonetech) and a ^{32}P labeled β_4 subunit probe (coding nucleotides 215-1628 plus approximately 300 bp 3' untranslated sequence). Molecular masses on right correspond to labeled blot markers. *C*, Human β_4 subunit genome map depicting the lengths of intron sequences (b = bases) between alternatively spliced β_{4a} and β_{4b} N-terminal exons and the beginning of exon 2. *Solid lines* represent exons and *dashed lines* introns. Numbers in parenthesis below solid lines indicate position on chromosome 2. *Boxes* indicate protein sequence (β_{4a} in parenthesis). First and last two amino acids of each sequence are indicated above each box.

Chapter 5

CONCLUSIONS

Voltage-gated Ca^{2+} channels are widely expressed in excitable cells and are involved in a broad array of cellular mechanisms. Release of neurotransmitter from pre-synaptic nerve terminals in response to changes in membrane potential is highly reliant on the influx of Ca^{2+} through voltage-gated Ca^{2+} channels. Evidence has shown that small changes in pre-synaptic Ca^{2+} concentrations can have a significant effect on neurotransmitter release and that release is an n^4 function of intracellular Ca^{2+} (Shneggenburger and Neher 2000; Bollman *et al*., 2000). While ten distinct Ca^{2+} channel α_1 subunit genes have been identified to date, 3 subtypes, $Ca_v2.1$, $Ca_v2.2$, and $Ca_v2.3$ channels have been localized to pre-synaptic membranes (Timmerman *et al*., 2002). $Ca_v2.1$ and $Ca_v2.2$ channels in particular are required for depolarization-coupled neurotransmitter release (Miljanich and Ramachandran, 1995). Beta 4 subunits co-localize with $Ca_v2.1$ and $Ca_v2.2$ channels *in vitro* and appear to be the predominant β subunit subtype expressed in neuronal tissues (Westenbroek *et al*., 1998).

Voltage-gated Ca^{2+} channel gating can be regulated by a variety of intracellular mechanisms including phosphorylation by PKA and PKC, and by activation of G-proteins (Catterall 2000). G-protein modulation of $Ca_v2.1$ and $Ca_v2.2$ channels has been shown to occur at pre-synaptic nerve terminals (Toth *et al*., 1993) and this mechanism is responsible for some of the pre-synaptic inhibition of synaptic transmission mediated by activation of $\alpha 2$ adrenergic and μ opioid receptors (Hille, 1992; Toth *et al*., 1993;

Dolphin, 1995). It has been determined that the Gβγ subunits of the G-protein complex are responsible for slowing the rate and right shifting the voltage-dependency of activation of $Ca_v2.1$ and $Ca_v2.2$ channels (Herlitze *et al*., 1996; Ikeda *et al*., 1997; Patil *et al*., 1996; Jones and Elmslie., 1997). This G-protein mediated inhibition can be relieved by strong depolarizing prepulses (facilitation) that restore the rate and voltage-dependence of activation to near pre-inhibition levels (Zhang *et al*., 1996; Jones and Elmslie, 1997). Chimeric experiments involving the G-protein sensitive $Ca_v2.1$ and $Ca_v2.2$ channels and G-protein insensitive $Ca_v1.2$ and $Ca_v2.3$ demonstrate that the primary G-protein interaction site is on the I-II linker region near the AID (De Waard *et al*., 1997; Herlitze *et al*., 1997; Page *et al*., 1997; Zamponi *et al*., 1997). The N- and C-terminus of $Ca_v2.1$ and $Ca_v2.2$ have also been shown to interact with Gβγ subunits and modulate channel inhibition (Cantí *et al*., 1999; Furukawa *et al*., 1998; Page *et al*., 1998; Qin *et al*., 1997; Zhang *et al*., 1998).

G protein inhibition can be mediated through $Ca_v2.1$ and $Ca_v2.2$ interactions with syntaxin and β subunits. G protein inhibition of $Ca_v2.2$ is facilitated through coexpression of syntaxin 1A (Lu *et al*., 2001; Jarvis and Zamponi, 2001; Jarvis *et al*., 2000; Stanley and Mirotznik, 1997). In contrast, co-expression of $Ca_v2.2$ channels with β_3 subunits significantly reduces the inhibitory effect of Gβγ subunits presumably by competing for a closely associated binding sites on the I-II linker near the AID (Roche and Treistman, 1995, 1998). Alternative splicing of the Ca^{2+} channel β_4 subunit could alter channel responsiveness to regulation by G-proteins, syntaxin, and other intracellular effectors through specific N-terminal interactions with regions of the α_1 subunit such as the II-III linker. This will be an interesting line of research to pursue in the future.

Voltage-gated Ca^{2+} channel alternative splicing leads to changes in the electrophysiological and pharmacological properties of channel complexes (Zhuchenko *et al*., 1997; Krovetz *et al*., 2000; Helton and Horne 2002). In this respect, alternative splicing of voltage-gated Ca^{2+} channels can aid in the fine tuning of specific neurons in response to stimuli making theme more or less sensitive leading to differential modulation of neurotransmission in neuronal pathways. Our data demonstrate that the association of alternatively spliced β_4 subunits (β_{4a} and β_{4b}) with $Ca_v2.1$ and $Ca_v2.2$ channels alters the voltage dependent properties of the channel. $Ca_v2.1$ and $Ca_v2.2$ channels expressed with β_{4b} are more sensitive to smaller changes in membrane potential as compared to $Ca_v2.1$ and $Ca_v2.2$ channels expressed with β_{4a}. In this respect, β_{4b} subunit expression leads to channel complexes that are more plastic in response to changes in membrane potential. This is reflected in the differential distribution of the alternatively spliced β_4 isoforms (see Figure 4.6) where β_{4a} is predominantly expressed in "reptilian" regions of the nervous system such as the spinal cord while β_{4b} is expressed primarily in "higher" brain regions like the frontal lobe. The greater synaptic flexibility afforded by expression of β_{4b} subunits would allow for more fine tuning of complex neuronal signaling in the more cognitive regions of the brain.

Alternative splicing of the β_4 subunit may also play a role in modulating pain responses. Using the Kim and Chung spinal cord ligation (SCL) rodent model of neuropathy (Kim and Chung, 1992), Matthews and Dickenson demonstrated that after SCL, the potency of the $Ca_v2.2$ channel blocker ω-Ctx-GVIA increased at low doses in comparison to control (Matthews and Dickenson, 2001). $Ca_v2.2$ channels are concentrated in laminae I and II of superficial dorsal horn of the spinal cord where

nocioceptive primary afferents synapse (Kerr *et al*., 1988; Gohil *et al*., 1994) and *in vivo* blockade of $Ca_v2.2$ channels by ω-Ctx-GVIA leads to antinocioception in the formalin test (Malmberg and Yaksh 1994, 1995; Bowersox *et al*., 1996) and intradermal capsaicin and knee joint inflammation pain models (Sluka, 1998). In the SCL model, spinal nerves L5 and L6 were ligated to induce a neuropathic state where experimental rats demonstrated allodynia and hyperalgesia of the affected hind limb. *In vivo* spinal cord application of ω-Ctx-GVIA significantly decreased the electrically- and naturally-evoked dorsal horn neuronal responses to innocuous and noxious stimuli (Matthews and Dickenson, 2001). While Matthews and Dickenson speculate that the selective enhancement of ω-Ctx-GVIA inhibitory actions are a result of an upregulation of the α_2/δ subunit, our data may suggest an alterntive theory. In our studies, we demonstrate that the primary β_4 subunit expressed in human spinal cord is β_{4a} (see chapter 4) and that β_{4a} right shifts the voltage-dependency of activation and inactivation of $Ca_v2.1$ and $Ca_v2.2$ compared to β_{4b} (Helton and Horne 2002). Of particular interest, we also demonstrate that $Ca_v2.1/Ca_v2.2$ β_{4a} complexes are 2-3 times less sensitive to ω-Ctx-MVIIC and ω-Ctx-GVIA block, respectively, than complexes expressed with β_{4b} (see chapter 4). This may explain the results demonstrated by Matthews and Dickenson where hyperalgesic pathways show an increased affinity for ω-Ctx-GVIA. In normal spinal cord nocioceptive pathways, $Ca_v2.1$ and $Ca_v2.2$ channels may be primarily associated with β_{4a} subunits and these complexes require a stronger, or normal, pre-synaptic membrane depolarization to activate and propagate a noxious stimulus. However, in hyperalgesic pathways, the alternatively spliced β_{4b} subunit would be upregulated leading to a more sensitive state

where normally non-noxious stimuli are perceived as allodynic and hyperalgesic. Upregulation of β_{4b} subunit expression would account for the increased effectiveness of block by ω-Ctx-GVIA. Further investigation, involving single cell analysis in normal and neuropathic pain pathways, of Ca^{2+} channel subunit expression and *in vivo* electrophysiological characterization is required to determine if alternative β_4 subunit splice variant expression plays a role in hyperalgesia and allodynia.

Traditionally, the treatment for chronic, intractable pain is the use of α2 agonists and opioids. While effective in modulating pain, opioids can have serious side effects including tolerance buildup and addiction. Recently, ziconotide, a $Ca_v2.2$ specific channel blocker was approved by the FDA for treatment of chronic pain. Ziconotide has been shown to be effective in modulating chronic pain without any indication of tolerance buildup (Jain 2000). However ziconotide must be delivered intrathecally and has deleterious side effects including nausea, sedation, nystagmus, and auditory and visual hallucinations (Penn and Paice, 2000). A better understanding of the role of alternative splicing in the regulation of voltage-gated Ca^{2+} channels in pre-synaptic nerve termini could lead to the design of better therapeutic agents with specific targeting and minimal side effects for the treatment of chronic pain.

References

Bollmann JH, Sakmann B, Borst JG (2000) Calcium sensitivity of glutamate release in a calyx-type terminal. Science. 289:953-957.

Bowersox SS, Gadbois T, Singh T, Pettus M, Wang YX, Luther RR. (1996) Selective N-type neuronal voltage-sensitive calcium channel blocker, SNX-111, produces spinal antinociception in rat models of acute, persistent and neuropathic pain. J Pharmacol Exp Ther. 279:1243-1249.

Canti C, Page KM, Stephens GJ, Dolphin AC. (1999) Identification of residues in the N terminus of alpha1B critical for inhibition of the voltage-dependent calcium channel by Gbeta gamma. J Neurosci. 19:6855-6864.

Catterall WA (2000) Structure and regulation of voltage-gated Ca2+ channels. Annu Rev Cell Dev Biol.16:521-555.

De Waard M, Liu H, Walker D, Scott VE, Gurnett CA, Campbell KP (1997) Direct binding of G-protein betagamma complex to voltage-dependent calcium channels. Nature. 385:446-450.

Dolphin AC. (1995) The G.L. Brown Prize Lecture. Voltage-dependent calcium channels and their modulation by neurotransmitters and G proteins. Exp Physiol. 80:1-36.

Furukawa T, Nukada T, Mori Y, Wakamori M, Fujita Y, Ishida H, Fukuda K, Kato S, Yoshii M. (1998) Differential interactions of the C terminus and the cytoplasmic I-II loop of neuronal Ca2+ channels with G-protein alpha and beta gamma subunits. I. Molecular determination. J Biol Chem. 273:17585-17594.

Gohil K, Bell JR, Ramachandran J, Miljanich GP. (1994) Neuroanatomical distribution of receptors for a novel voltage-sensitive calcium-channel antagonist, SNX-230 (omega-conopeptide MVIIC). Brain Res. 653:258-266.

Helton TD, Horne WA (2002) Alternative splicing of the beta 4 subunit has alpha1 subunit subtype-specific effects on Ca2+ channel gating. J Neurosci. 22:1573-1582.

Herlitze S, Garcia DE, Mackie K, Hille B, Scheuer T, Catterall WA (1996) Modulation of Ca2+ channels by G-protein beta gamma subunits. Nature. 380:258-262.

Herlitze S, Hockerman GH, Scheuer T, Catterall WA (1997) Molecular determinants of inactivation and G protein modulation in the intracellular loop connecting domains I and II of the calcium channel alpha1A subunit. Proc Natl Acad Sci U S A. 94:1512-1516.

Hille B. (1992) G protein-coupled mechanisms and nervous signaling. Neuron. 9:187-195.

Ikeda SR. (1996) Voltage-dependent modulation of N-type calcium channels by G-protein beta gamma subunits. Nature. 380:255-258.

Jain KK. (2000) An evaluation of intrathecal ziconotide for the treatment of chronic pain. Expert Opin Investig Drugs. 9:2403-2410.

Jarvis SE, Magga JM, Beedle AM, Braun JE, Zamponi GW. (2000) G protein modulation of N-type calcium channels is facilitated by physical interactions between syntaxin 1A and Gbetagamma. J Biol Chem. 275:6388-6394.

Jarvis SE, Zamponi GW. (2001) Distinct molecular determinants govern syntaxin 1A-mediated inactivation and G-protein inhibition of N-type calcium channels. J Neurosci. 2001 May 1;21(9):2939-48.

Jones SW, Elmslie KS (1997) Transmitter modulation of neuronal calcium channels. J Membr Biol. 155:1-10.

Kerr LM, Filloux F, Olivera BM, Jackson H, Wamsley JK. (1988) Autoradiographic localization of calcium channels with [125I]omega-conotoxin in rat brain. Eur J Pharmacol. 146:181-183.

Kim SH, Chung JM. (1992) An experimental model for peripheral neuropathy produced by segmental spinal nerve ligation in the rat. Pain. 50:355-363.

Krovetz HS, Helton TD, Crews AL, Horne WA. (2000) C-Terminal alternative splicing changes the gating properties of a human spinal cord calcium channel alpha 1A subunit. J Neurosci. 20:7564-7570.

Lu Q, AtKisson MS, Jarvis SE, Feng ZP, Zamponi GW, Dunlap K. (2001) Syntaxin 1A supports voltage-dependent inhibition of alpha1B Ca2+ channels by Gbetagamma in chick sensory neurons. J Neurosci. 21:2949-2957.

Malmberg AB, Yaksh TL. (1994) Voltage-sensitive calcium channels in spinal nociceptive processing: blockade of N- and P-type channels inhibits formalin-induced nociception. J Neurosci. 14:4882-4890.

Malmberg AB, Yaksh TL. (1995) Effect of continuous intrathecal infusion of omega-conopeptides, N-type calcium-channel blockers, on behavior and antinociception in the formalin and hot-plate tests in rats. Pain. 60:83-90.

Matthews EA, Dickenson AH. (2001) Effects of spinally delivered N- and P-type voltage-dependent calcium channel antagonists on dorsal horn neuronal responses in a rat model of neuropathy. Pain. 92:235-246.

Page KM, Canti C, Stephens GJ, Berrow NS, Dolphin AC. (1998) Identification of the amino terminus of neuronal Ca2+ channel alpha1 subunits alpha1B and alpha1E as an essential determinant of G-protein modulation. J Neurosci. 18:4815-4824.

Page KM, Stephens GJ, Berrow NS, Dolphin AC. (1997) The intracellular loop between domains I and II of the B-type calcium channel confers aspects of G-protein sensitivity to the E-type calcium channel. 17:1330-1338.

Patil PG, de Leon M, Reed RR, Dubel S, Snutch TP, Yue DT. (1996) Elementary events underlying voltage-dependent G-protein inhibition of N-type calcium channels. Biophys J. 71:2509-2521.

Penn RD, Paice JA. (2000) Adverse effects associated with the intrathecal administration of ziconotide. Pain. 85:291-296.

Qin N, Platano D, Olcese R, Stefani E, Birnbaumer L. (1997) Direct interaction of gbetagamma with a C-terminal gbetagamma-binding domain of the Ca2+ channel alpha1 subunit is responsible for channel inhibition by G protein-coupled receptors. Proc Natl Acad Sci U S A. 94:8866-8871.

Roche JP, Anantharam V, Treistman SN. (1995) Abolition of G protein inhibition of alpha 1A and alpha 1B calcium channels by co-expression of the beta 3 subunit. FEBS Lett. 371:43-46.

Roche JP, Treistman SN. (1998) Ca2+ channel beta3 subunit enhances voltage-dependent relief of G-protein inhibition induced by muscarinic receptor activation and Gbetagamma. J Neurosci. 18:4883-4890.

Schneggenburger R, Neher E (2000) Intracellular calcium dependence of transmitter release rates at a fast central synapse. Nature. 406:889-893.

Sluka KA. (1998) Blockade of N- and P/Q-type calcium channels reduces the secondary heat hyperalgesia induced by acute inflammation. Pharmacol Exp Ther. 287:232-237.

Stanley EF, Mirotznik RR. (1997) Cleavage of syntaxin prevents G-protein regulation of presynaptic calcium channels. Nature. 385:340-343.

Timmermann DB, Westenbroek RE, Schousboe A, Catterall WA (2002) Distribution of high-voltage-activated calcium channels in cultured gamma-aminobutyric acidergic neurons from mouse cerebral cortex. J Neurosci Res. 67:48-61.

Toth PT, Bindokas VP, Bleakman D, Colmers WF, Miller RJ. (1993) Mechanism of presynaptic inhibition by neuropeptide Y at sympathetic nerve terminals. Nature. 364:635-639.

Westenbroek RE, Hoskins L, Catterall WA. (1998) Localization of Ca2+ channel subtypes on rat spinal motor neurons, interneurons, and nerve terminals. J Neurosci. 18:6319-6330.

Zamponi GW, Bourinet E, Nelson D, Nargeot J, Snutch TP (1997) Crosstalk between G proteins and protein kinase C mediated by the calcium channel alpha1 subunit. Nature. 385:442-446.

Zhang JF, Ellinor PT, Aldrich RW, Tsien RW. (1996) Multiple structural elements in voltage-dependent Ca2+ channels support their inhibition by G proteins. Neuron. 17:991-1003.

Zhuchenko O, Bailey J, Bonnen P, Ashizawa T, Stockton DW, Amos C, Dobyns WB, Subramony SH, Zoghbi HY, Lee CC. (1997) Autosomal dominant cerebellar ataxia (SCA6) associated with small polyglutamine expansions in the alpha 1A-voltage-dependent calcium channel. Nat Genet. 15:62-69.